To the Graduate Council:

I am submitting herein a thesis written by Lek Song Chua entitled "Out-of-plane Behavior of Unreinforced Hollow Clay Tile Masonry Infilled Wall Panels." I have examined the final copy of this thesis for form and content and recommend that it be accepted in partial fulfillment of the requirements for the degree of Master of Science, with a major in Civil Engineering.

Richard M. Bennett, Major Professor

We have read this thesis
and recommend its acceptance:

Edwin G. Burdette

Accepted for the Council:

Vice Provost
and Dean of The Graduate School

STATEMENT OF PERMISSION TO USE

In presenting this thesis in partial fulfillment of the requirements for a Master's degree at The University of Tennessee, Knoxville, I agree that the Library shall make it available to borrowers under rules of the Library. Brief quotations from this thesis are allowable without special permission, provided that accurate acknowledgement of the source is made.

Requests for permission for extensive quotation from or reproduction of this thesis in whole or in parts may be granted by the copyright holder.

Signature 

Date April 22, 1991

OUT-OF-PLANE BEHAVIOR OF UNREINFORCED HOLLOW CLAY TILE MASONRY INFILLED WALL PANELS

A Thesis

Presented for the

Master of Science

Degree

The University of Tennessee, Knoxville

Lek Song Chua

May 1991

Copyright © Lek Song Chua, 1991

All Right Reserved

DEDICATION

To my wife, Noy Cheng Heng [王進真]

and

daughter, Florence [麥靖雯] with love.

ACKNOWLEDGEMENTS

First and foremost I wish to express my sincere appreciation to my major professor, Dr. Richard M. Bennett, for his guidance and encouragement throughout the course of my graduate studies. With his invaluable assistance, generous support, unlimited patience and friendship, I was able to complete this thesis otherwise impossible. I am also grateful for the contributions and valuable comments of Dr. Edwin G. Burdette and Dr. James H. Deatherage who both served as members of my thesis committee. Their knowledge and consultation help educate me throughout my studies at this university.

I wish to acknowledge Martin Marietta Energy Systems for the financial support and the opportunity to participate in this research. In addition, a special thank to Chin Kong Seah for providing me with valuable information which made this work possible. Appreciation is also due to George Barclay who plotted most of the graphs for this thesis.

I am indebted to my family, especially my parents, Kim Cheong Chua [蔡勤昌] and Ho Kiang Chai [谢惠娟], and my brother Chaw Song Chuah [蔡昭松]. I thank them for their love and support which make my studies possible and successful.

As a final note, I especially would like to extend my sincere thanks to my wife and daughter whom were my primary source of inspiration for completing this thesis.

ABSTRACT

The structural integrity of existing unreinforced masonry infilled walls under earthquake generated forces is of primary importance in seismically active zones. One of the seismic excitations is in the out-of-plane direction of the wall panel. The inertial out-of-plane forces due to the mass of the panel are investigated and may be simulated by a uniformly distributed lateral load normal to the wall surface. Two in-situ wall panels designated for testing will be analyzed in this study. The testing will be done by inflating an air bag positioned between the wall panel and a reaction frame consisting of metal reinforced plywood board.

Analytical models and techniques were developed to predict the initial crack load and the ultimate strength. The first cracking analysis is based on linear elastic finite element stress analysis. With the estimated material properties and appropriate failure criteria, the analytical model is verified with experimental results from published literature. A parametric study was performed on several parameters suspected to influence the initial cracking strength of the wall panel. These parameters include modulus of elasticity, Poisson's ratio, modulus of rupture, and boundary conditions.

The ultimate strength prediction is based on yield line analysis with arching action of the infill confined in a steel frame. It also includes the infill strength and stiffness orthotropies in the analysis. The technique is used to examine various parameters thought to affect the ultimate load capacity of the wall panel. The parameters investigated include compressive strength, modulus of elasticity, face shell thickness and frame rigidity.

The boundary interfaces of the panel, modeled with various support conditions, were investigated. The boundary condition is a major factor in determining the initial cracking and ultimate loads. The effect of the air bag size was also examined for the strength in two limit states. It does not affect the capacity of the wall panel significantly.

TABLE OF CONTENTS

CHAPTER		PAGE
1.	**INTRODUCTION**	1
1.1	Introduction	1
	1.1.1 General	1
	1.1.2 Testing Program	2
1.2	Scope	9
1.3	Description of Wall Panels	13
	1.3.1 Panel in Building 9207	13
	1.3.2 Panel in Building 9212	13
2.	**FIRST CRACKING STRENGTH CALCULATIONS**	18
2.1	Introduction	18
2.2	Analytical Methods	18
2.3	Material Properties	22
	2.3.1 Modulus of Elasticity	22
	2.3.2 Poisson's Ratio	24
	2.3.3 Modulus of Rupture	26
2.4	Failure Criteria	29
2.5	Model Verification	46
2.6	Building 9207	53
	2.6.1 Wall Panel	53
	2.6.2 Analysis of Results	57
	2.6.3 Natural Frequencies	60
	2.6.4 Parametric Study	62
2.7	Building 9212	70
	2.7.1 Wall Panel	70
	2.7.2 Analysis of Results	72
2.8	Summary of Results	72

3. ULTIMATE STRENGTH CALCULATIONS 76

3.1 Introduction 76

3.2 Analytical Methods 76

3.3 Predicted Ultimate Load Behavior 87

3.3.1 Description of Failure Modes 88
3.3.2 Effects of Failure Modes 91
3.3.3 Estimated Ultimate Strength 101
3.3.4 In-plane Membrane Action 108
3.3.5 Parametric Study 113

3.4 Summary of Results 136

4. CONCLUSIONS AND RECOMMENDATIONS 137

4.1 Conclusions 137

4.2 Recommendations 140

REFERENCES 142

VITA 146

LIST OF TABLES

TABLE		PAGE
2.3.1	Modulus of Elasticity in Compression Normal to the Bed Joint from Johnson and Matthys	23
2.3.2	Modulus of Elasticity in Ultimate Transverse Strength from Johnson and Matthys	25
2.3.3	Estimated Values of Poisson's Ratio	27
2.3.4	Modulus of Rupture from Plummer, and Johnson and Matthys	28
2.4.1	The Differences in Predictions Using Equation 2.4.2	31
2.5.1	Material Properties for Concrete Block Wall from Seah	49
2.5.2	Cracking Load Predictions for Fixed Base and Simply supported Base for Seah's Panels	50
2.5.3	First Panel Cracking Predictions for Seah's Panels	52
2.6.1	Estimated Material Properties for Hollow Clay Tile Walls in Buildings 9207 and 9212	56
2.6.2	Cracking Load Predictions for Fixed Base and Simply Supported Base in Building 9207	58
2.6.3	First Panel Cracking Predictions for Building 9207	59
2.6.4	Predicted and Measured Frequencies on Panel in Building 9207	61
2.6.5	Predicted Frequencies and First Panel Cracking Load Using Elastic Spring Models	63
2.6.6	Effects of Poisson's Ratio on First Panel Cracking in Building 9207	66
2.6.7	Effects of Modulus of Elasticity on First Panel Cracking in Building 9207	67

2.6.8 Effects of Modulus of Rupture on First Panel Cracking in Building 9207 69

2.6.9 Effects of Air Bag Sizes in Building 9207 71

2.7.1 First Panel Cracking Predictions for Building 9212 74

3.3.1 Effects of Coefficient of Friction on Ultimate Pressure for Panel 28'x12' in Building 9207 97

3.3.2 Effects of Coefficient of Friction on Ultimate Pressure for Panel 24'x20.5' in Building 9212 .. 103

3.3.3 Effects of Top Beam Sizes on Ultimate Pressure for Panel 28'x12' in Building 9207 128

3.3.4 Effects of Bottom Beam Sizes on Ultimate Pressure for Panel 28'x12' in Building 9207 129

3.3.5 Effects of Top Beam Sizes on Ultimate Pressure for Panel 24'x20.5' in Building 9212..... 131

3.3.6 Effects of Bottom Beam Sizes on Ultimate Pressure for Panel 24'x20.5' in Building 9212 .. 132

LIST OF FIGURES

FIGURE		PAGE
1.1.1	Typical Hollow Clay Tile Wall Framing	4
1.1.2	12-inch Hollow Clay Tile Wall Framing in Building 9212	5
1.1.3	Air Bag Test Setup with Reaction Frame	7
1.1.4	Self-equilibrating Air Bag Test Setup	8
1.1.5	Instrumentation Locations of Hollow Clay Tile Wall	10
1.1.6	Instrumentation Locations on Steel Frame	11
1.1.7	Instrumentation Locations on Steel Frame with Crackmeters	12
1.3.1	Typical 8-inch Tile Wall Panel in Building 9207.	14
1.3.2	Typical 12-inch Tile Wall Panel in Building 9212	15
1.3.3	Sketch of the 12-inch Tile Construction	17
2.2.1	Eight Nodes Shell Element	20
2.2.2	Beam in Space Element	20
2.4.1	Direct and Torsional Moment	33
2.4.2	Direct and Torsional Resisting Moment	34
2.4.3	Failure Surface of Tensile Strength	36
2.4.4	Various Mode of Failures	39
2.4.5	Debonding along Bed Joint	40
2.4.6	Vertical Splitting Through Head Joints and Units	41
2.4.7	Debonding along Bed and Head Joints	42
2.4.8	Splitting Through Mortar and Units	44
2.4.9	Failure Envelope in Biaxial Stress Fields	45

2.5.1 Finite Element Mesh Configuration for Specimen WE2, WE4, WE6, and WE8 47

2.6.1 Finite Element Mesh Configuration for Wall Panel in Building 9207 54

2.6.2 Different Boundary Conditions for Wall Panel in Building 9207 and 9212 55

2.6.3 Elastic Spring Model with Spring Stiffness of 50 kips per Foot for Panel in Building 9207 64

2.7.1 Finite Element Mesh Configuration for Wall Panel in Building 9212 73

3.2.1 Loading System for Test Wall Panel 79

3.2.2 Predicted Failure Load Versus Aspect Ratio for Simple Support at All Edges Wall Panel 82

3.2.3 Uniformly Loaded Slab with All Edges Fixed against Out-of-Plane Translation 86

3.3.1 Modes of Failures 90

3.3.2 Pressure Versus zy, Mode A of Panel 28'x12' (Assuming zx1 = zx2 = 0.3) 93

3.3.3 Pressure Versus zx1 and zx2, Mode A of Panel 28'x12' (Assuming zy = 0.62) 94

3.3.4 Pressure Versus zx1 and zx2, Mode C of Panel 28'x12' (Assuming zy = 0.5) 95

3.3.5 Pressure Versus zy, Mode C of Panel 28'x12' (Assuming zx1 = zx2 = 0.38) 96

3.3.6 Pressure Versus zy, Mode D of Panel 28'x12' 98

3.3.7 Pressure Versus zy, Mode A of Panel 24'x20.5' (Assuming zx1 = zx2 = 0.25) 99

3.3.8 Pressure Versus zx1 and zx2, Mode A of Panel 24'x20.5' (Assuming zy = 0.5) 100

3.3.9 Pressure Versus zy, Mode B of Panel 24'x20.5' (Assuming zx = 0.5) 102

3.3.10 Pressure Versus zy, Mode D of Panel 24'x20.5' .. 104

3.3.11 Pressure Versus Deflection for Wall Panel in Building 9207 105

3.3.12 Pressure Versus Deflection for Wall Panel in Building 9212 107

3.3.13 In-Plane Compressive Forces in Panel 28'x12' ... 109

3.3.14 In-Plane Compressive Forces in Panel 28'x12', Top Beam = W36 x 300 111

3.3.15 In-Plane Compressive Forces in Panel 24'x20.5' . 112

3.3.16 In-Plane Compressive Forces in Panel 24'x20.5', Top Beam = W36 x 300 114

3.3.17 In-Plane Compressive Forces in Panel 24'x20.5', Column Sizes = W36 x 300's 115

3.3.18 Pressure Versus Compressive strength 117

3.3.19 Pressure Versus Deflection with Various Compressive Strength for Panel 28'x12' 118

3.3.20 Pressure Versus Deflection with Various Compressive Strength for Panel 24'x20.5' 119

3.3.21 Pressure Versus Modulus of Elasticity 121

3.3.22 Pressure Versus Deflection with Various Modulus of Elasticity for Panel 28'x12' 122

3.3.23 Pressure Versus Deflection with Various Modulus of Elasticity for Panel 24'x20.5' 123

3.3.24 Pressure Versus Deflection with Various Face Shell Thickness for Panel 28'x12' 125

3.3.25 Pressure Versus Deflection with Various Face Shell Thickness for Panel 24'x20.5' 126

3.3.26 Pressure Versus Deflection with Various Column Sizes for Panel 28'x12' 130

3.3.27 Pressure Versus Deflection with Various Column Sizes for Panel 24'x20.5' 133

3.3.28 Pressure Versus Deflection for Different Air Bag Sizes 135

CHAPTER 1

INTRODUCTION

1.1 INTRODUCTION

1.1.1 General

The recent United States Department of Energy "General Design Criteria", DOE 6430.1A (1987) mandated that several existing building structures in the Y-12 plant in Oak Ridge, Tennessee, be evaluated for seismic structural integrity. Typical construction for most of the buildings consists of simply connected steel frames with unreinforced hollow clay tile infilled walls. As most of the structures were constructed during the 1940's and early 1950's, there was no consideration of seismic events in the original design. The behavior of the existing unreinforced masonry infilled walls under earthquake forces is of primary importance in earthquake-prone areas.

Two of the primary forces generated by an earthquake are in-plane and out-of-plane forces, depending upon the direction of the ground motion with respect to the wall. Axley (1979) in his study of infilled frame systems recommended that the

evaluation of an infilled frame structure should consider not just in-plane, but also out-of-plane behavior. While the in-plane aspect is vital in the survival of the structure, this thesis focuses on the out-of-plane behavior of the panel subjected to lateral earthquake forces. Two types of out-of-plane forces are generated in a wall panel. The first is imposed boundary displacements due to in-plane displacements of perpendicular panels. The second is inertial forces due to the mass of the panel. The inertial out-of-plane forces may be simulated by a uniform lateral loading normal to the surface of the infilled wall panel. The analysis herein focuses on the inertial forces developed in the wall and capacity of the wall to resist these forces.

1.1.2 Testing Program

Uncertainties exist with both the material properties and the behavior of the infilled frames. Therefore, an experimental testing program was proposed (Bennett and Burdette, 1989). This testing program would supplement and run parallel to analytical analysis of the wall panels.

The first portion of the program addressed various aspects of the existing conditions of the structural components, such as the construction of the hollow clay tile walls, the beam to column and column to baseplate connections, and the wall to frame interface conditions. The construction

of the clay tile wall panels are described later in Section 1.3. Typical girder to column connections are clip angles riveted to the respective webs and flanges. Typical column to baseplate connections are rivets to back to back angles on the column webs. The horizontal leg of the angle is anchor bolted through the baseplate and into the floor slab. Both types of connections are capable of resisting only minimum moments.

There are at least two types of wall to frame interfaces. One is where the infill frames into the column flanges, shown in Figure 1.1.1. The other is where the infill surrounds the column to form a pilaster at the column, Figure 1.1.2. A third type of interface would be where the infill frames against the column flange. Preliminary inspection shows that the wall to frame interfaces exhibit highly variable conditions, in some cases being very good and other cases being very poor (Fricke, 1990).

The second portion of the program is a test plan that varies from material property tests to full scale in-situ tests. Since the infill is the primary resisting structure, material property tests are necessary to determine the constitutive models to be used in the numerical analysis. Some of the material property tests include prism compression tests, flexural bond strength tests (both normal and parallel to the bed joint), splitting tensile strength of masonry units, and in-situ normal stress and shear tests.

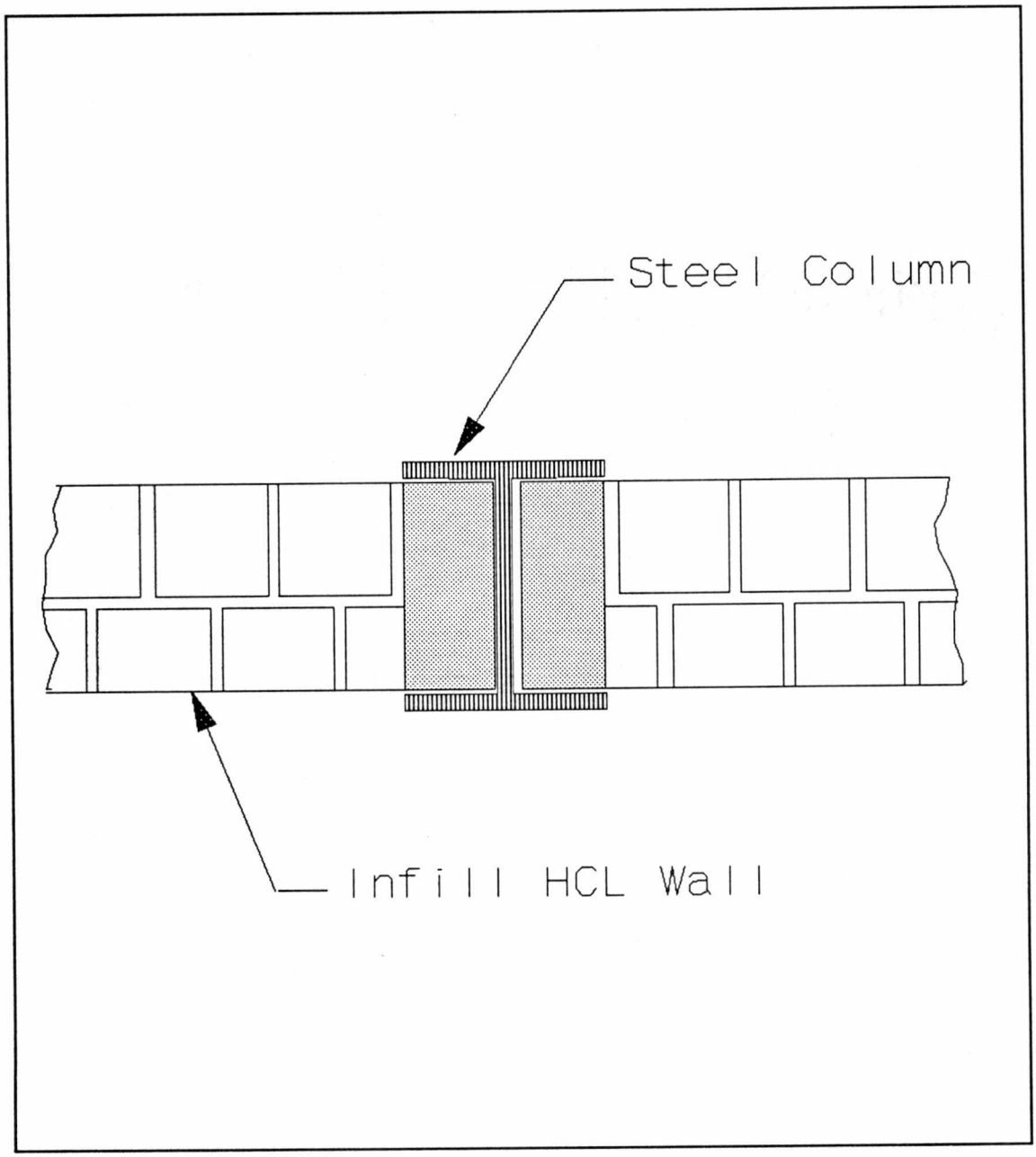


Figure 1.1.1 Typical Hollow Clay Tile Wall Framing

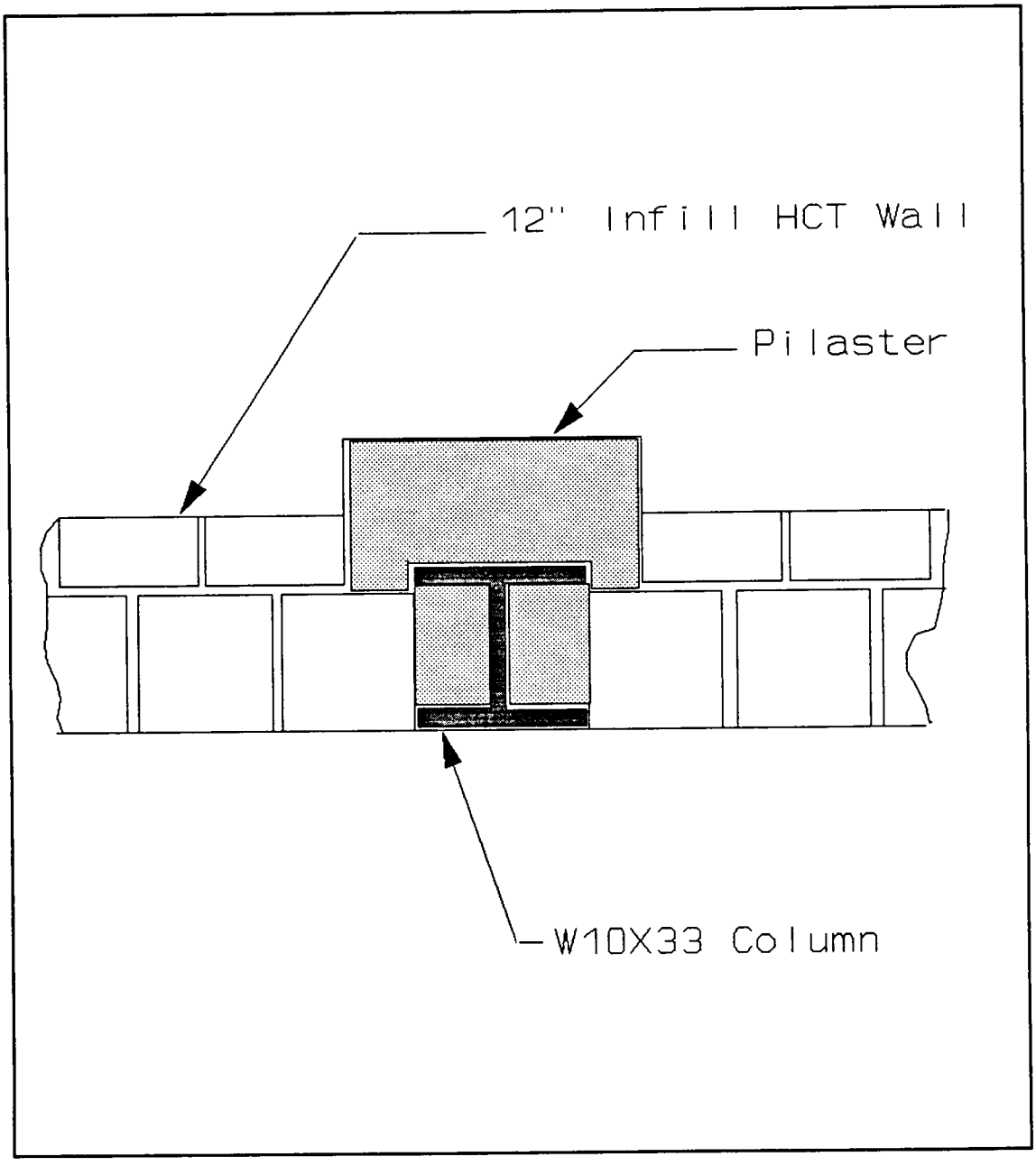


Figure 1.1.2 12-inch Hollow Clay Tile Wall Framing in Building 9212

Full scale infilled structure tests are proposed to observe the actual behaviors of the infilled wall panel as a structural system. The loading conditions of the full scale tests are in-plane and out-of-plane. The in-plane infilled frame static tests are conducted to observe the actual infilled wall panel conditions under static loads. Load reversal will be used to develop a hysteresis loop. To determine the bending strength and to observe the boundary conditions, cracking patterns and failure modes, out-of-plane full scale static air bag tests to failure are proposed. Two in-situ tests will be performed on existing walls. A detailed test plan has been developed by the Martin Marietta Energy Systems Committee for Structural Testing of Hollow Clay Tile Wall Panels (1990).

The air bag test set-up is illustrated in Figure 1.1.3. The full size air bag being one foot shorter in length than the actual length of the panel because of the offset of the flanges of the columns by one-half foot on each side. The uniform loading is provided by inflating an air bag sandwiched between the test wall panel and the supporting frame. An alternate self-equilibrating air bag set-up is shown in Figure 1.1.4. The self-equalibrating system has an advantage of minimum space occupation. It is believed that both set-ups will perform equally well under careful supervision. Air bag pressure is monitored using a pressure transducer and a

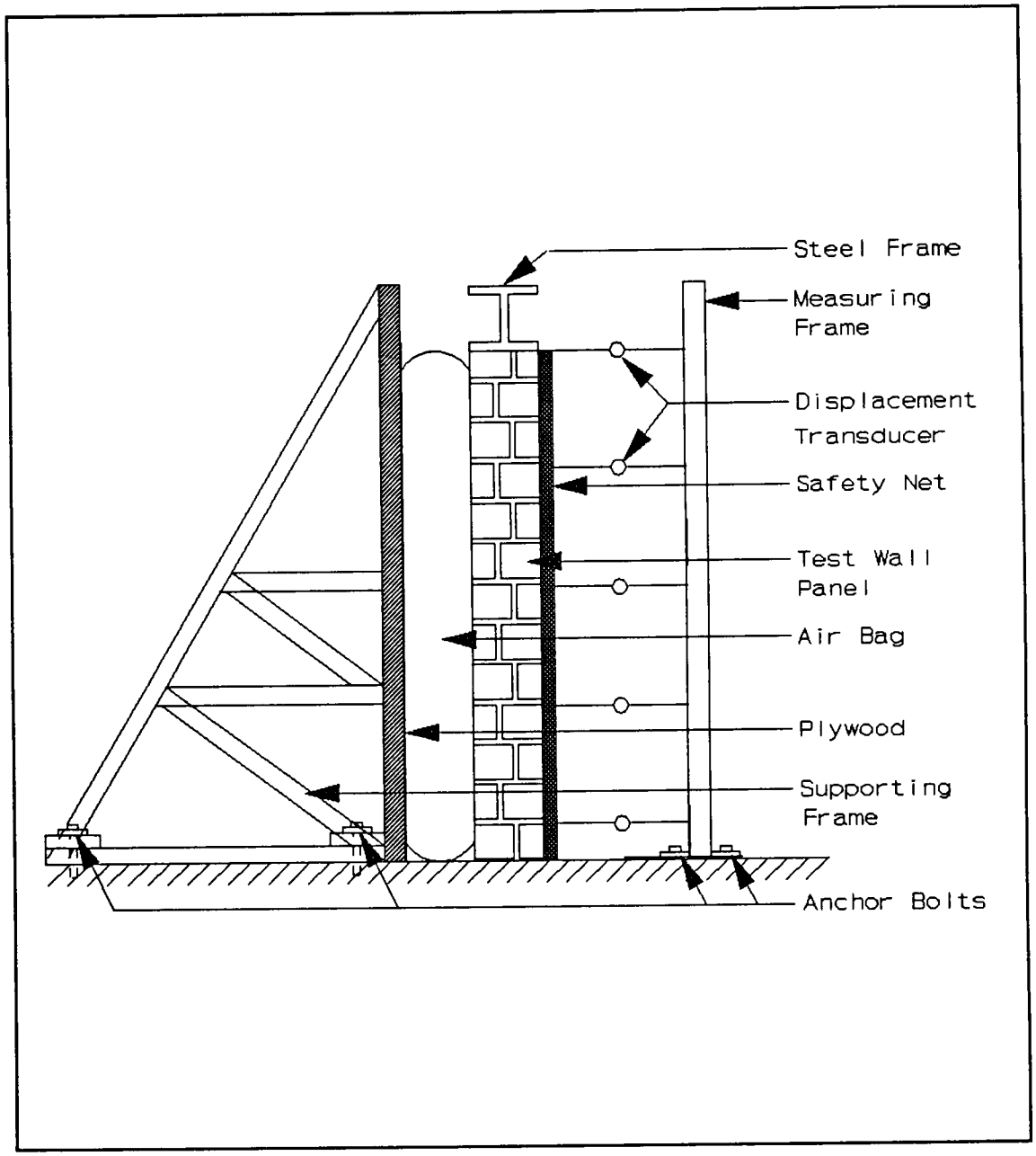


Figure 1.1.3 Air Bag Test Setup with Reaction Frame (After Bennett and Burdette, 1989)

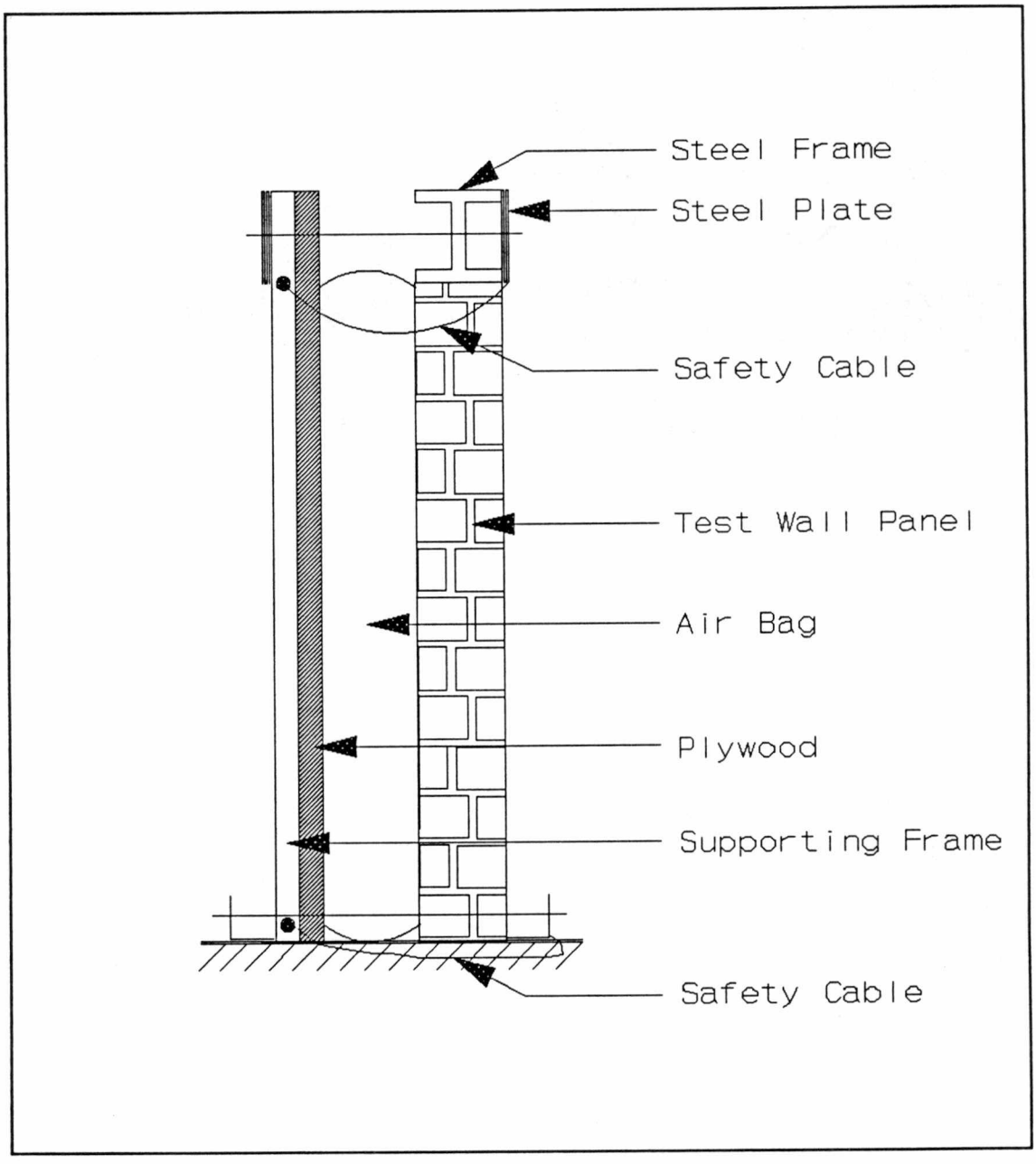


Figure 1.1.4 Self-equilibrating Air Bag Test Setup (After Bennett and Burdette, 1989)

regulator increases or decreases the pressure at a slow rate. The test wall panel will be loaded to imminent failure to determine the ultimate capacity and the failure mode. The deformations are monitored using Linear Variable Displacement Transducers (LVDT's) throughout the test. Movement between the frame and the infills is monitored by crackmeters. The instrumentation locations are shown in Figures 1.1.5, 1.1.6 and 1.1.7.

1.2 SCOPE

The scope of this research is to predict the strengths of two existing wall panels in two limit states, the first panel cracking and the ultimate load capacity. Analyses will be conducted using numerical techniques to estimate the maximum loads in the two limit states, to determine the parameters affecting the strength of the wall panels, and to study the variation of capacity in different failure modes.

The results of this study are a preliminary analysis of the wall panels with estimated material properties in anticipation of out-of-plane lateral load testing. The details of the wall panels to be tested are described in the following section.

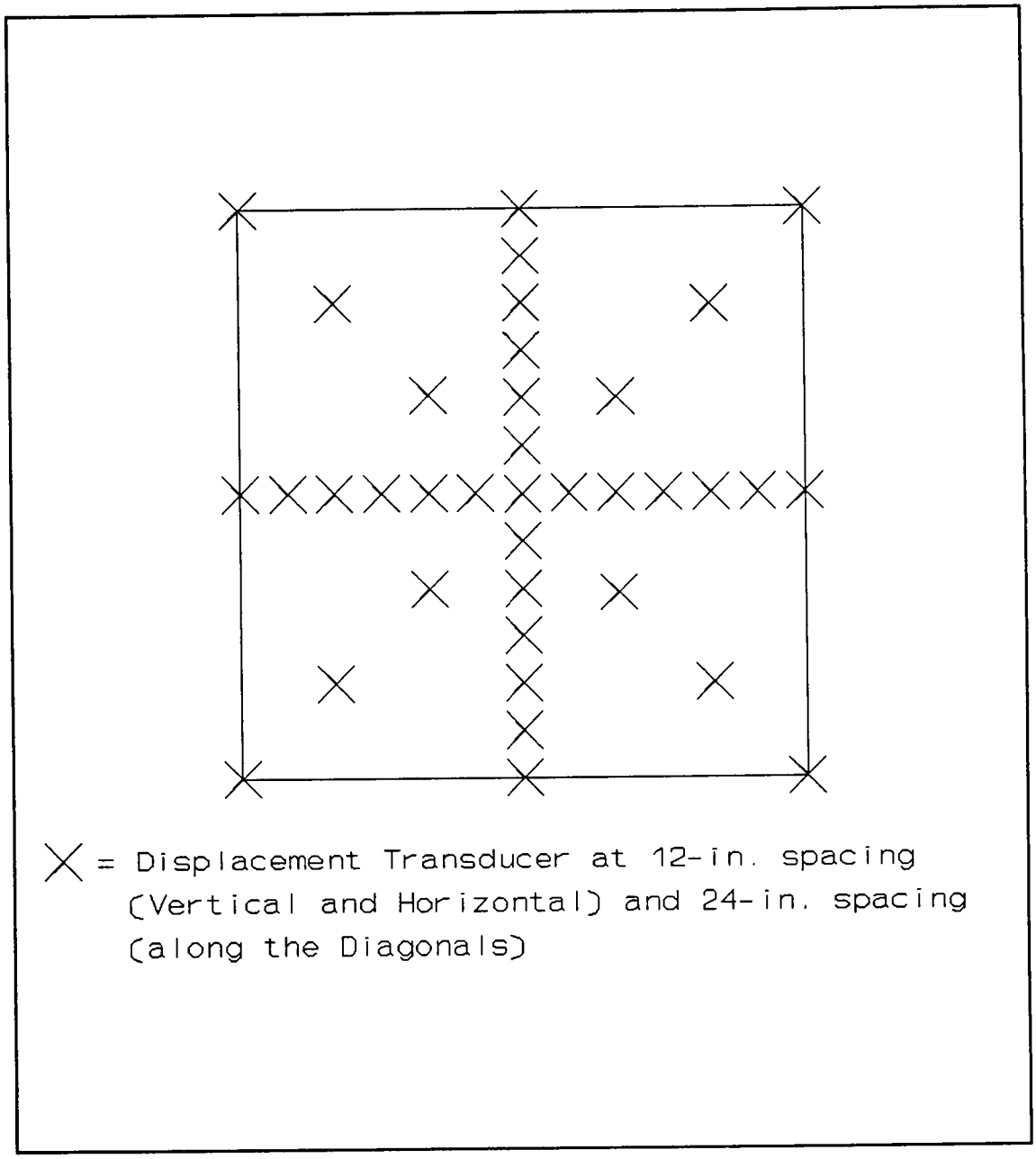


Figure 1.1.5 Instrumentation Locations of Hollow Clay Tile Wall (After Bennett and Burdette, 1989)

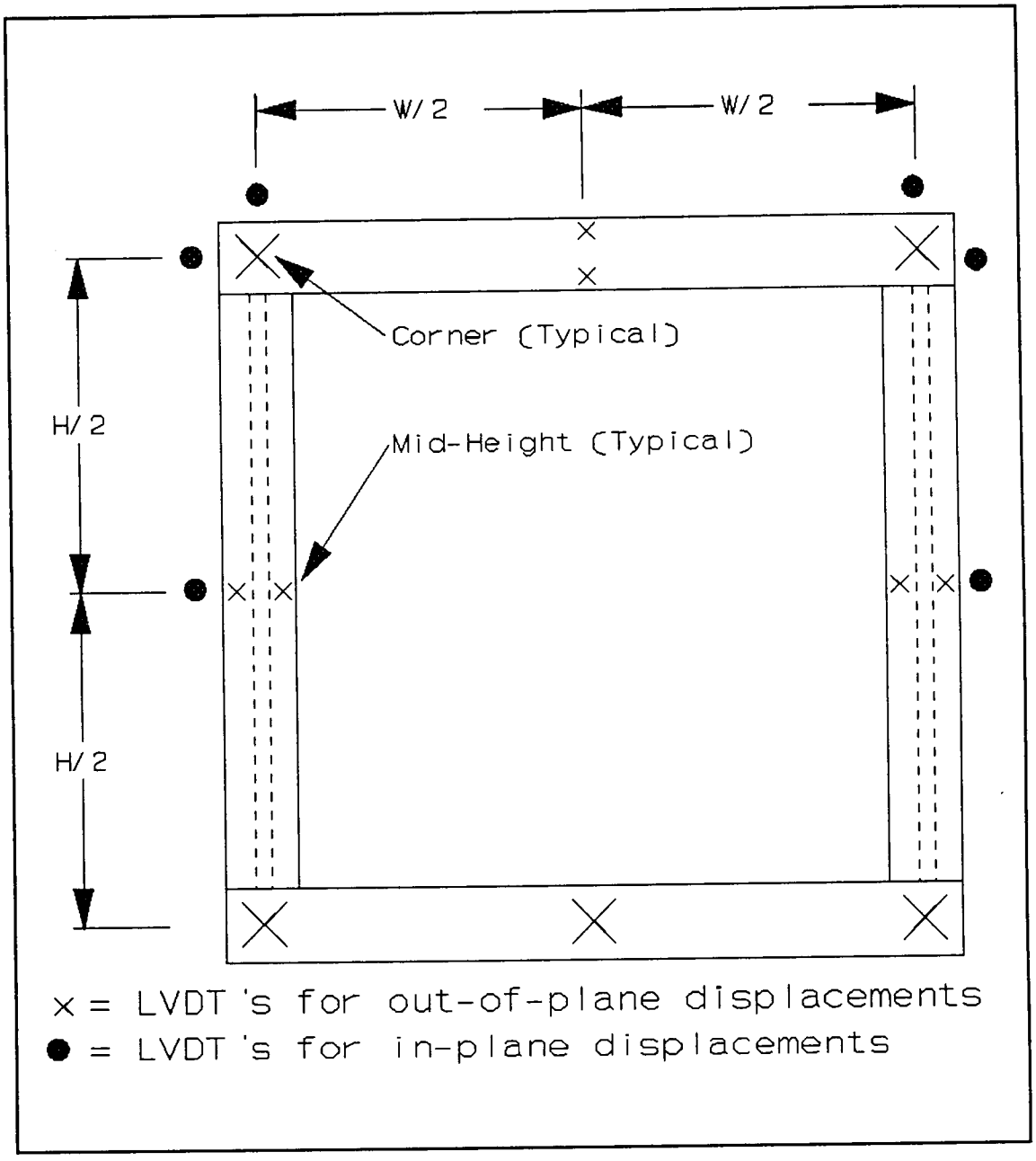


Figure 1.1.6 Instrumentation Locations on Steel Frame (After Bennett and Burdette, 1989)

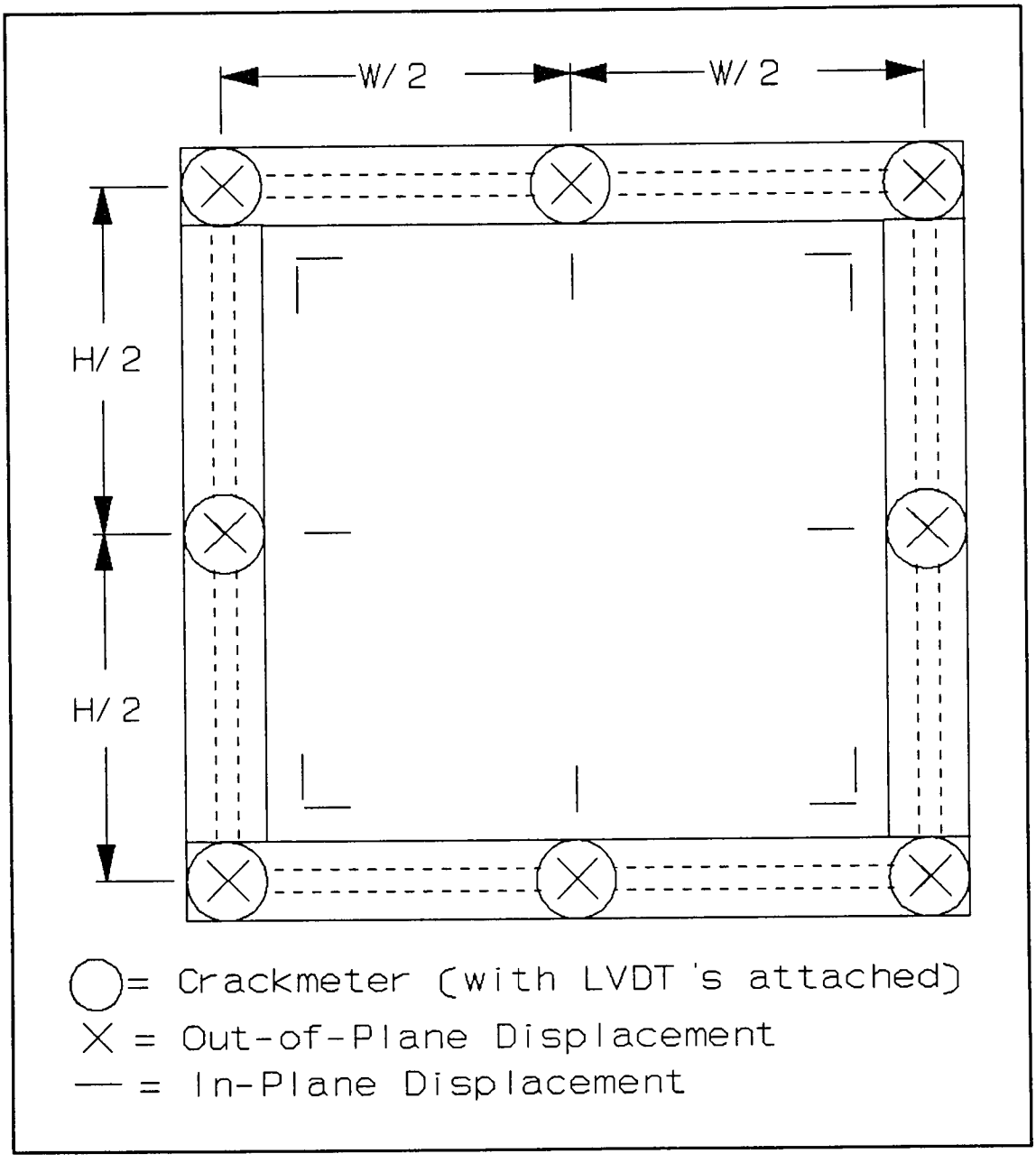


Figure 1.1.7 Instrumentation locations on Steel Frame with Crackmeters (After Bennett and Burdette, 1989)

1.3 DESCRIPTION OF WALL PANELS

Both 8-inch and 12-inch hollow clay tile wall panels are present in the Y-12 Plant in Oak Ridge. Building 9207 primarily has 12-inch exterior walls and 8-inch interior wall panels. Building 9212 has 12-inch exterior wall panels. The face shell thickness of the masonry units is approximately 0.75 inch, and the bed joint is about one-half inch thick.

1.3.1 Panel in Building 9207

The wall panel in Building 9207 designated for testing is a first floor panel 28 ft. in length and 12 ft. in height. The panel consists of 8-inch hollow clay tile units. The wall panel is constructed with running bond and the cores run horizontally. It is enclosed by a steel frame of a W30x116 girder and W14x176 columns, as shown in Figure 1.3.1. The hollow clay tile frames between the column flanges.

1.3.2 Panel in Building 9212

The wall panel designated for testing in Building 9212 is shown in Figure 1.3.2, and is 24 ft. in length and 20.5 ft. in height. The 12-inch wall panel is constructed from 8-inch and 4-inch hollow clay tile units. The cores run horizontally similar to those in Building 9207. The wall panel is built in running bond with 8-inch and 4-inch units placed alternating

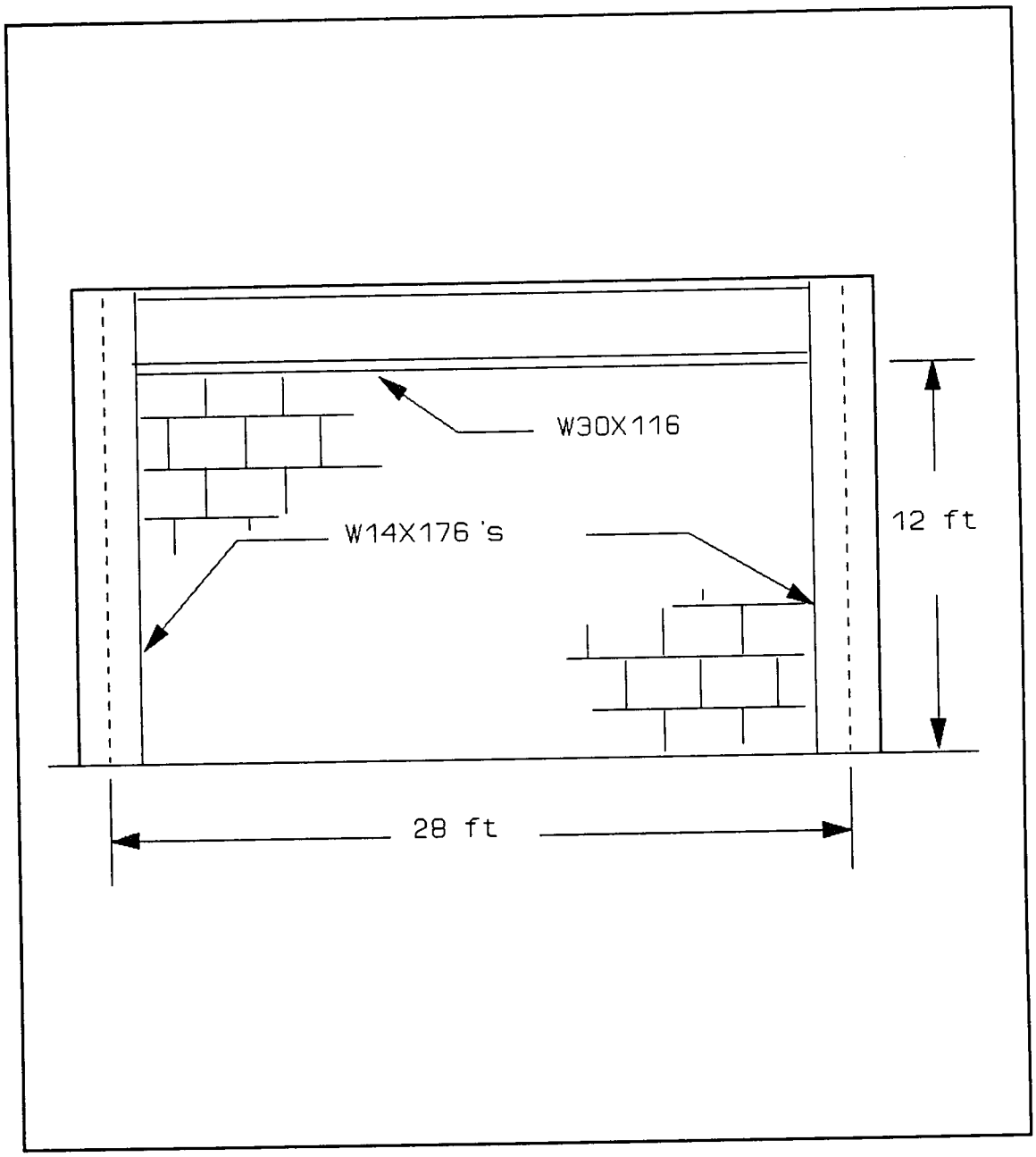


Figure 1.3.1 Typical 8-inch Tile Wall Panel in Building 9207

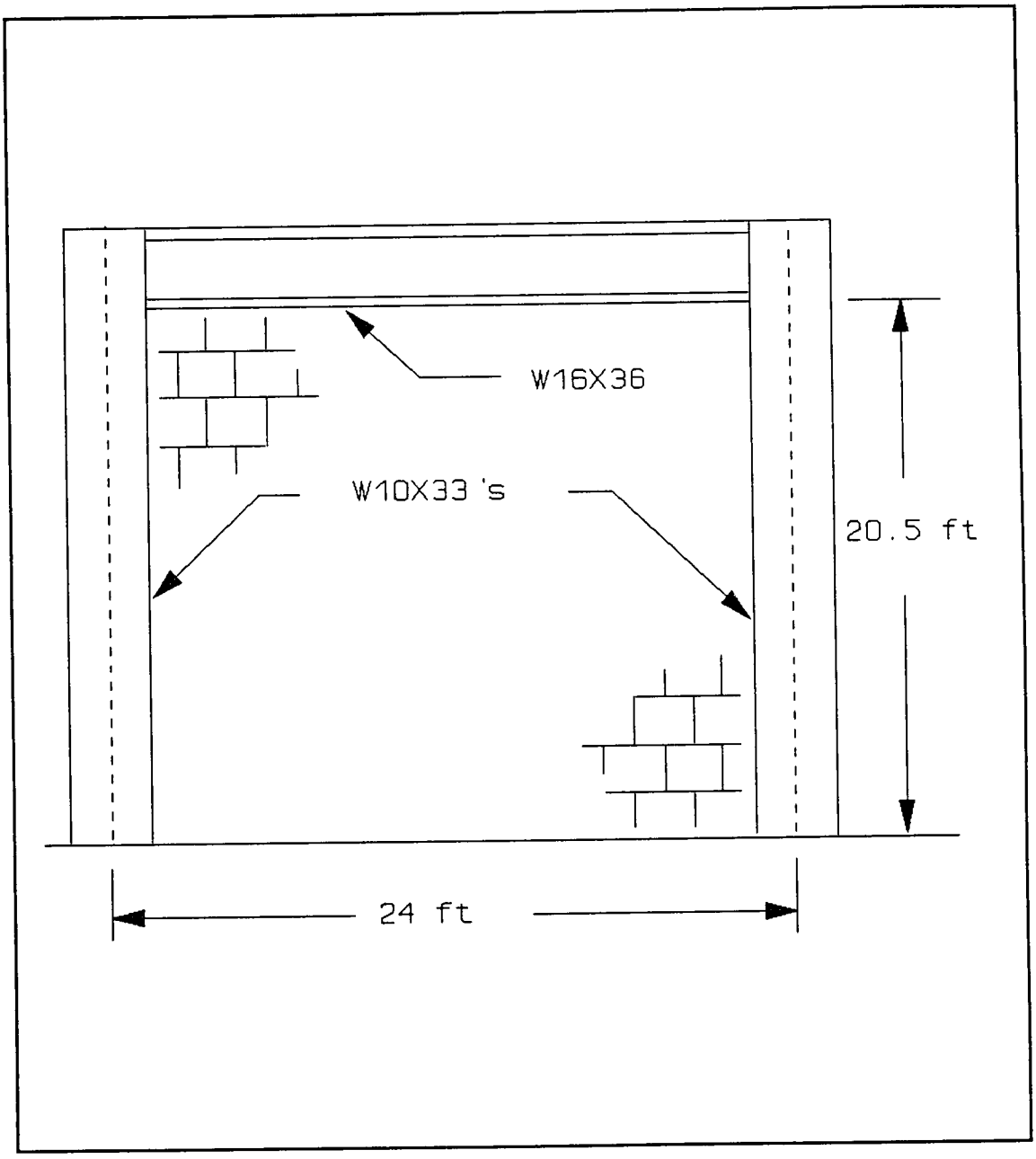


Figure 1.3.2 Typical 12-inch Tile Wall Panel in Building 9212

each other and staggered throughout the courses as shown in Figure 1.3.3. The panel is enclosed in a steel frame with a W16x36 top beam and W10x33 columns. The hollow clay tile is actually offset slightly from the centroid of the steel frame, as shown in Figure 1.1.2. This feature is not, however, considered in the subsequent analysis.

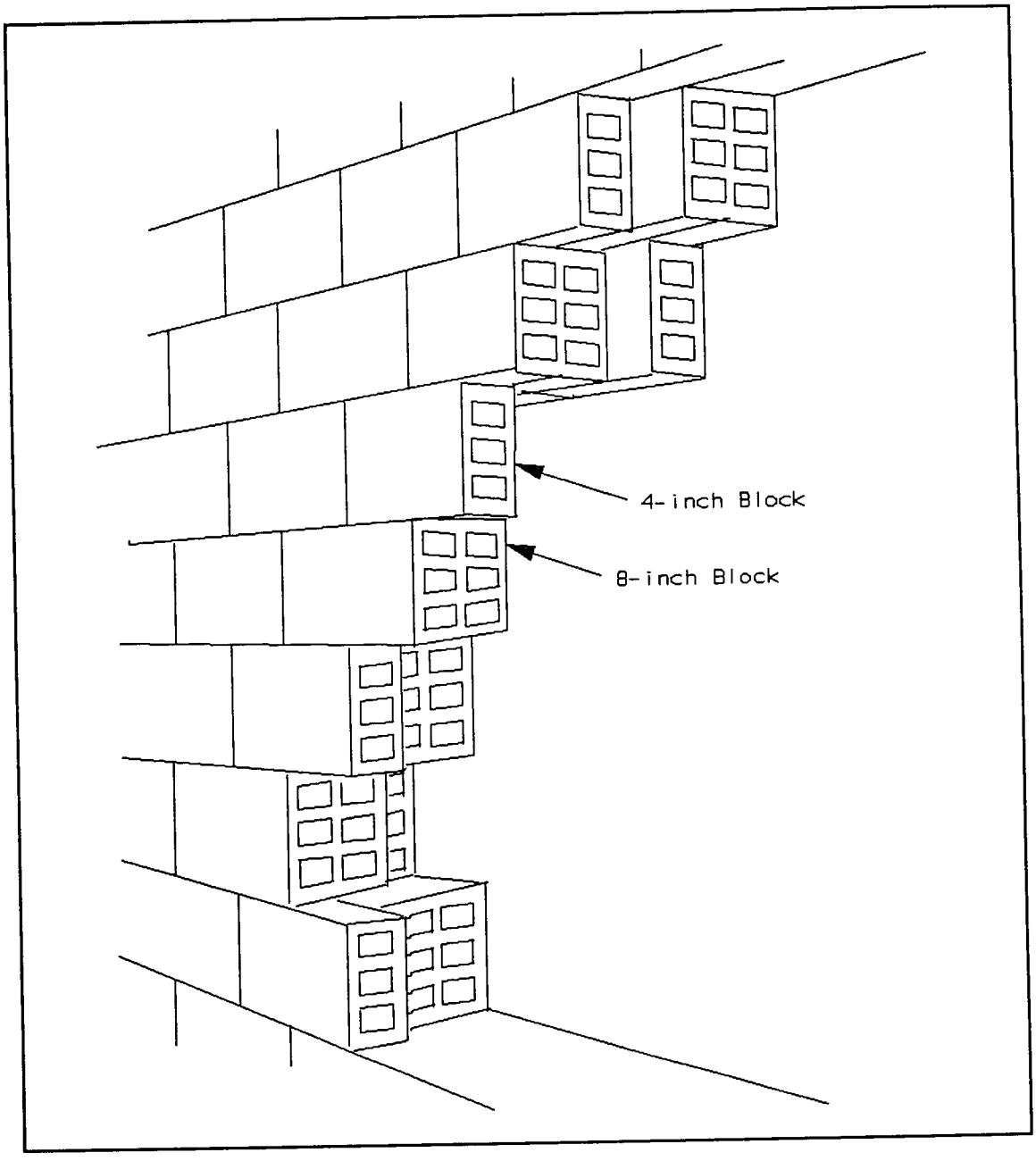


Figure 1.3.3 Sketch of the 12-inch Tile Construction

CHAPTER 2

FIRST CRACKING STRENGTH CALCULATIONS

2.1 INTRODUCTION

This chapter performs several tasks. First is to design an analytical model that includes the relevant material properties and appropriate failure criteria. Second is to verify the validity of the model with the experimental results from the published literature. Third is to use the validated model to predict the approximate first cracking load of the hollow clay tile masonry wall panel subjected to uniformly distributed load, normal to the surface of the wall. The final task is to investigate parametrically various factors that influence the first cracking capacity of the wall panel.

2.2 ANALYTICAL METHODS

Adopting an appropriate analytical method to predict the flexural strength of a masonry wall has been difficult. With the advancement of numerical computations and computer

technologies, the finite element method has been a convenient tool in structural analysis. Despite the complication in modeling the boundary conditions of the actual wall panels, and the non-homogeneous nature of masonry, the analytical results prove useful.

Haseltine et al (1977) found that in the working range, a brick wall behaves elastically. It was suggested that isotropic elastic plate methods are adequate in spite of the fact that brickwork is orthotropic. One or the other direction of bending governs the result regardless of the reserve strength in the other direction. Essawy and Drysdale (1987) later concluded that the elastic plate theory assuming isotropic properties produced fairly good predictions for the first cracking loads for the whole range of aspect ratios of panels supported on four sides. Seah (1988) also indicated that masonry behaved linearly prior to first cracking.

The ABAQUS finite element program (1989) is used for the present study to predict the first cracking loads for the masonry infilled walls. An orthotropic linear elastic material model was used even though results from isotropic material models have proven satisfactory. Shell elements used for the infilled masonry include membrane and transverse shear deformation. The element consists of eight peripheral nodes as shown in Figure 2.2.1. Steel frames are modeled using beams in space elements such as shown in Figure 2.2.2. The

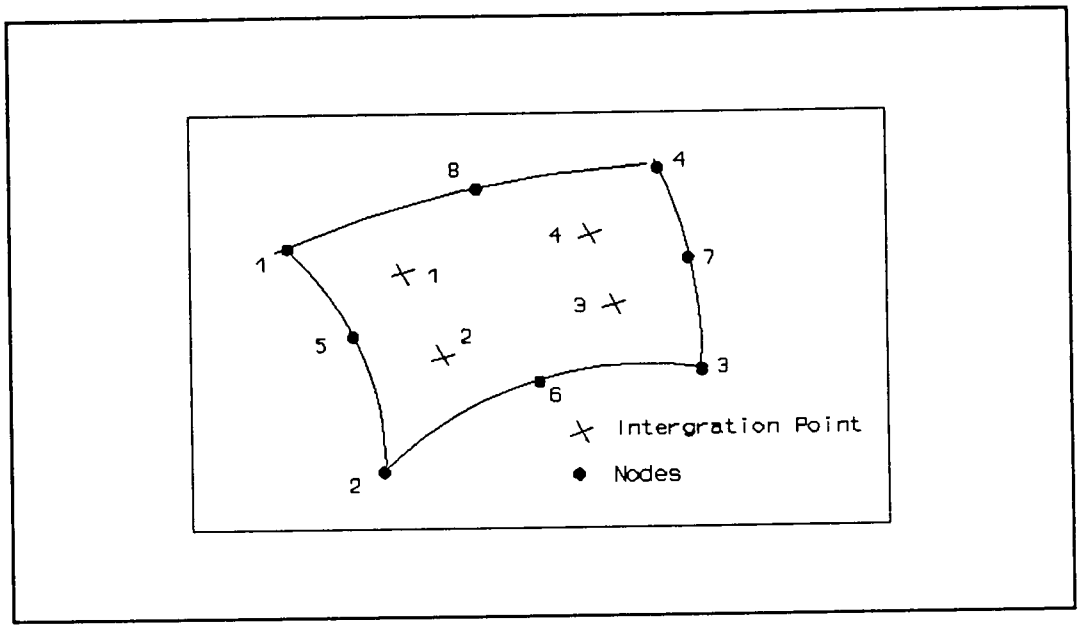


Figure 2.2.1 Eight Nodes Shell Element

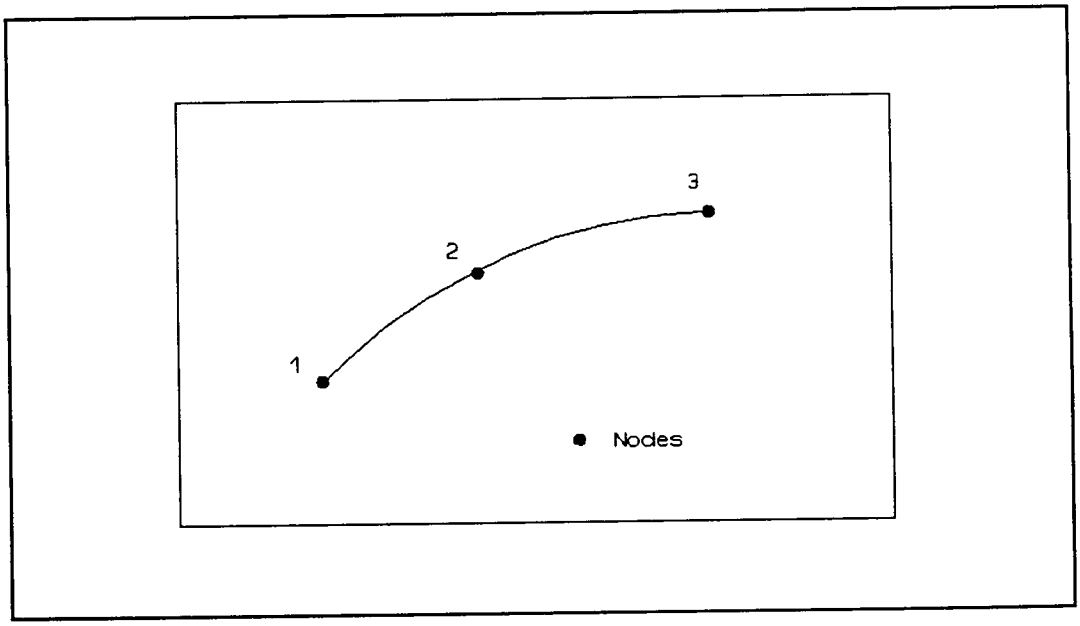


Figure 2.2.2 Beam in Space Element

gravity loading of wall panel is considered, but other superimposed normal load is not accounted.

ABAQUS gives stresses at extreme fibers. These include membrane stresses as shown below :

$$(S_x)_1 = (S_x)_{membrane} + \frac{6M_x}{h^2} \qquad [2.2.1]$$

Where h = *Thickness of plate.*
M_x = *Moment in x-direction.*
$(S_x)_1$ = *Stress on the face.*
$(S_x)_{membrane}$ = *Membrane Stress.*

The membrane stress will be the average of the stresses of the two faces.

$$(S_x)_{membrane} = \frac{(S_x)_1 + (S_x)_3}{2} \qquad [2.2.2]$$

Where $(S_x)_1$ = *Stress on one face.*
$(S_x)_3$ = *Stress on opposite face.*

The moment can be found from

$$M_x = [(S_x)_1 - (S_x)_{membrane}] \frac{h^2}{6}$$
$$= [(S_x)_1 - (S_x)_3] \frac{h^2}{12} \qquad [2.2.3]$$

This relation holds true for S_y and S_{xy} also.

2.3 MATERIAL PROPERTIES

There is a general lack of experimental information pertaining to the structural behavior and properties of hollow clay tile masonry walls. A parametric study on some of the parameters thought to affect the first cracking strength of the wall panel subjected to out-of-plane loading is performed in section 2.6. Johnson and Matthys (1973) tested a few series of hollow clay tile assemblages on 4-inch, 6-inch and 8-inch blocks. Some of the properties are listed below.

2.3.1 Modulus of Elasticity

(i) Loaded normal to bed joint.

The modulii of elasticity normal to the bed joints based on gross and net areas for various block sizes are tabulated in Table 2.3.1. The values exhibit no consistent trend. If the 4-inch data is neglected, then $E_{gross} \approx 0.75 \times 10^6$ psi. Plummer (1962) suggested an approximate equation of

$$E \approx 1000 f'_m \qquad [2.3.1]$$

Where f'_m = *Compressive Strength of the Assemblage (Psi).*

The assumed $E_{gross} = 0.75 \times 10^6$ psi implies a compressive strength of 750 psi.

TABLE 2.3.1

MODULUS OF ELASTICITY IN COMPRESSION NORMAL TO THE BED JOINT FROM JOHNSON AND MATTHYS (1973)

BLOCK SIZES	E_{gross} x 10^6 psi	E_{net} x 10^6 psi
4 - inch.	1.47	4.28
6 - inch.	0.76	3.06
8 - inch.	0.72	2.04

(ii) Loaded parallel to bed joint.

The modulii of elasticity normal and parallel to the bed joint based on net areas are tabulated in Table 2.3.2. By obtaining the ratio of modulus of elasticity parallel to bed joint to modulus of elasticity normal to bed joint, the results are 1.30 and 1.34 for 4-inch and 6-inch blocks respectively. Using the ratio as 1.33, the modulus of elasticity parallel to bed joint can be calculated as follows:

$$E = 1.33\,(0.75 \times 10^6\ Psi)$$
$$= 1.00 \times 10^6\ Psi$$

2.3.2 Poisson's Ratio

For an orthotropic linear elastic material, the various constitutive parameters may be related as follows (Weaver and Johnston, 1984).

$$\frac{1}{G_{xy}} \approx \frac{1+\nu_{yx}}{E_x} + \frac{1+\nu_{xy}}{E_y} \qquad [2.3.2]$$

$$\frac{E_y}{E_x} = \frac{\nu_{xy}}{\nu_{yx}} \qquad [2.3.3]$$

Where G_{xy} = *Shear Modulus.*
ν_{xy} = *Strain in the x-direction due to strain in the y-direction.*
ν_{yx} = *Strain in the y-direction due to strain in the x-direction.*

TABLE 2.3.2

MODULUS OF ELASTICITY IN ULTIMATE TRANSVERSE STRENGTH FROM JOHNSON AND MATTHYS (1973)

BLOCK SIZES	E_{net} x 10^6 psi	
	Normal to Bed Joint	Parallel to Bed Joint
4 - inch.	2.25	2.93
6 - inch.	1.16	1.55
8 - inch.	----	6.75

For the ratio of modulii of elasticity of 1.33 assumed in the present study,

$$\frac{1}{G_{xy}} = \frac{1+\nu_{yx}}{E_x} + \frac{1+1.33\ \nu_{yx}}{1.33\,E_x} \qquad [2.3.4]$$

Rewriting, Equation 2.3.4 becomes

$$\nu_{yx} = \frac{E_x}{2G_{xy}} - 0.875 \qquad [2.3.5]$$

Data from Johnson and Matthys (1973) based on gross areas and horizontal cells are used. The values of Poisson's ratios are calculated for various block sizes as shown on Table 2.3.3. The Poisson's ratios are impossible. A Poisson's ratio of 0.25 will be assumed, and the effects of this parameter are examined in section 2.6 through a parametric study.

2.3.3 Modulus of Rupture

Values of modulus of rupture are listed in Table 2.3.4. These are based on gross areas. The value of the 4-inch block from Johnson and Matthys (1973) is neglected since it is quite different from the remainder of the data. Averaging the remaining values gives the modulii of rupture normal and parallel to bed joints of 63 psi and 87 psi respectively.

TABLE 2.3.3

ESTIMATED VALUES OF POISSON'S RATIO

BLOCK SIZES	E_x	G_{xy}	ν_{yx}
4 - inch.	1.47	0.221	2.45
6 - inch.	0.76	0.133	1.98
8 - inch.	0.72	0.105	2.55

TABLE 2.3.4

MODULUS OF RUPTURE FROM PLUMMER (1962) AND JOHNSON AND MATTHYS (1973)

REFERENCES	NORMAL TO BED JOINT (Psi)	PARALLEL TO BED JOINT (Psi)
Plummer (1962)	51	---
Plummer (1962)	42	---
Plummer (1962)	98	---
Plummer (1962)	64	---
Johnson and Matthys (4-inch.)	130	253
Johnson and Matthys (6-inch.)	64	94
Johnson and Matthys (8-inch.)	57	81

2.4 FAILURE CRITERIA

Failure is defined in this section as a crack forming in the masonry. Many researchers have proposed failure criteria for masonry panels or assemblages subjected to either in-plane or out-of-plane loadings. The existing failure criteria for masonry subjected to biaxial stress is rather broad. Some of the criteria are established using experimental results, others are based on isotropic material failure theories and on composite material failure theories.

Hendry (1973) used elastic theory calculations using finite element analysis to obtain the maximum tensile principal stress under out-of-plane loading. The attainment of the modulus of rupture at the point of maximum tensile principal stress was considered failure. This requires knowing the modulus of rupture at any angle with respect to the bed joint.

Thurlimann and Guggisberg (1988) investigated eight brick masonry panels to develop a failure criterion for laterally loaded masonry. The failure criterion was based on the bending moments in two directions at failure. An elliptical interaction relationship between the failure moments M_x and M_y, similar to that proposed by Baker (1979), was developed. The elliptical interaction failure criterion is as follows:

$$A \cdot (M_x^2+M_y^2+2M_{xy}^2) \pm B \cdot \left| (M_x+M_y)\sqrt{(M_x-M_y)^2+4M_{xy}^2} \right| - 2C = 0 \quad [2.4.1]$$

$A = (M_{xo}^2+M_{yo}^2)$
$B = (M_{xo}^2-M_{yo}^2)$
$C = (M_{xo}^2 \cdot M_{yo}^2)$

The positive sign is used for B if M_x is less than M_y and neg sign is used if M_x is greater than M_y in the above equation.

Where M_x = *Moment in x-direction.*
M_y = *Moment in y-direction.*
M_{xo} = *Failure moment with* $M_y = 0$.
M_{yo} = *Failure moment with* $M_x = 0$.
M_{xy} = *Twisting moment.*

The cracking occurred when Equation 2.4.1 is positive.

For the case of no twisting moments, Equation 2.4.1 reduces to

$$\left(\frac{M_x}{M_{xo}}\right)^2 + \left(\frac{M_y}{M_{yo}}\right)^2 - 1 = 0 \quad [2.4.2]$$

Using their test results, the differences of the predictions obtained using Equation 2.4.2 is tabulated in Table 2.4.1. Thus, failure is underpredicted by about 8%. In other words, capacity of the wall is about 8% greater than predicted.

The Normal Moment Method used by Fried et al (1988) is

TABLE 2.4.1

THE DIFFERENCES IN PREDICTIONS USING EQUATION 2.4.2 (THURLIMANN AND GUGGISBERG, 1988)

TEST SPEC.	M_x (KNm/m)	M_y (KNm/m)	M_{xo} (KNm/m)	M_{yo} (KNm/m)	RESULTS USING EQUATION 2.4.2
Q1	12.56	1.77	18.5	2.15	0.139
Q2	4.90	0.60	5.0	2.0	0.050
Q3	4.15	1.50	5.0	2.0	0.251
Q4	0.00	2.00	5.0	2.0	0.000
Q5	1.35	1.95	5.0	2.0	0.024
Q6	15.55	1.30	18.5	2.15	0.072
Q7	0.53	1.63	1.5	1.7	0.044
Q8	3.95	1.35	5.0	2.0	0.080
				AVERAGE	0.082

adapted from the failure criteria proposed by Kemp (1965) for reinforced concrete slabs. The direct and twisting moments for applied and resisting moments are shown in Figures 2.4.1 and 2.4.2 respectively. The equations for the normal moments are as follows:

$$M_n = M_x Cos^2\theta + M_y Sin^2\theta - M_{xy} Sin(2\theta) \qquad [2.4.3]$$

$$M_{nr} = M_{hr} Cos^2\theta + M_{vr} Sin^2\theta \qquad [2.4.4]$$

Where M_n = *Normal applied moment.*
M_{nr} = *Normal resisting moment.*
M_x, M_y, M_{xy} = *Applied moments acting on the element.*
M_{hr}, M_{vr} = *Resisting moments of the element.*

When the normal applied moment is equal to the normal resisting moment, failure in the element of masonry is assumed to occur through a plane inclined at an angle to the vertical. Note that in the absence of membrane stresses, the normal moment method is identical to the stepped mode failure criteria proposed by Gazzola et al (1985).

Gazzola et al (1985) tested 25 wallettes and 92 prisms constructed with bed joints at different angles from the direction of bending to develop a failure criterion for concrete block masonry subjected to out-of-plane bending. Three modes of failure were suggested : bond failure along the bed joint, bond failure in a stepped or toothed pattern

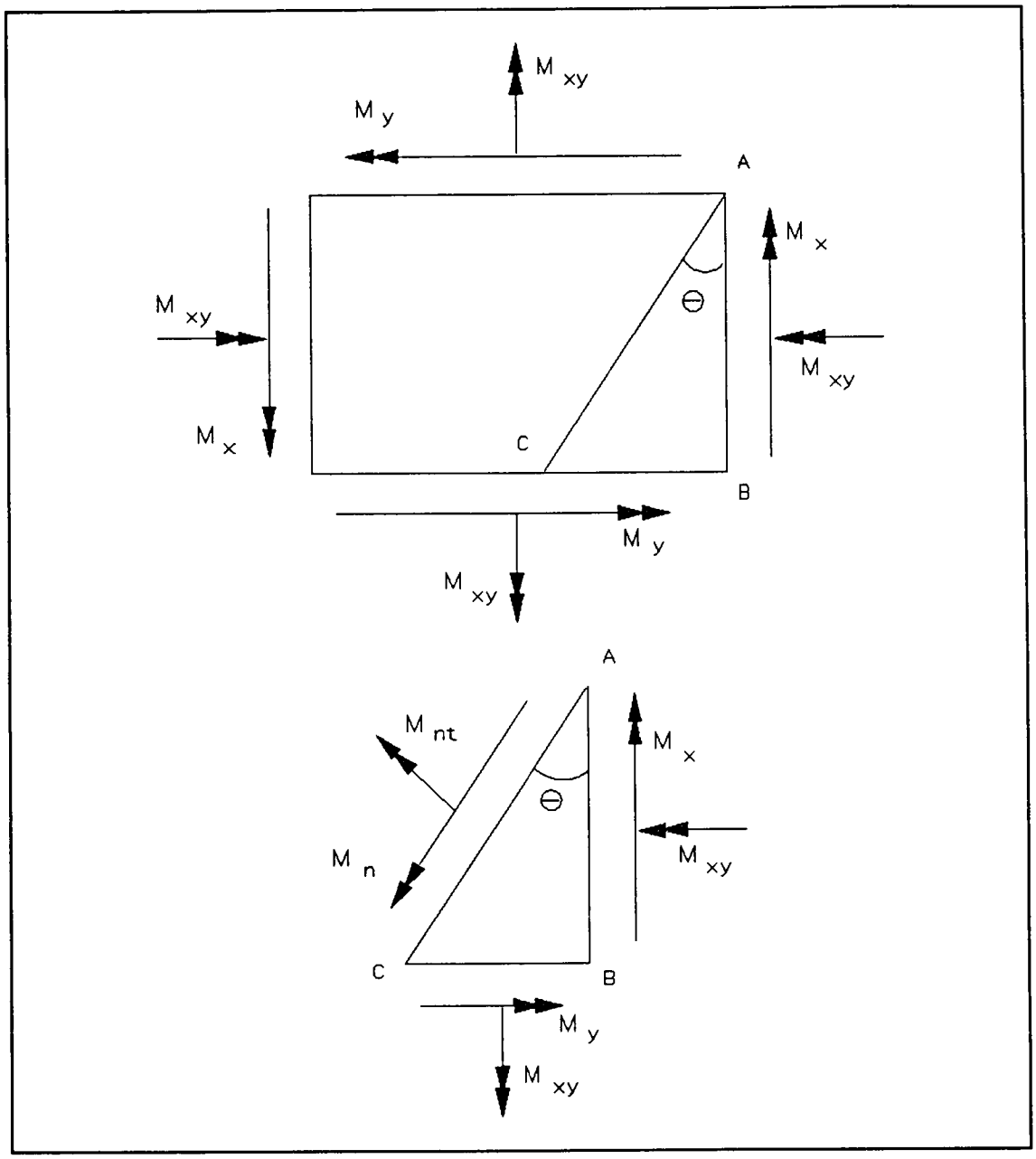


Figure 2.4.1 Direct and Torsional Moment

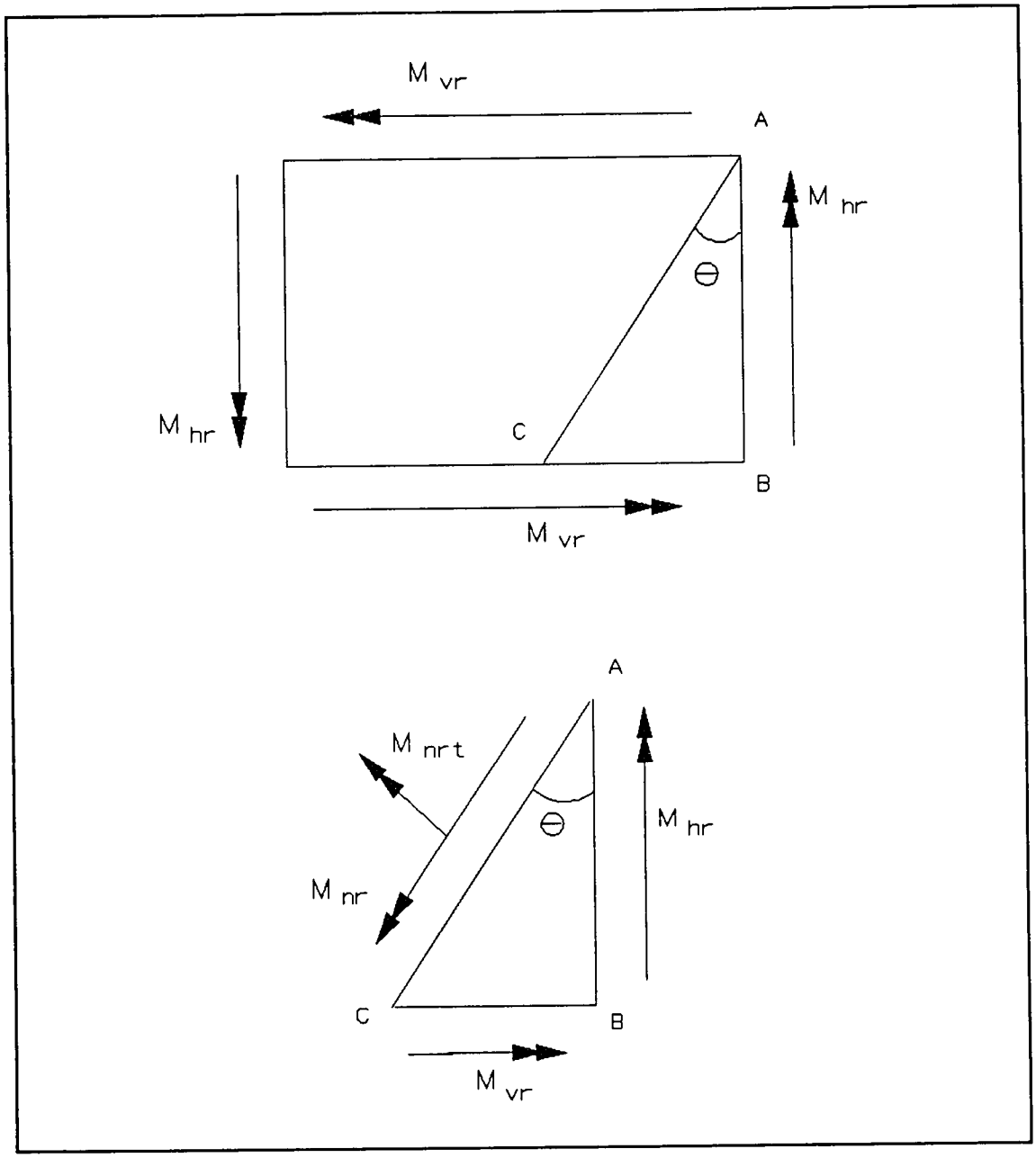


Figure 2.4.2 Direct and Torsional Resisting Moment

through a combination of bed and head joints, and failure along the head joints and splitting of the block units. It was believed that the mode of failure has a great influence on the degree of interaction for biaxial tension. Failure by tension parallel to the bed joint has little effect on the tensile strength normal or perpendicular to the bed joint. Likewise failure by tension perpendicular to the bed joints through failure of the head joints and splitting of the block units has little effect on the tensile strength parallel to the bed joints. Thus there is no interaction between the two, as shown in Figure 2.4.3 and failure occurs only if one of the tensile strengths is exceeded. A combined failure through head and bed joints will decrease the tensile strength to some extent due to interaction. It is proposed that the tensile strength at some angle θ to the bed joint be obtained as

$$S'_{t\theta} = S'_{tn} Sin^2\theta + S'_{tp} Cos^2\theta \qquad [2.4.5]$$

Where $S'_{t\theta}$ = *Tensile strength at* θ° *to the bed joint.*
S'_{tn} = *Tensile strength normal to bed joint.*
S'_{tp} = *Tensile strength parallel to bed joint.*

This tensile strength interaction is shown in Figure 2.4.3. The suggested failure criterion was used with the finite element analysis to predict first cracking loads of

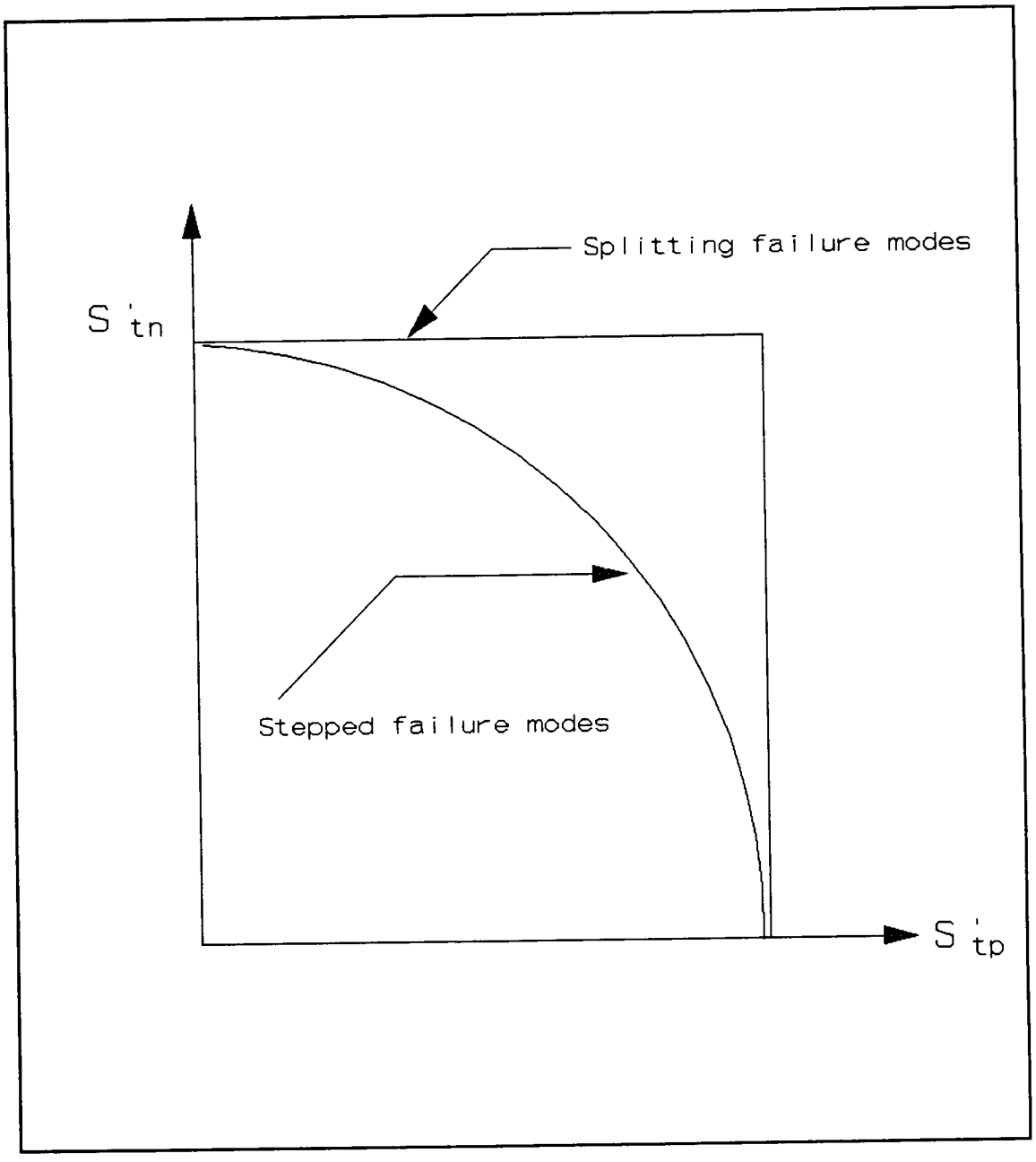


Figure 2.4.3 Failure Surface of Tensile Strength (After Gazzola et al, 1985)

experimental panels. The ratio of predicted to experimental results ranged from 0.70 to 1.20.

Hamid and Drysdale (1981) in the in-plane loading analysis, stated that the mortar joints in masonry are relatively weak compared to masonry units. Therefore the bed joint and head joint directions are the critical planes where failure is likely to occur. The masonry also can be treated as a laminated composite material because the mortar bed joints divide the media into layers of equal thickness. The failure criterion used was based on the shear failure along either the bed joints or the head joints and tension failure in the block and mortar.

Drysdale and Hamid (1984) in their earlier works for in-plane loading, developed tension failure criteria for unreinforced concrete masonry and proposed two possible failure modes. One of the modes is tension failure by cracking passing through head joints and face shells. The other is combined shear-tension failure by stepped cracking at the block-mortar interfaces. The mode of failure is governed by the block's strength and geometric characteristics such as aspect ratio and the net-to-gross area ratio in orthogonal directions.

Essawy and Drysdale (1986) later proposed a macroscopic failure criterion incorporating the anisotropic and composite nature of masonry, possible transverse failure modes, various

possible units strengths and geometries, and the mortar bonding characteristics. The criterion also considered the interaction of the shear and normal stresses on mortar joints as a primary contributor to the interaction between strengths.

Four different failure modes under biaxial stress were suggested as shown in Figure 2.4.4 and the respective equations were developed as follows :

(i) Mode 1 (Figure 2.4.5)

-Debonding along bed joints.

$$S_n - S_{tbmo}(1-\frac{t_{np}}{S_{sbmo}}) = 0 \qquad [2.4.6]$$

(ii) Mode 2 (Figure 2.4.6)

-Debonding of head joints and splitting of block units in alternating courses.

$$\frac{1}{2}[S_{tbmo}(1-[\frac{1+2\frac{E_m}{G_b}}{1+\frac{E_m}{G_m}+\frac{E_m}{G_b}}]\frac{t_{np}}{S_{sbmo}})+S_{tbl}] - S_p = 0 \qquad [2.4.7]$$

(iii) Mode 3 (Figure 2.4.7)

-Debonding of a combination of head and bed joints in diagonally stepped or vertically toothed patterns. The former is mainly due to biaxial stresses and the latter is likely to

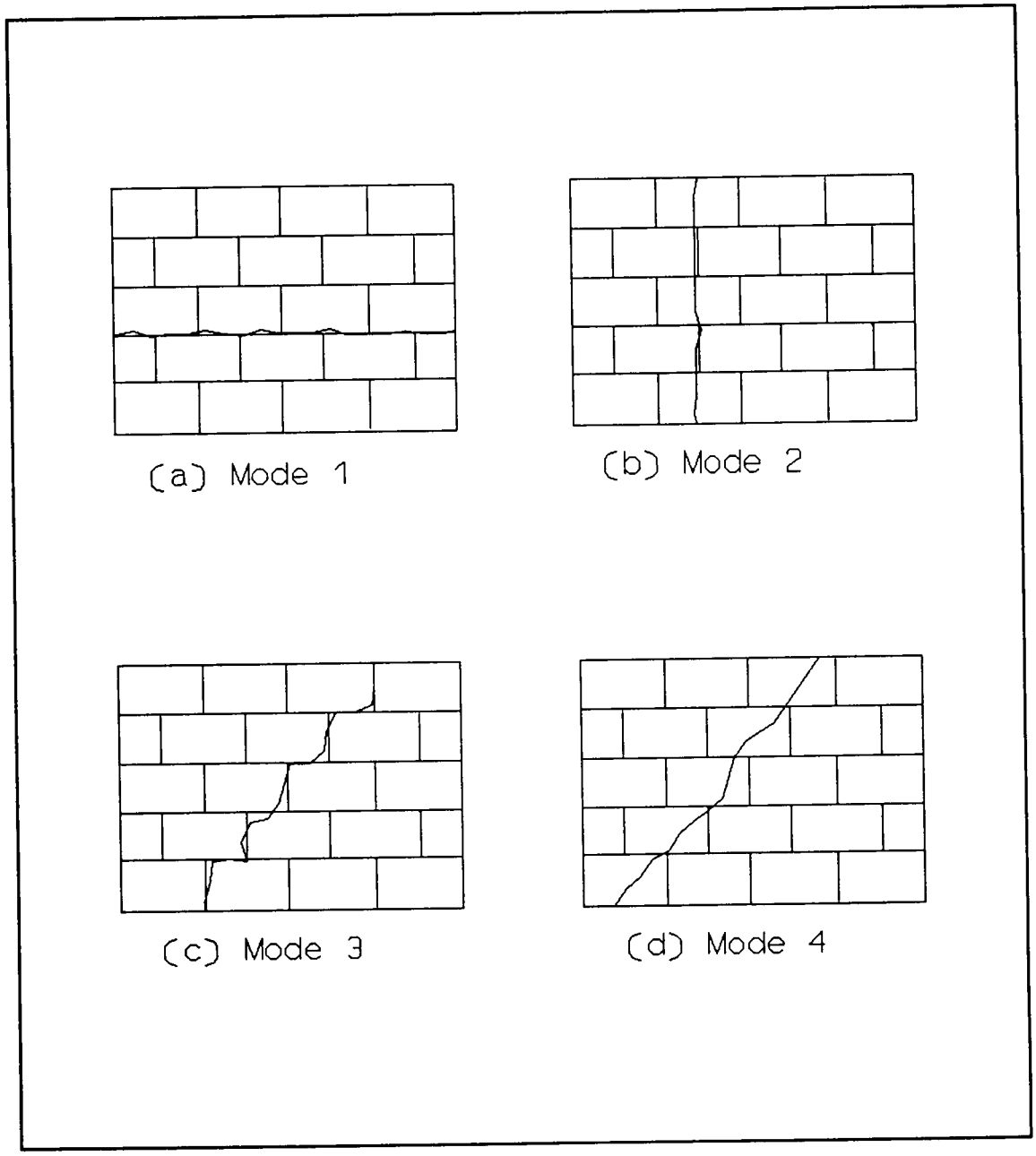


Figure 2.4.4 Various Mode of Failures

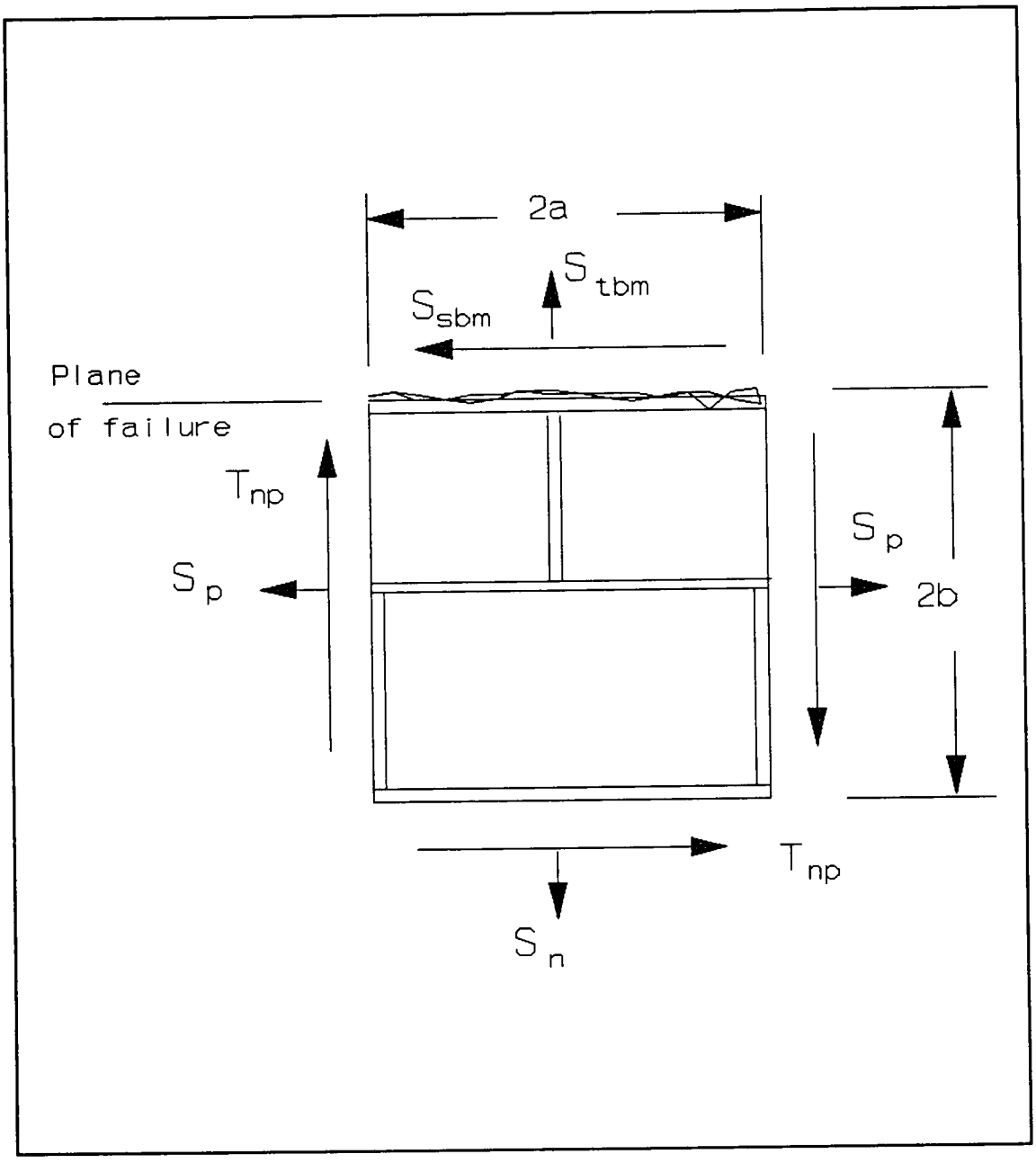


Figure 2.4.5 Debonding along Bed Joint (After Essawy et al, 1986)

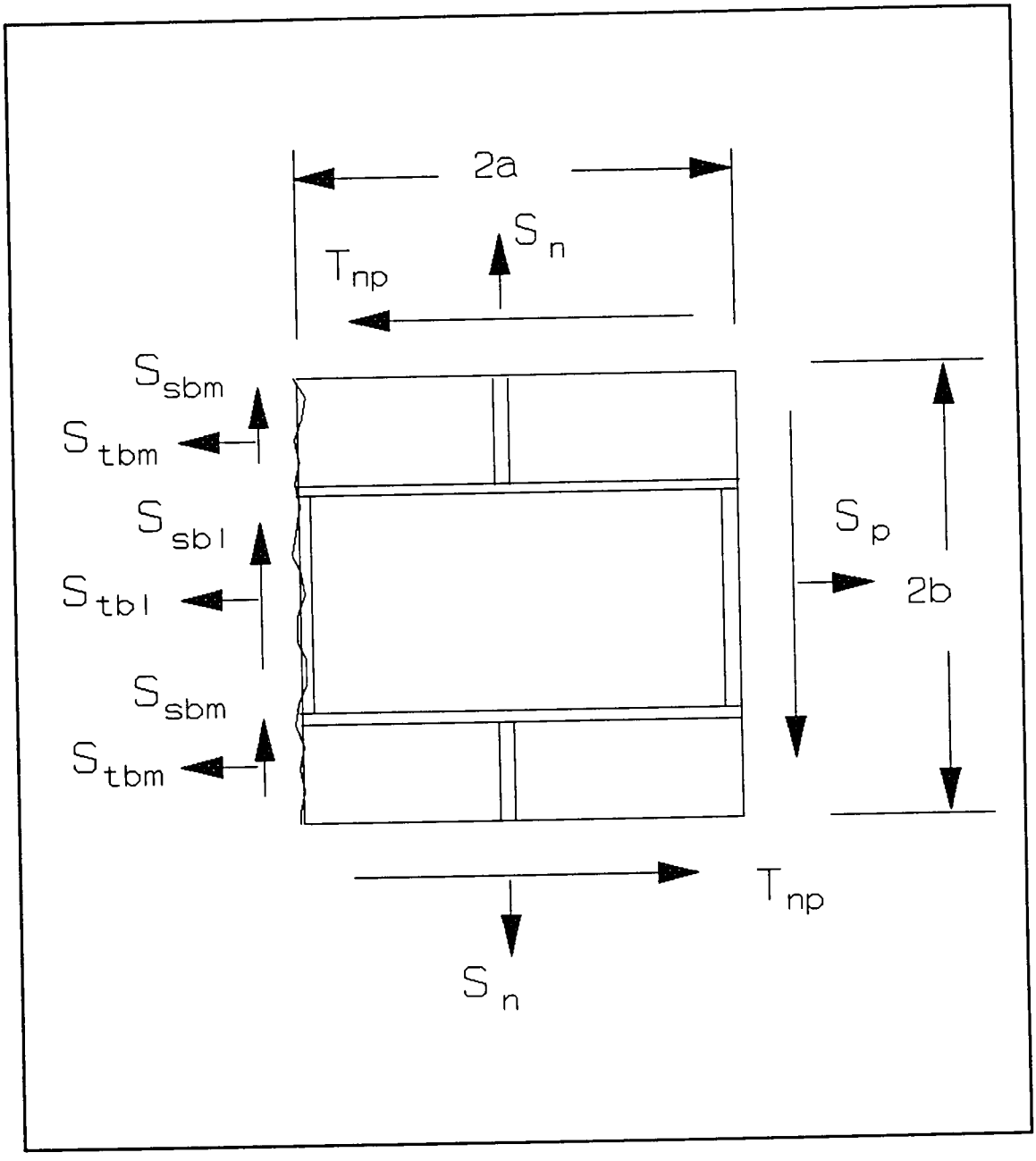


Figure 2.4.6 Vertical Splitting Through Head Joints and Units (After Essawy et al, 1986)

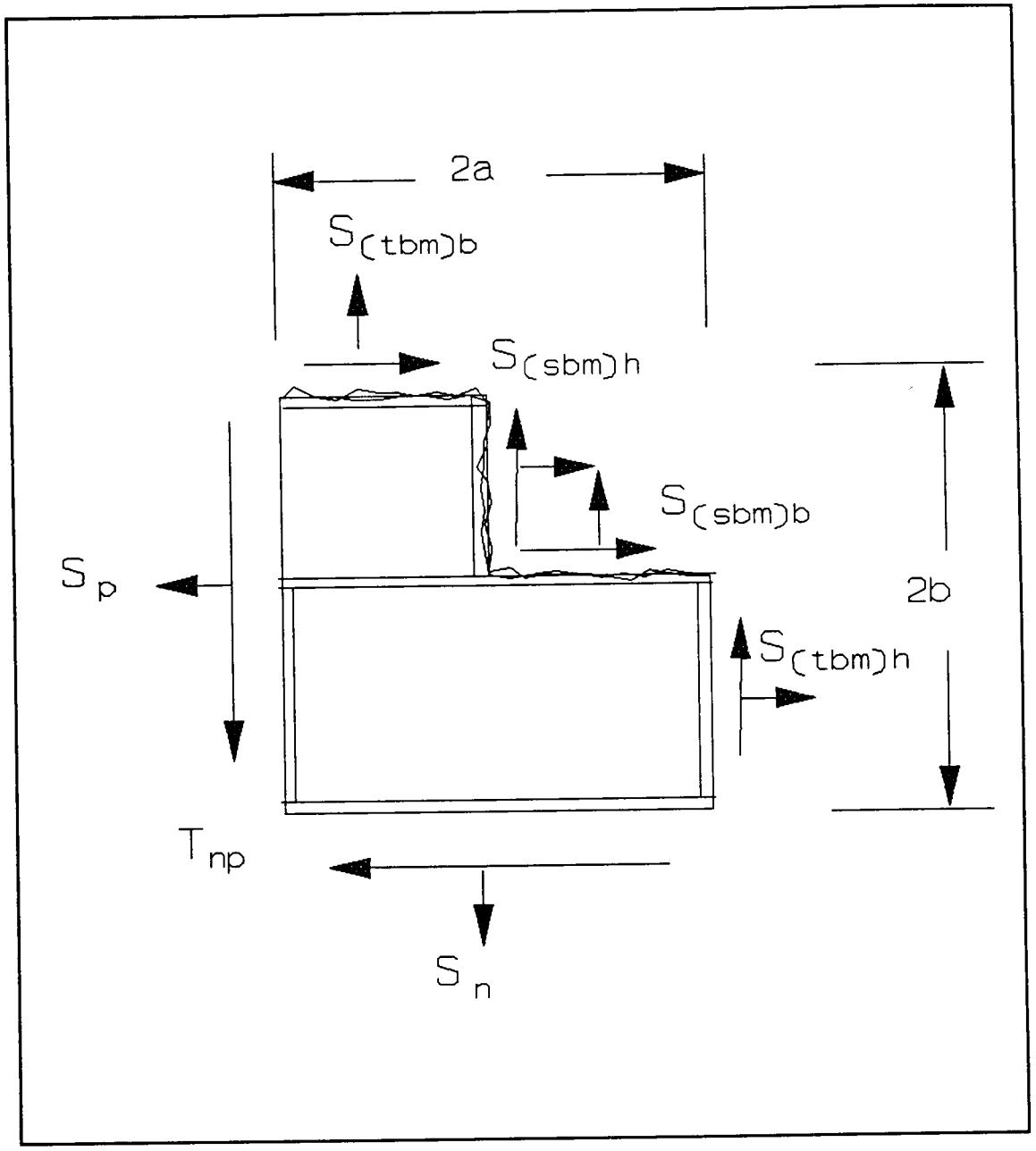


Figure 2.4.7 Debonding along Bed and Head Joints (After Essawy et al, 1986)

occur under tension parallel to the bed joints.

$$\frac{S_n}{((\frac{b}{a})S_{sbmo}+S_{tbmo})} + \frac{S_p}{((\frac{a}{b})S_{sbmo}+S_{tbmo})} + \frac{t_{np}}{(S_{sbmo}+(\frac{a}{b})S_{tbmo})} + \frac{t_{np}}{(S_{sbmo}+(\frac{b}{a})S_{tbmo})} - 1 = 0 \qquad [2.4.8]$$

(iv) Mode 4 (Figure 2.4.8)

-Splitting through the block units. For the practical range of values of most masonry, other modes are predominant.

$$(\frac{t_{np}}{S_{tbl}})^2 - (1-\frac{S_n}{S_{tbl}})(1-\frac{S_p}{S_{tbl}}) = 0 \qquad [2.4.9]$$

Where E_m = *Modulus of elasticity of mortar joint.*
G_m, G_b = *Shear modulus of mortar joint and block units respectively.*
$2a, b$ = *Nominal unit length and unit height respectively*
S_n, S_p = *Stresses at the extreme fibers of the assemblage normal and parallel to the bed joint respectively*
t_{np} = *Shear stress.*
S_{sbmo}, S_{tbmo} = *Pure shear and pure tensile bond strength of the mortar joints.*
S_{tbl} = *Tensile strength of masonry units.*

By combining the different failure modes described above, a failure envelope can be constructed such as shown in Figure 2.4.9. Both the strength and the failure mode can be

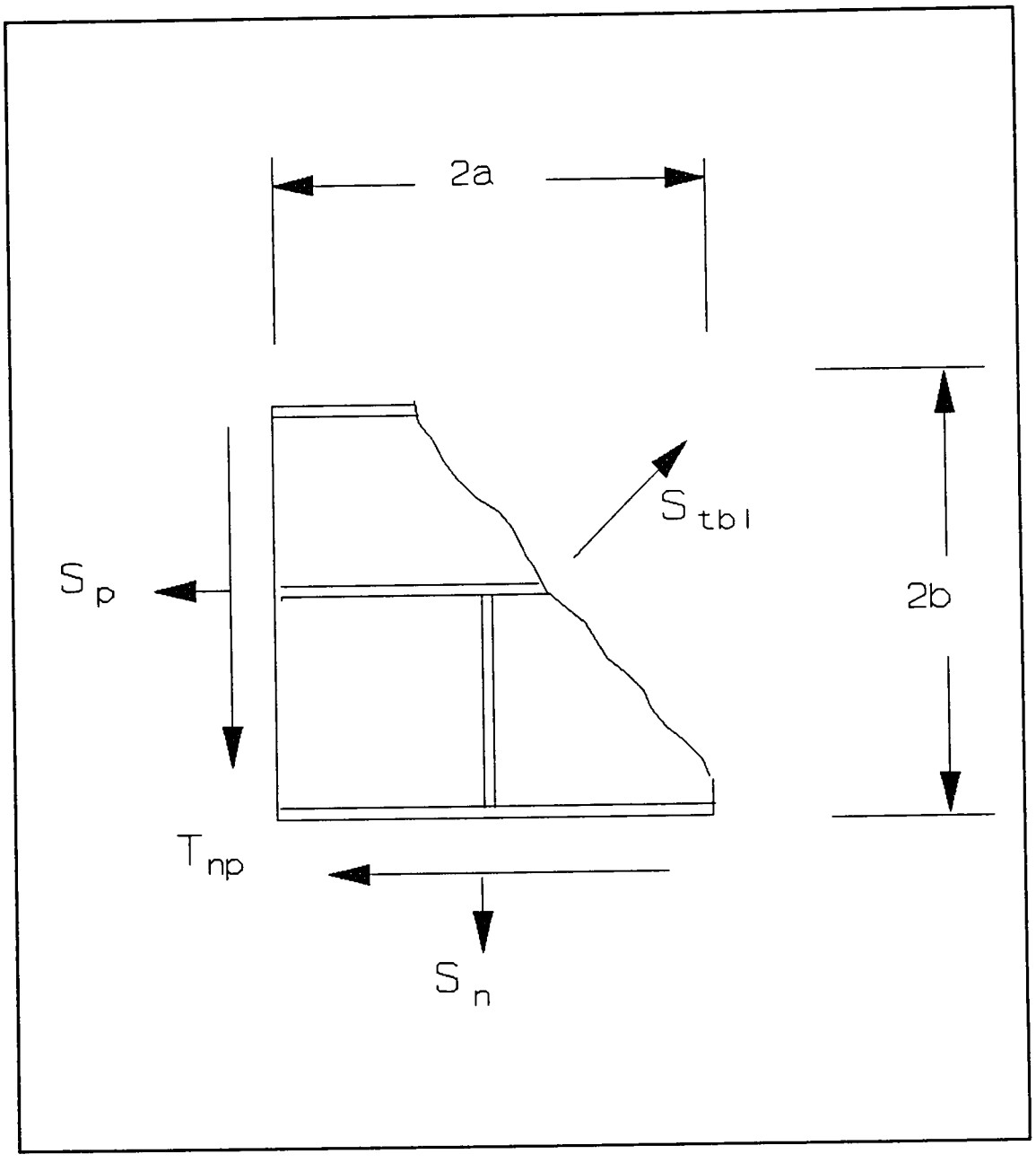


Figure 2.4.8 Splitting Through Mortar and Units (After Seah, 1988)

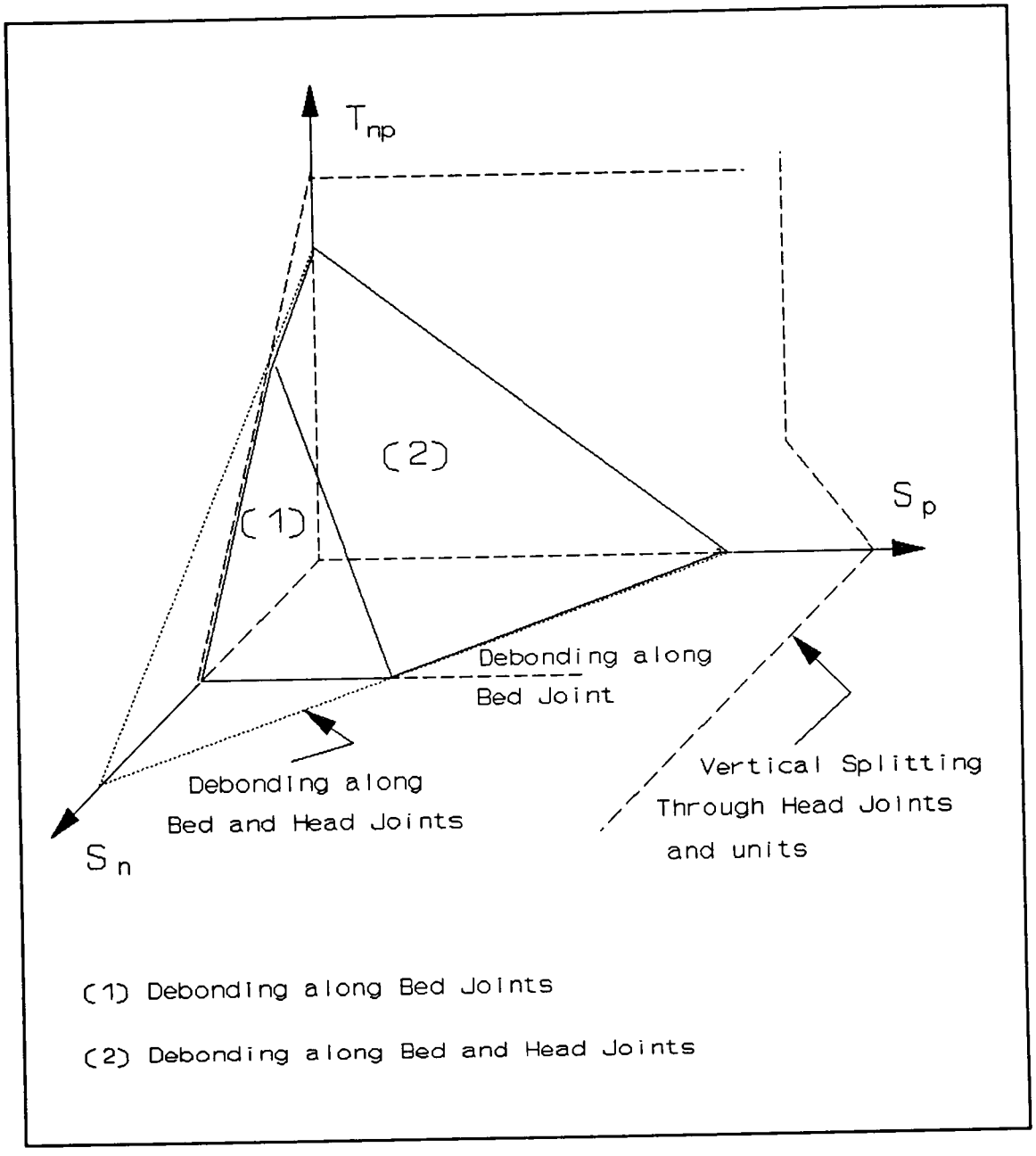


Figure 2.4.9 Failure Envelope in Biaxial Stress Fields (After Essawy et al, 1986)

estimated for any combination of the stresses. The failure envelope may vary from one condition to another depending on the geometry and the strength of the materials of the panel.

Essawy and Drysdale (1987) used the proposed failure criterion with the finite element model to predict the strength and mode of failure of masonry assemblages. The proposed criterion was also adapted and implemented into a finite element technique by Seah (1988) and Dawe and Seah (1988,1989) to predict the first cracking load of laterally loaded infilled panels. The ratios of predicted to experimental values vary from 0.77 to 1.12, which is reasonable considering the high variability of the tensile bond strength of masonry construction.

2.5 MODEL VERIFICATION

To verify and calibrate the prediction of first cracking, a finite element mesh consisting of 42 elements and 195 nodes was developed to model test specimens WE2, WE4, WE6, and WE8 from Seah (1988). The finite element mesh configuration is shown in Figure 2.5.1. This mesh models half of the specimen's dimension of 3600 mm in length and 2800 mm in height. These specimens are symmetrical about the center line of the panel in the y-direction. They are made of hollow

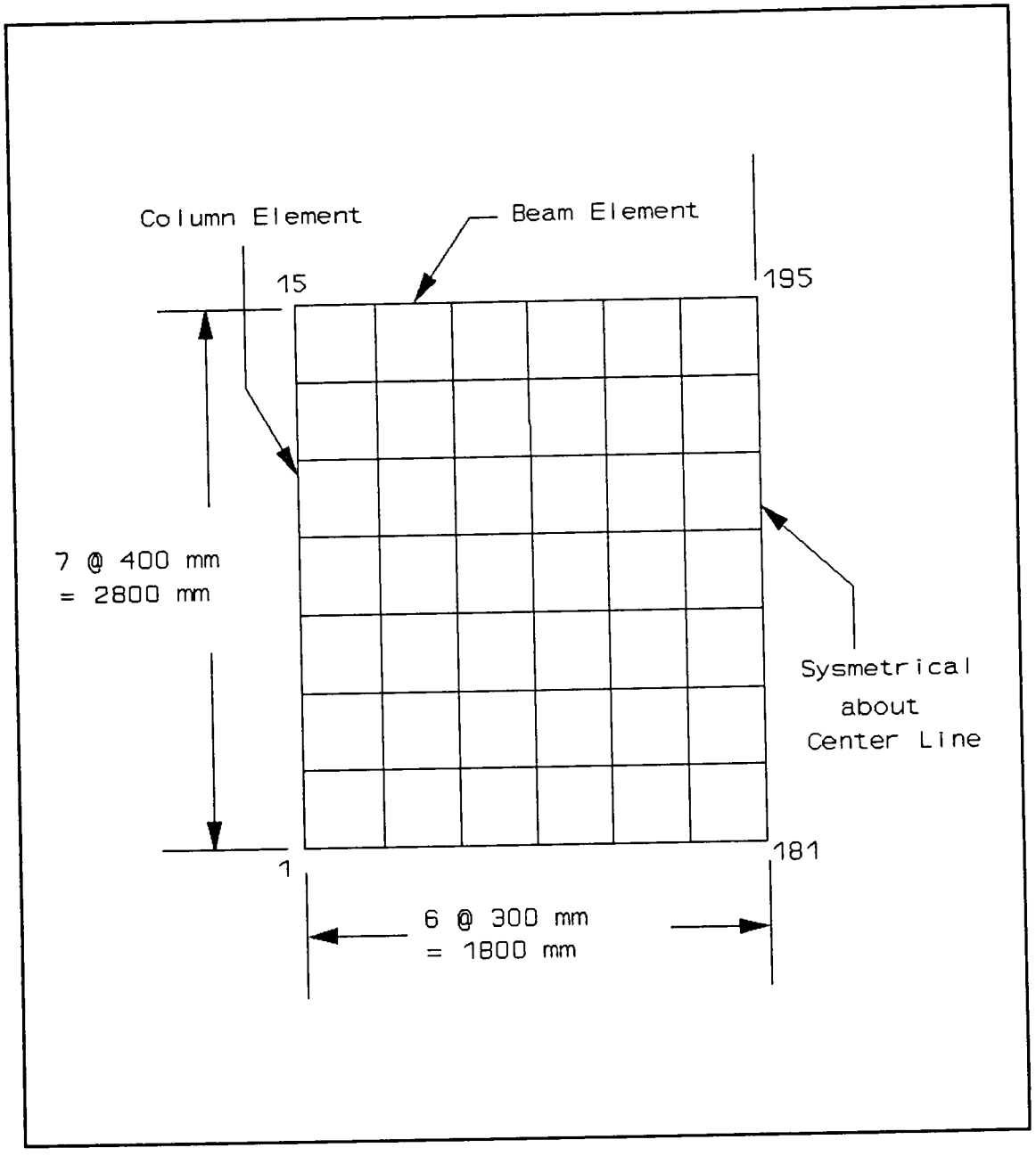


Figure 2.5.1 Finite Element Mesh Configuration for Specimen WE2, WE4, WE6 and WE8

concrete masonry units enclosed in a steel frame with W250x58 columns and a W200x46 beam. The thickness for WE2 and WE6 is 190 mm and for WE4 and WE8 is 140 mm.

The modulus of rupture normal and parallel to the bed joints are 0.291 MPa and 1.08 MPa respectively for the 190 mm blocks, and 0.390 MPa and 0.94 MPa respectively for the 140 mm blocks. Other material properties such as Poisson's ratio, shear modulus, modulus of elasticity normal and parallel to the bed joints, and the boundary conditions are tabulated in Table 2.5.1.

The highest stresses were in the y-directions at the fixed base for most of the specimens. This might induce early stage cracking at the base. Predicted uniform loads to cause base cracking are shown in Table 2.5.2. Both the Normal Moment Method failure criteria (Fried et al., 1988) and the elliptical interaction method failure criteria (Thurlimann and Guggisberg, 1988) are considered. The predicted cracking loads were about 38% to 75% below the experimental results. The specimens were remodelled with simply supported bases to simulate the behavior after base cracking. The first cracking load values are underpredicted by 25% for WE4 and WE6, 46% for WE8, and overpredicted by 75% for WE2, Table 2.5.2. Neither the fixed base model or simply supported base model correlates well with the experimental results.

The fixed base model is thought to be valid because of

TABLE 2.5.1

MATERIAL PROPERTIES FOR CONCRETE BLOCK WALL FROM SEAH (1988)

TEST SPEC.	MATERIAL PROPERTIES				BOUNDARY CONDITIONS Bottom: Fixed For All Cases
	ELASTIC MODULUS (MPa)		SHEAR MODULUS (MPa)	POISSON RATIO	
	Normal	Parallel			
WE2	23000	17250	8353	0.18	Top: Pinned Sides: Free
WE4	13800	17900	5994	0.30	Top: Pinned Sides: Free
WE6	17200	15600	6874	0.19	Top: Free Sides: Pinned
WE8	16200	18800	7374	0.18	Top: Fixed Sides: Fixed

TABLE 2.5.2

CRACKING LOAD PREDICTIONS FOR FIXED BASE AND SIMPLY SUPPORTED BASE FOR SEAH'S PANELS

TEST SPEC.	EXPT. RESULTS (KPa)	NORMAL MOMENT METHOD (KPa)		ELLIPTICAL INTERACTION METHOD (KPa)	
		Base Cracking	Simply Supported Base	Base Cracking	Simply Supported Base
WE2	3.8	1.9	6.7	1.9	6.7
WE4	2.4	1.5	1.8	1.5	1.7
WE6	5.2	1.3	3.9	1.3	3.6
WE8	4.8	2.6	2.6	2.6	2.6

the in-plane arching effect or membrane action developed after the wall panel cracks at the base. The base will continue to carry some moment and the panel will eventually crack away from the base. It is conjectured that the experimental cracking loads reported are those for panel cracking, since base cracking would be almost impossible to observe due to the air bag.

The predicted results for cracking away from the base using the Normal Moment Method (Fried et al., 1988), are about 18% higher than the experimental results for WE4, WE6 and WE8, whereas it is 10% lower for the WE2 specimen, shown in Table 2.5.3. With the elliptical interaction failure criteria (Thurlimann and Guggisberg, 1988), the predicted results for WE4, WE6 and WE8 are 14%, 4% and 13% higher than the experimental results, respectively. A 10% lower cracking load than the experimental is predicted for WE2 as before. Predicted cracking loads from Seah (1988) are also shown in Table 2.5.3. These were obtained using biaxial stress fields failure criteria developed by Essawy and Drysdale (1986).

Considering the uncertainties of various parameters of the material properties involved, the predicted first cracking loads by both methods are satisfactory. However, the elliptical interaction method of Thurlimann and Guggisberg (1988) provides closer results to the experimental values than the Normal Moment Method of Fried et al (1988). The

TABLE 2.5.3

FIRST PANEL CRACKING PREDICTIONS FOR SEAH'S PANELS

TEST SPEC.	EXPT. RESULTS (KPa)	SEAH'S RESULTS (KPa)	NORMAL MOMENT METHOD (KPa)	ELLIPTICAL INTERACTION METHOD (KPa)
WE2	3.8	3.4	3.4	3.4
WE4	2.4	2.2	2.8	2.7
WE6	5.2	4.1	6.2	5.4
WE8	4.8	3.7	5.7	5.4

elliptical interaction method is used in the following sections to predict the first cracking loads of the wall panels in Building 9207 and 9212.

2.6 BUILDING 9207

2.6.1 Wall Panel

The wall panel in Building 9207 described in section 1.3 and illustrated in Figure 1.3.1 is investigated with respect to the first panel cracking load. A finite element mesh consisting of 42 elements and 195 nodes for half of the panel was utilized. The mesh configuration is shown in Figure 2.6.1.

Three boundary conditions were investigated, as shown in Figure 2.6.2. Case 1 has a restraint at the upper corners of the panel. Case 2 has a simple support along the columns, and Case 3 has simple supports along the columns as well as the top beam. The infilled to floor interface was assumed to be fixed. To better understand the effects of the base support conditions on all three cases, a simply supported base model was included in this section.

The modulus of rupture and the elastic constants such as Poisson's ratio, modulus of elasticity and shear modulus were estimated in Section 2.3 and are tabulated in Table 2.6.1.

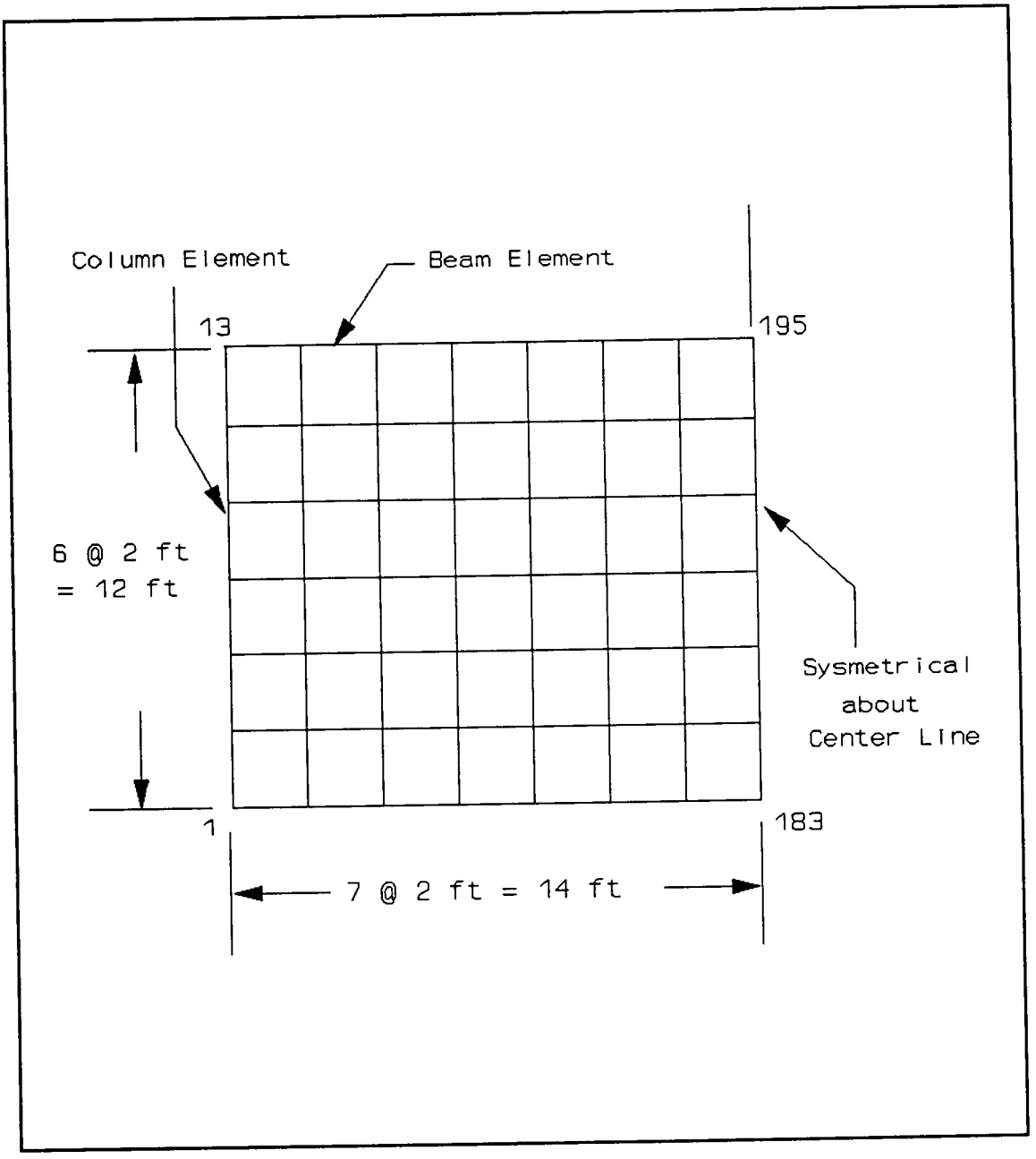


Figure 2.6.1 Finite Element Mesh Configuration for Wall Panel in Building 9207

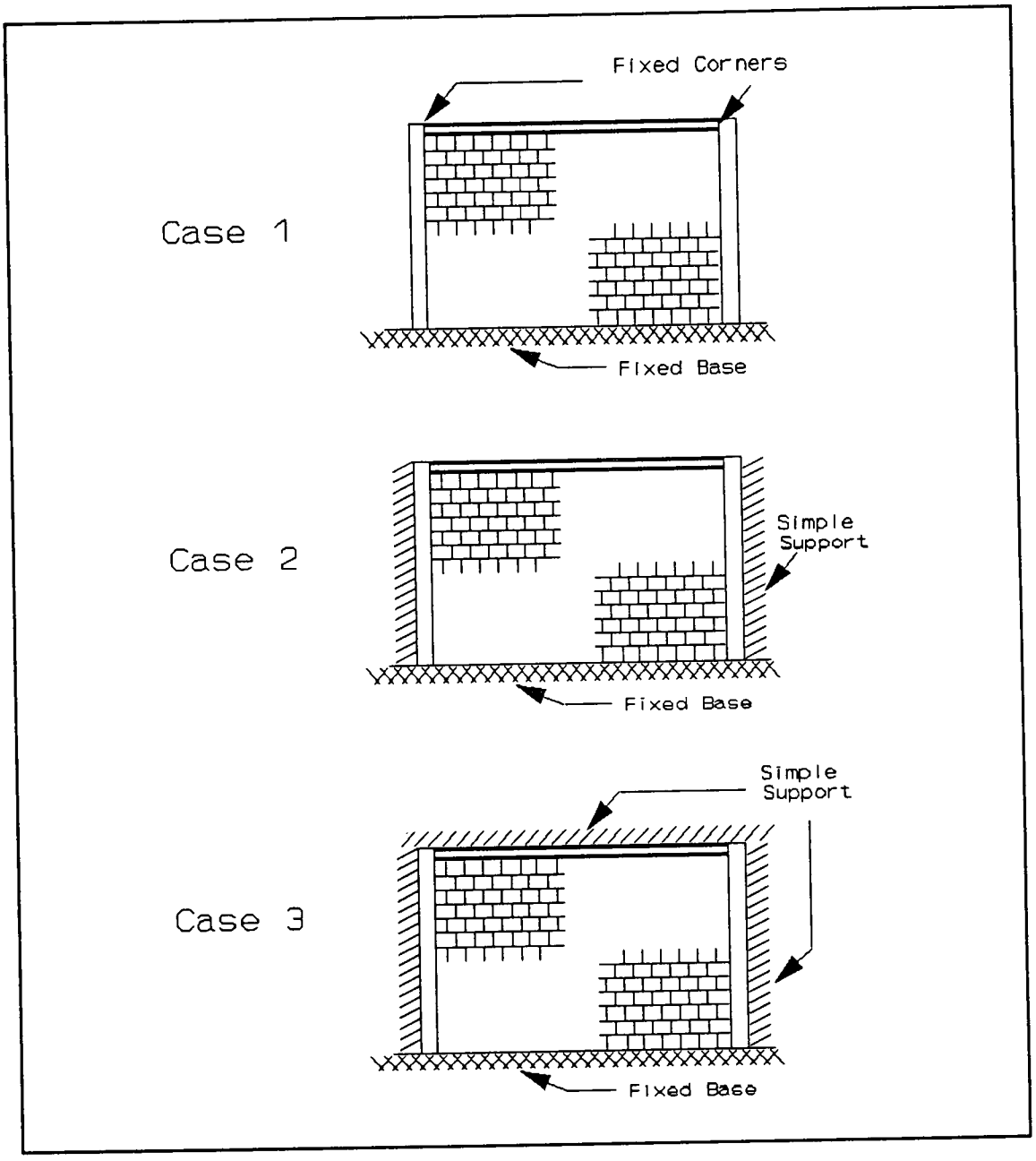


Figure 2.6.2 Different Boundary Conditions for Wall Panel in Building 9207 and 9212

TABLE 2.6.1

ESTIMATED MATERIAL PROPERTIES FOR HOLLOW CLAY TILE WALLS IN BUILDINGS 9207 AND 9212

MATERIAL PROPERTIES					
ELASTIC MODULUS (Ksi)		MODULUS OF RUPTURE (Psi)		SHEAR MODULUS (Ksi)	POISSON'S RATIO
Normal	Parallel	Normal	Parallel		
750	1000	63	87	343	0.25

The estimated material properties for the 8-inch hollow clay tile unit were used in the ABAQUS finite element program (1989).

2.6.2 Analysis of Results

Table 2.6.2 shows the predicted results of the base cracking load from the fixed base model and the simply supported base model using the elliptical interaction method (Thurlimann and Guggisberg, 1988). The highest stresses, as in section 2.5, occurred in the y-direction at the fixed base and the x-direction at the top boundary near to the center line of the panel for case 1 and 2. For case 3, because it is simply-supported along the top boundary, the highest stresses in the x-direction occurred around 4 ft. below the top interface.

The base cracking loads are approximately 0.12 Psi for case 1 and 2, and 0.26 Psi for case 3. For the simply supported base, the cracking loads are about twice as much as the base cracking loads for case 1 and 2, and just slightly greater, about 0.29 Psi, for case 3.

Based on the model described in section 2.5, the predicted panel cracking loads away from the base correlates well with the experimental results. Hence, the fixed base model with first panel cracking was determined as shown in Table 2.6.3. The predicted uniform first panel cracking loads

TABLE 2.6.2

CRACKING LOAD PREDICTIONS FOR FIXED BASE AND SIMPLY SUPPORTED BASE IN BUILDING 9207

CASE	ELLIPTICAL INTERACTION METHOD	
	Base Cracking (Psi)	Simply Supported Base (Psi)
1	0.12	0.23
2	0.12	0.23
3	0.26	0.29

TABLE 2.6.3

FIRST PANEL CRACKING PREDICTIONS FOR BUILDING 9207

CASE	ELLIPTICAL INTERACTION METHOD (Psi)
1	0.46
2	0.46
3	0.45

are 0.46 Psi for the first two cases, and 0.45 Psi for the third case. The differences between the predicted loads were minimal for the various boundary conditions. The stress distribution obtained from the numerical analysis indicates that the cracks are expected to span vertically for the first two cases, and horizontally for the last case where the boundaries are restrained.

2.6.3 Natural Frequencies

A low amplitude dynamic test was performed on the wall panel in Building 9207. The first measured frequency was 17.5 Hertz (Huff, 1990). A frequency analysis was included in the numerical analysis to determine the proximity of the models to the panel in Building 9207. The first and second frequencies were predicted for all three cases as tabulated in Table 2.6.4. The first frequencies were 11.8 Hertz for case 1 and 2, and 30.7 Hertz for the third case. The frequencies predicted are approximately 48% smaller than the measured frequency for the first two cases, and about 43% larger for the third case. Part of the discrepancies can be attributed to the uncertainty of the elastic constants. However, since the frequency is directly proportional only to the square root of the modulus of elasticity, there appears to be other factors affecting the result. It is conjectured that the top boundary is between simply supported and free. A model using

TABLE 2.6.4

PREDICTED AND MEASURED FREQUENCIES ON PANEL IN BUILDING 9207

PANEL IN BUILDING 9207	PREDICTED FREQUENCIES (Hertz)			MEASURED FREQUENCY (Hertz)
	Case 1	Case 2	Case 3	
First	11.8	11.8	30.7	17.5
Second	44.6	44.6	57.2	----

out-of-plane elastic springs at the top boundary is utilized. Various spring stiffness were investigated and the first two frequencies and the predicted panel cracking loads are tabulated in Table 2.6.5. The natural frequency of 17.7 Hertz determined using a spring stiffness of 50 Kips per foot has excellent correlation with the measured frequency. The predicted first cracking pressure is 0.52 Psi or a total load of 24 Kips. The first cracking load remains relatively constant with the various models.

2.6.4 Parametric study

Case 2 with the boundary conditions described as before (fixed base, simply supported sides and free at the top) is chosen to study some of the parameters suspected to influence the first cracking capacity of the wall panel. The parameters investigated are Poisson's ratio, modulus of elasticity and modulus of rupture. The model with spring stiffness of 50 Kips per foot, shown in Figure 2.6.3 is also used to study the effects of modulus of rupture and the air bag size.

(i) Effects of the Poisson's ratio

Changing of Poisson's ratio will affect the shear modulus. Decreasing the value of Poisson's ratio by 0.1 to 0.15 causes the shear modulus to increase by 9%, and increases the first cracking load by 2%. Increasing the value of

TABLE 2.6.5

PREDICTED FREQUENCIES AND FIRST PANEL CRACKING LOAD USING ELASTIC SPRING MODELS

SPRING STIFFNESS (Kips/ft.)	FREQUENCIES (Hertz)		PREDICTED CRACKING LOAD (Psi)
	First	Second	
0.0	11.8	44.6	0.46
50.0	17.7	47.5	0.52
87.6	20.3	49.6	0.50
113.6	21.6	51.0	0.49
175.2	23.7	52.5	0.48
∞	30.7	57.2	0.45

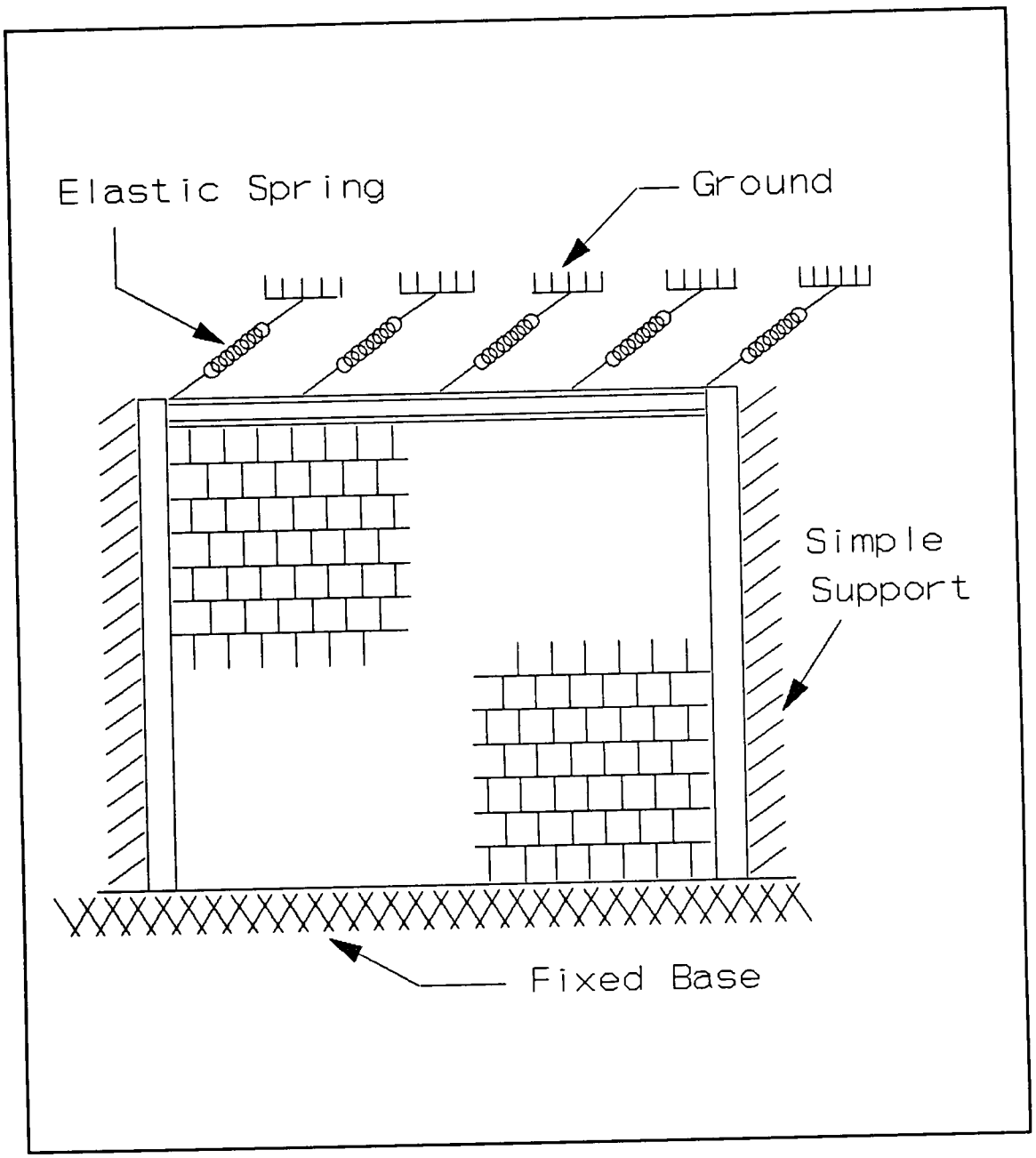


Figure 2.6.3 Elastic Spring Model with Spring Stiffness of 50 kips per foot for Panel in Building 9207

Poisson's ratio from 0.25 to 0.35 leads to a reduction of the shear modulus of 8%, and decreases the first cracking load by 2%. The first cracking load for Poisson's ratios of 0.15 and 0.35 are 0.47 Psi and 0.45 Psi respectively as shown in Table 2.6.6. The first panel cracking load is not very sensitive to a change of Poisson's ratio and shear modulus.

(ii) Effects of Modulus of Elasticity

Consider the isotropic elastic case by setting both of the orthogonal modulii of elasticity to 1000 Ksi. The increase of the modulus of elasticity normal to the bed joint by 25% increases the shear modulus about 17%. It reduces the first cracking capacity to 0.38 Psi, which is 17% lower than the result from the original model. This infers that the isotropic model predicts a lower cracking load than the orthotropic model. Thus, the isotropic model yields conservative predictions.

Reducing the modulus of elasticity normal to the bed joint to half the modulus of elasticity parallel to the bed joint causes a reduction of shear modulus of 22%. It increase the first cracking load by 17%. The results for both cases are shown in Table 2.6.7.

TABLE 2.6.6

EFFECTS OF POISSON'S RATIO ON FIRST PANEL CRACKING IN BUILDING 9207

CASE	MATERIAL PROPERTIES		PREDICTED CRACKING LOAD (Psi)
	Poisson's Ratio	Shear Modulus (Ksi)	
2	0.25	343	0.46
2(A)	0.15	373	0.47
2(B)	0.35	318	0.45

TABLE 2.6.7

EFFECTS OF MODULUS OF ELASTICITY ON FIRST PANEL CRACKING IN BUILDING 9207

CASE	MATERIAL PROPERTIES			PREDICTED CRACKING LOAD (Psi)
	Elastic Modulus (Psi)		Shear Modulus (Ksi)	
	Normal	Parallel		
2	1000	750	343	0.46
2(C)		500	267	0.54
2(D)		1000	400	0.38

(iii) Effects of Modulus of Rupture

Table 2.6.8 shows the results for the modulus of rupture normal and parallel to the bed joint. Decreasing the modulus of rupture normal to the bed joint by 25% decreases the first cracking load of the elastic spring model by 23% and the free at top model by 6%. Increasing the modulus of rupture by 25% increases the first cracking load of the elastic spring model by 19%. However, it does not change the first cracking load significantly for the free at top model.

Decreasing the modulus of rupture parallel to the bed joint by 25% decreases the first cracking capacity by 8% for the elastic spring model and 24% for the free at top model. Increasing the modulus of rupture by 25% increases the first cracking load by 4% for the elastic spring model and 20% for the free at top model. Therefore, the effects of the modulus of rupture normal and parallel to the bed joint of the panel in Building 9207 depend on the stiffness of the girder and the top boundary conditions.

(iv) Effects of Air Bag Size

Present plans are to use a smaller air bag size, 24 ft. x 10 ft., to accommadate restrictions at the test location. For ease of numerical modeling, the size of the air bag was reduced to 24 ft. x 8 ft., which is about 59% of the original air bag size. The effect of the reduced air bag size was

TABLE 2.6.8

EFFECTS OF MODULUS OF RUPTURE ON FIRST PANEL CRACKING IN BUILDING 9207

CASE	MODULUS OF RUPTURE (Psi)		PREDICTED CRACKING LOAD (Psi)	
	Normal	Parallel	Elastic Spring Model	Free at Top Model
2	63	87	0.52	0.46
2(E)	47	87	0.40	0.43
2(F)	79	87	0.62	0.46
2(G)	63	65	0.48	0.35
2(H)	63	109	0.54	0.55

examined using the elastic spring model. The first cracking pressure increases about 8% to 0.56 Psi, as shown in Table 2.6.9. The total load required to cause the first panel cracking is reduced to 15.5 Kips from 24.2 Kips using the full size air bag. A reduction of 36% of the total load is determined using the 24 ft. x 8 ft. air bag size. Thus, using a reduced air bag size does not significantly affect the pressure to cause cracking.

2.7 BUILDING 9212

2.7.1 Wall Panel

The wall panel in Building 9212 described earlier in section 1.3 consists of 4-inch blocks and 8-inch blocks alternating to form a total thickness of a 12-inch masonry unit. The panel's configuration is shown in Figure 1.3.2. Assumptions regarding the material properties for the 12-inch block wall panel in Building 9212 are necessary because of the lack of experimental values on this arrangement of hollow clay tile. The material properties are assumed the same as those for 8-inch block panel in Building 9207, as shown in Table 2.6.1. The wall panel is assumed symmetrical about the center line in the y-direction, and a finite element mesh consisting of 60 elements and 273 nodes for the numerical analysis was

TABLE 2.6.9

EFFECTS OF AIR BAG SIZES IN BUILDING 9207

AIR BAG SIZE	PREDICTED CRACKING LOAD (Psi)
27 ft. x 12 ft.	0.52
24 ft. x 8 ft.	0.56

developed to model half the dimension of the panel, Figure 2.7.1.

2.7.2 Analysis of Results

Using the elliptical interaction method of Thurlimann and Guggisberg (1988), the fixed base model with three different boundary conditions similar to those in Building 9207 in Section 2.6, were investigated. Table 2.7.1 provides the first cracking uniform loads predicted for the panels in Building 9212. The initial cracking for Case 1 and 2 appeared to be at the top of the panel near the center line of the panel. They are 0.17 Psi and 0.21 Psi respectively. Case 3 experienced base cracking at the uniform load of 0.34 Psi.

2.8 SUMMARY OF RESULTS

Analytical models and methods to predict first cracking loads were developed and validated by comparison with experimental results obtained from Seah (1988). The predictions using an elliptical interaction failure method for a fixed base model but considering cracking away from the base resulted in close agreement. The model was used to predict the panel cracking load in Building 9207 and 9212 using the estimated material properties.

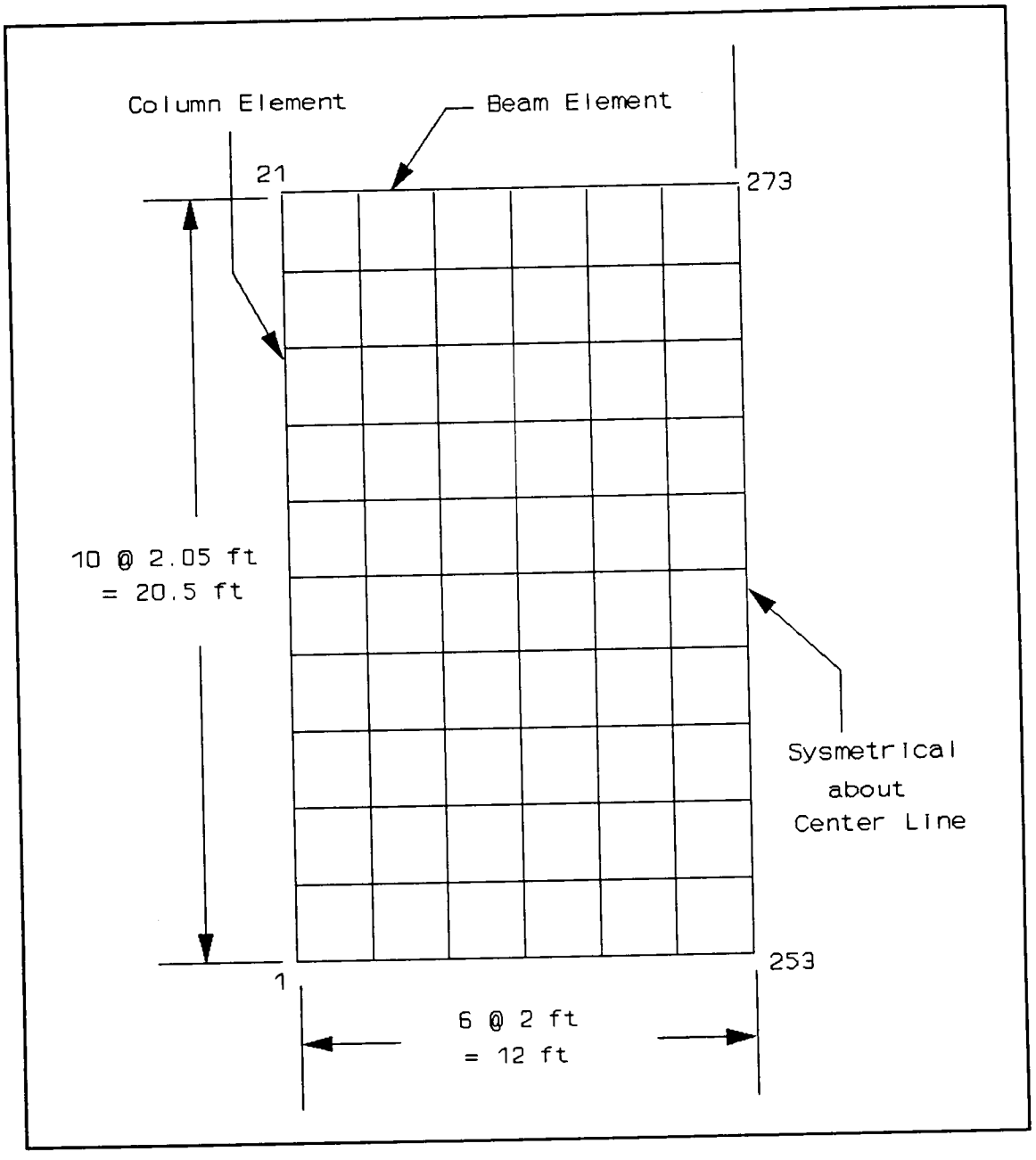


Figure 2.7.1 Finite Element Mesh Configuration for Wall Panel in Building 9212

TABLE 2.7.1

FIRST PANEL CRACKING PREDICTIONS FOR BUILDING 9212

CASE	ELLIPTICAL INTERACTION METHOD (Psi)
1	0.17
2	0.21
3	0.34

For most cases, early stage cracking at the bases may occur. It is hardly visible due to the placement of the air bag. According to the model verification in Section 2.6, the base may be able to sustain moment after cracking.

The estimated first panel cracking capacities for Case 1, 2, and 3 were determined as 22 Kips, 22 Kips, and 21 Kips respectively for Building 9207, and 12 Kips, 14 Kips, and 23 Kips respectively for Building 9212. The natural frequency analysis reveals that a model using elastic spring at the top boundary is more appropriate to predict the first cracking load in Building 9207, and it was determined as 24 Kips. These results are influenced by the modulus of rupture normal and parallel to the bed joint for panel in Building 9207. The cracking capacity of panel free at the top boundary is significantly affected by the modulus of rupture parallel to the bed joint. The modulus of rupture in the orthogonal direction plays an important role in the panel that has an elastic spring at the top boundary. Using a different air bag size also changes the results of the cracking load moderately. The other parameter having a significant effect on the results is the modulus of elasticity of the infilled panel. Poisson's ratio has marginal effect on the first cracking capacity. Changes in either modulus of elasticity or Poisson's ratio causes significant changes in the shear modulii, however, the fluctuation in shear modulii does not contribute significantly to the first cracking capacity.

CHAPTER 3

ULTIMATE STRENGTH CALCULATIONS

3.1 INTRODUCTION

The objectives of this chapter are twofold. The first is to determine the important variables that affect the ultimate strength of a hollow clay tile infilled wall when subjected to a uniform lateral load. This is done through a parametric study. The second objective is to predict the approximate ultimate loading capacity and deflection of the hollow clay tile masonry infilled wall panels under a uniformly distributed pressure applied by an air-bag, normal to the surface of the wall panel.

3.2 ANALYTICAL METHODS

A review of the published literature reveals that limited studies have been done on the out-of-plane resistance of masonry infilled walls. The work that has been done has primarily focused on the behavior of concrete block and clay

brick masonry infilled wall panels; few deal with the hollow clay tile masonry infilled panel in steel frame. Several analytical techniques are expected to be very helpful in the initial modeling of the proposed tests.

Sinha, Loftus and Temple (1979) carried out a testing program on model brickwork panels of different aspect ratios (L/H = 0.5-2), with simply supported boundary conditions on top and bottom, and continuous on one or both ends, continuity being simulated by returns. A uniform lateral loading condition was provided to the test wall panel by means of an air-bag sandwiched between the wall and a rigid reaction frame. Three analytical methods were employed separately to calculate the failure pressure. First, the yield-line analysis, as applied to reinforced concrete slabs, tends to overestimate the failure pressure because the behavior of brickwork is brittle and does not yield after cracks have appeared. It was predicted that after cracking, the material can carry little or no moment. Second, the Grashoff-Rankine Method of mid-span deflection compatibility, an elastic theory based on stiffness orthotropy, always underestimates the failure pressure of the panels. The failure pressure was determined when either the bending moment in the horizontal or vertical direction achieved the corresponding moment of resistance obtained from wallette tests, without considering the reserve strength in other directions. Third, the

idealized fracture line analysis proposed by Sinha (1978) to analyze low tensile strength brickwork was used. The proposed simplified idealized fracture line analysis is similar to the yield line method except that the former includes both stiffness and strength orthotropies in the analysis. Although the fracture line pattern formed at failure pressure resembles the yield line in ductile plates, the use of the term "yield line" is inaccurate. Moreover, it is difficult to account for fully plastic behavior in a brittle material such as brickwork. Therefore, the term "fracture line" is used for this analysis. The proposed fracture line technique predicted the ultimate pressure very close to the experimental pressure for panels supported on four sides.

Anderson (1985) used the yield line technique to predict the ultimate load on wall panels subjected to uniform lateral and edge loadings. The technique for applying lateral loading to the tested wall panel is known as "Christmas Tree" or "Wiffle Tree", a mechanical system of beams and wires pulled by a single jack as shown in Figure 3.2.1. Therefore, a series of equal loads is applied normal to the surface of the wall panel to simulate uniform wind loading. The technique is further modified to include the additional series of point loads along the free edge of the wall, in order to simulate wind load transferred from the adjoining horizontal spanning panel. It was concluded that the use of the characteristic

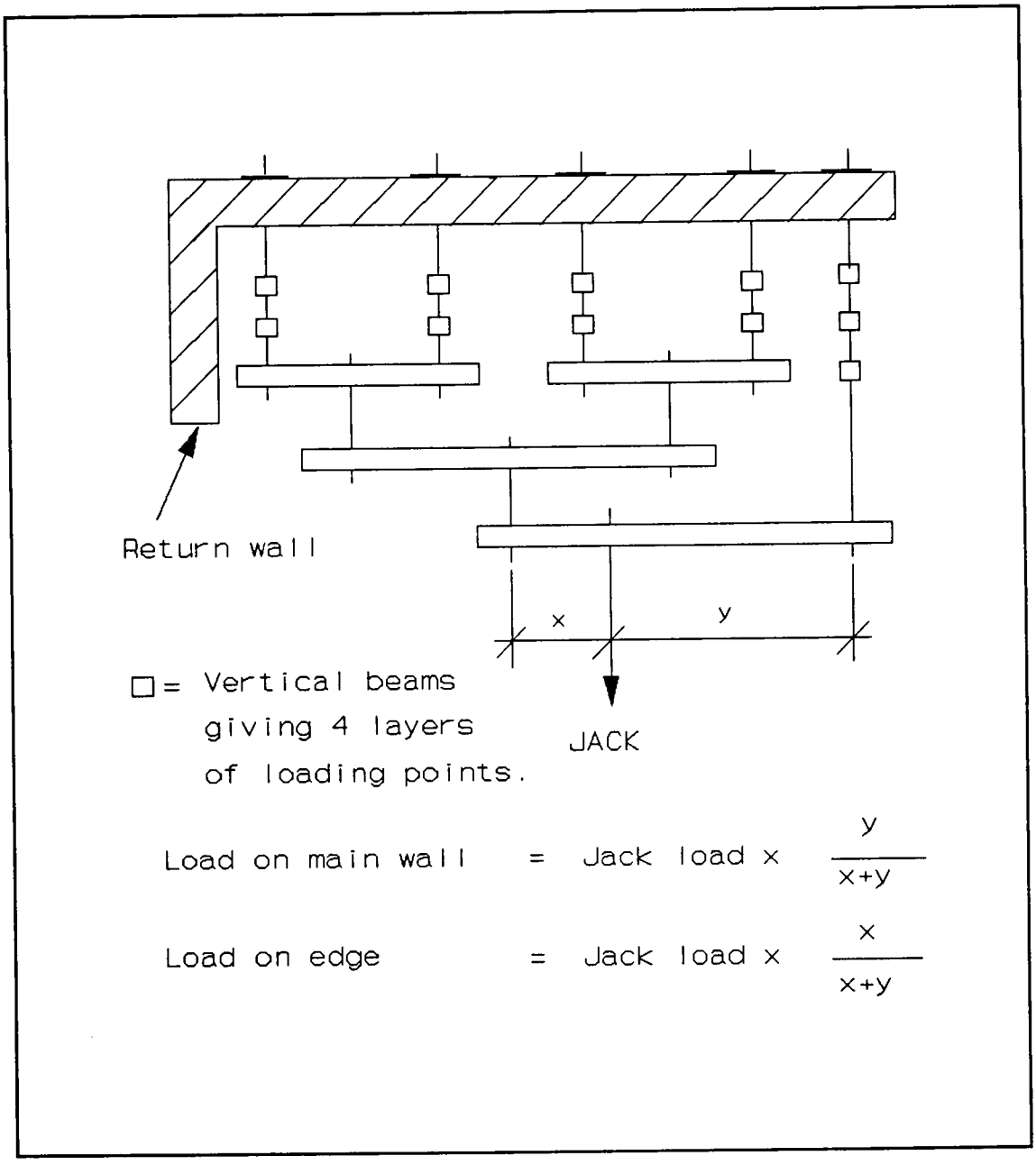


Figure 3.2.1 Loading System for Test Wall Panel (After Anderson, 1985)

wallette flexural strengths and yield-line theory generally underestimates the strength of the walls and thus is conservative. Moreover, it was pointed out that if the yield line theory is used to analyze brittle unreinforced material which can not withstand a moment after cracked, the secondary effects need to be considered. The secondary effects include self weight effects, in-plane membrane action, and partial arching action from the enclosing frame, which can introduce eccentric compression forces across the cracks. The ultimate load was approximately twice the first cracking load in the wall. The deflection at the ultimate load was found to be a function of the length of the wall panel.

Fried et al. (1988) studied and utilized five different analytical techniques to predict the strength of masonry walls subjected to lateral loadings. These methods were Simplified Principal Stress Method (PSM), Elastic Plate Method (EPM), Strip Method (SM), Yield Line Method (YLM) and Normal Moment Method (NMM). Strip Method (SM) and Yield Line Method are wall design methods used in Australia and United Kingdom respectively. The Normal Moment Method (NMM) assumes failure to occur along a plane inclined at a certain angle to the vertical when the normal applied moment is equal to the normal resisting moment. In other words, the ratio of normal resisting moment to normal applied moment equals 1.0 at the point of failure and is influenced by the angle along the

plane of failure to the vertical. The minimization of this ratio is obtained numerically and the failure pattern of a panel can be observed by elements with the lowest ratios. Predictions of the failure load versus the aspect ratio (L/H) using the PSM, EPM, SM and YLM are shown in Figure 3.2.2 for a simply supported wall on four sides. The YLM has the maximum prediction. The EPM, only considers stresses in the vertical or horizontal directions, but the high torsional stresses set up at the corners of a simply supported panel are ignored. Consequently, the EPM always predicts failure at the geometric center of the panel. On the other hand, the NMM, which is not shown on the figure, predicts failure near the left or right corners of the panel where there is likely to be high torsion. It also predicts the ultimate and first cracking loads to be nearly equal. The NMM predictions were always less than the YLM predictions, and less than or equal to the EPM predictions. Fried et al. (1988) concluded that although there are variations in the upper bound strengths by the yield line technique and the Strip Method, the difference can be reduced when the flexural properties used for both analytical methods are determined using the British and Australian methods respectively. Thus, material properties have significant effects on each analytical technique. The yield line and strip methods were recommended to predict the ultimate strength of the wall panel because these two methods

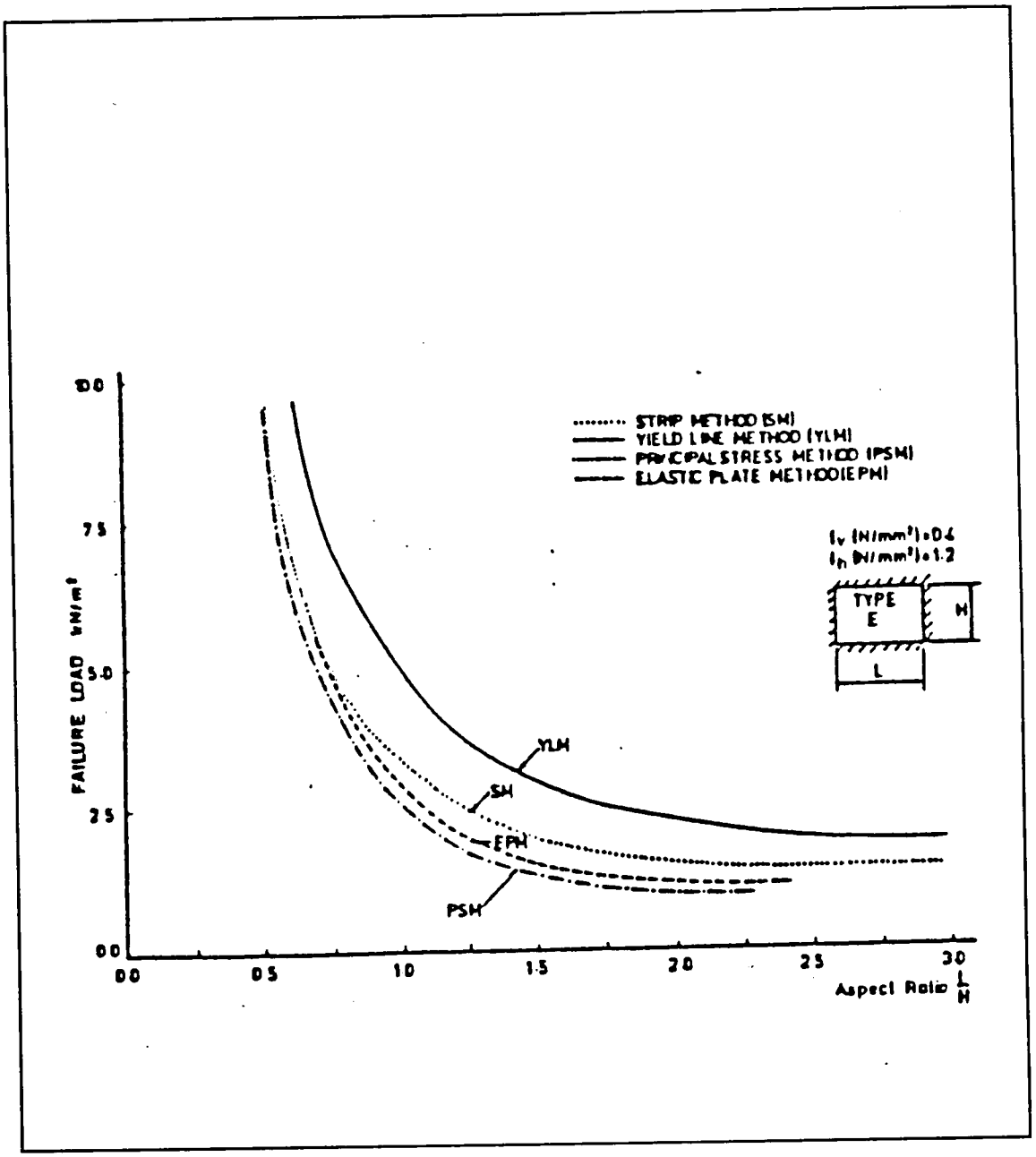


Figure 3.2.2 Predicted Failure load Versus Aspect Ratio for Simple Support at All Edges Wall Panel (Fried et al., 1988)

always produced maximum predictions in their investigations. They also suggested that the in-plane membrane action by the built-in edges usually contributes to the enhancement of strength, even though the masonry did not have full rotational restraint along the built-in edges.

Drysdale and Essawy (1988) investigated a series of concrete block wall panels with well-defined boundary conditions with various lengths. The lateral loadings were furnished by means of an air bag placed between the test wall and a backup wall composed of a plywood covering on steel grid framework tied back to the support frame. The linear elastic plate analysis and yield line analysis techniques with continuity and without continuity along center crack assumptions were used. Yield line analysis with continuity assumption considered full moment capacity along the "yield line", whereas analysis without continuity considered the "yield moment" was lost by the pre-cracking at considerably lower than failure pressure. In general, the latter always predicts a lower ultimate pressure. It was observed in the wall panel simply supported on all four sides that an increase in the horizontal span decreased the failure pressure, and an increase in the length of the center horizontal crack and horizontal span increased the amount of deflection that occurred during formation of the horizontal crack. They concluded that both the elastic-plate and yield line methods

produced reasonable results of the ultimate pressure. However, the yield line analysis with continuity across the early horizontal crack, was found to be slightly unconservative. It was suggested that either the elastic plate analysis or the yield line method without continuity were adequate analytical methods.

Seah (1988) predicted the ultimate load capacities on hollow concrete block infilled panels subjected to uniformly distributed pressure perpendicular to the surface of the wall, using a modified conventional yield line technique, which accounts for the arching effect between the infills and the enclosing steel frame. Nine large scale infilled panels with different boundary conditions and thicknesses were tested. A uniformly distributed pressure perpendicular to the surface of the infilled wall panel was provided by an air bag set-up. Auxiliary tests were used to obtain appropriate strength and stiffness parameters, and later used to predict the first crack as well as ultimate load capacity. It was assumed that the fracture line pattern forming a failure mechanism divided the infilled wall panel into different sub-panels, and the subpanels act as a rigid plate rotating about the fractured lines. At every given deflection, the load resisted by the panel is then computed using the virtual work method. In the computation process, the wall panel was divided into a series of horizontal and vertical strips spanning each way as

suggested by Park (1964). A typical fracture line pattern with horizontal and vertical strips as shown in Figure 3.2.3. The level of uncertainty in this approximation can be reduced by increasing the number of strips.

Comparison of predicted ultimate loads with the corresponding experimental values showed that the ratios of predicted to experimental values vary from 0.94 to 1.14 with a coefficient of variation of 6% and a mean of 1.02. Overall, there are excellent correlation between experimental and predicted behavior. Dawe and Seah (1989) stated that the main lateral load resisting mechanism for infilled panels is by flexural action before first major cracking and by arching action in the post cracking range. The predicted capacities were more realistic with the inclusion of arching action than the values obtained by the conventional yield line technique. They also suggested that deformation of the enclosing frame be included in the analysis to simulate the true behavior of the system.

Two empirical relations suitable for design were proposed by Dawe and Seah (1989) as follows :

(a) For a panel supported on three sides and free at the top.

$$q_{ult} = 800 (f'_m)^{0.75} t^2 \alpha / L^{2.5} \qquad [3.2.1]$$

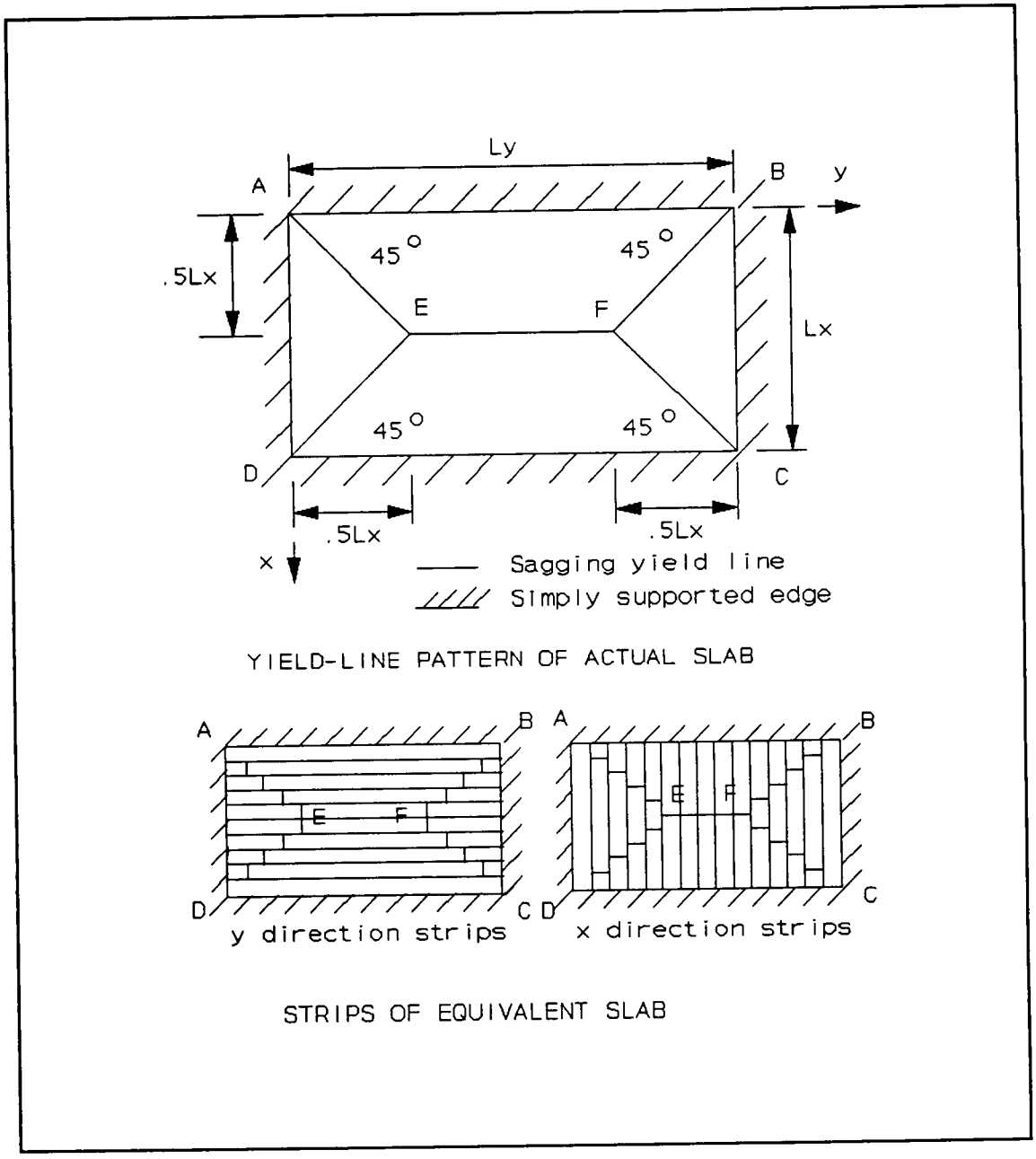


Figure 3.2.3 Uniformly Loaded Slab with All Edges Fixed Against Out-of-Plane Translation (After Park, 1964)

$$\text{where} \quad \alpha = \frac{1}{H}(EI_cH^2 + GJ_ctH)^{0.25} \leq 75$$

(b) For a panel supported on four sides

$$q_{ult} = 800(f'_m)^{0.75}t^2(\alpha/L^{2.5} + \beta/H^{2.5}) \qquad [3.2.2]$$

$$\text{where} \quad \alpha = \frac{1}{H}(EI_cH^2 + GJ_ctH)^{0.25} \leq 50$$
$$\beta = \frac{1}{L}(EI_bL^2 + GJ_btL)^{0.25} \leq 50$$

q_{ult} = *ultimate load (KPa)*
t = *panel thickness (mm)*
L = *panel length (mm)*
H = *panel height (mm)*
E = *Young's modulus of frame member (MPa)*
G = *Shear modulus of frame member (MPa)*
I_c, I_b = *Moments of inertia of columns and beams respectively* (mm^4)
J_c, J_b = *Torsional constants of columns and beams respectively* (mm^4)

3.3 PREDICTED ULTIMATE LOAD BEHAVIOR

The two panels described earlier and shown in Figure 1.3.1 and Figure 1.3.2 are examined with respect to their ultimate strength behavior. The boundary conditions of both panels were assumed to be fixed against out-of-plane

deflection on top, bottom and both sides. A bottom beam of a W36x260 was assumed to simulate the infilled-floor interface.

The compressive strength of the wall was assumed to be 1000 psi, the modulus of elasticity of the wall to be 1500 ksi, and the face shell thickness to be 0.75 inch in the 8 inch wall and 1 inch in the 12 inch wall. The effect of these assumptions will be examined later in a parametric study.

The post-cracking analytical technique developed by Seah (1988) was used to investigate the two wall panels because it considered flexibility of the confining steel frame, secondary effects due to the infills arching action and in-plane membrane action. It will also be shown that the only important masonry material property parameter in this method is the compressive strength, which is generally the most common material property available. The method has also been shown to have good correlation with full scale experimental results.

3.3.1 Description of Failure Modes

It is difficult to postulate an exact fracture line pattern because the cracking line pattern at failure depends on various factors such as the material properties of the infill, the infilled-enclosing steel members interface and the boundary conditions.

Judging from the construction and boundary conditions of

the wall panels in building 9207 and 9212, four probable modes of failures were examined with respect to their fracture line patterns. The modes are illustrated in Figure 3.3.1.

Mode A : Mode A occurs when slippage at the interface between the infills and the enclosing frame members is prevented. The horizontal crack occurs near the mid-height of the panel in the bed joints followed by diagonal cracks propagating to each of the four corners.

Mode B : When there is slippage at the interface between the infill and the top beam, while other interfaces are prevented from slippage, mode B could be the fracture line pattern for wall panels with low aspect ratio (L/H). The vertical crack near the mid-length propagates from the top of the infills to the mid-height due to the push out of the infills at the top interface with respect to the top beam. The fracture line proceeds with diagonal cracks to both corners at the bottom.

Mode C : Mode C could be another mode of failure if mode B is unlikely to occur when slippage occurrs at the top interface; mode C is most probable if the aspect ratio is relatively large. Two parallel vertical cracks at a small distant apart near the mid-length of the panel propagate to

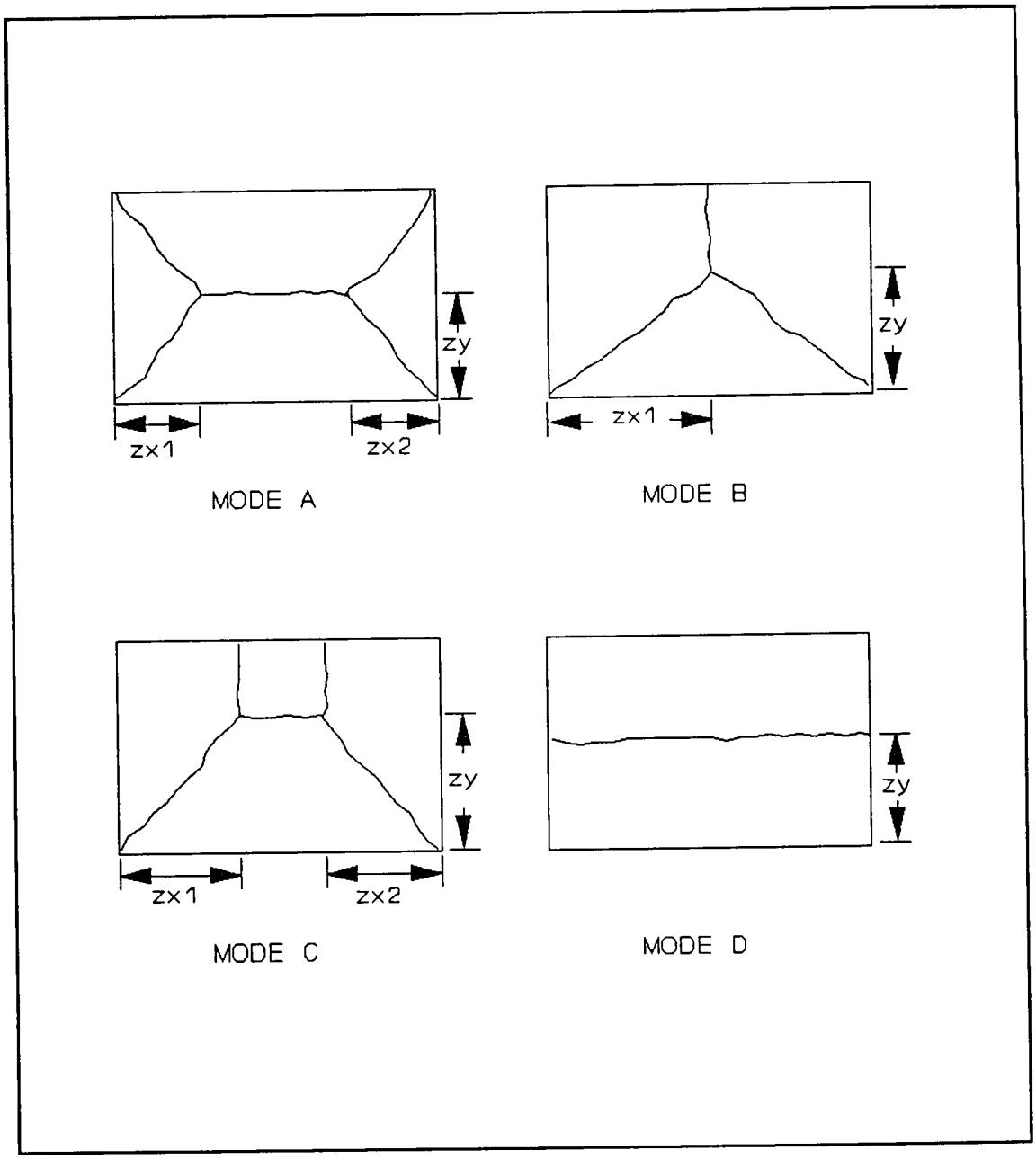


Figure 3.3.1 Modes of Failures

the center of the panel where a horizontal crack near mid-height along the bed joint is formed. The cracking continues with diagonal cracks proceeding to both sides of the lower corners.

Mode D : When slippage on both sides of the interfaces between the infills and the columns happens, mode D is the probable mode of failure. A horizontal crack spanning from side to side of the panel occurs near the mid-height due to the push out of the infills away from the columns. The wall panel acts like a panel simply supported on two opposite sides.

3.3.2 Effects of Failure Modes

Various modes of failure were examined to observe the effects of different fracture line patterns on the ultimate load capacity. The procedure to determine the fracture line dimensions of zy, zx1 and zx2 employed herein is trial and error. The locations of zy, zx1,and zx2 (if applicable) are shown in Figure 3.3.1. First, assume a reasonable value between zero and 0.5 for zx1 and zx2. Vary the value of zy between zero and 1.0 and determine corresponding ultimate pressure. The zy value corresponding to the lowest value of ultimate pressure is the value of zy used in the analyses. Similarly, by assuming the value of zy or using the zy value

obtained from above, the dimensions of zx1 and zx2 that correspond to the lowest ultimate pressure were used.

(i) 28 ft. X 12 ft. Wall Panel in Building 9207

The dimensions zy, zx1 and zx2 of mode A were determined as shown in Figures 3.3.2 and 3.3.3 with the results being zy=0.5, and zx1=zx2=0.17. The dimensions of the fracture line pattern of mode C were obtained as shown in Figures 3.3.4 and 3.3.5, with the results being zx1=zx2=0.38, and zy=0.77. The ultimate load capacity in Mode C was drastically reduced, by approximately 80%, as compared to mode A. It was also found that the amount of ultimate load capacity is a function of the coefficient of friction at the interface between the infill and the top beam. The results of various coefficients of friction and different modes of failures are tabulated in Table 3.3.1. Mode D has the zy dimension determined as in Figure 3.3.6, or 0.5. The slippage at both columns cuts the ultimate load capacity in half, because the load enhancement arching action is found only in the vertical direction.

(ii) 24 ft. X 20.5 ft. Wall Panel in Building 9212

The parameters for Mode A are the same as those obtained above. The values of zx1, zx2 and zy are shown in Figures 3.3.7 and 3.3.8. Mode B is considered to be a predominant mode of failure over Mode C due to the 1.17 aspect ratio. The

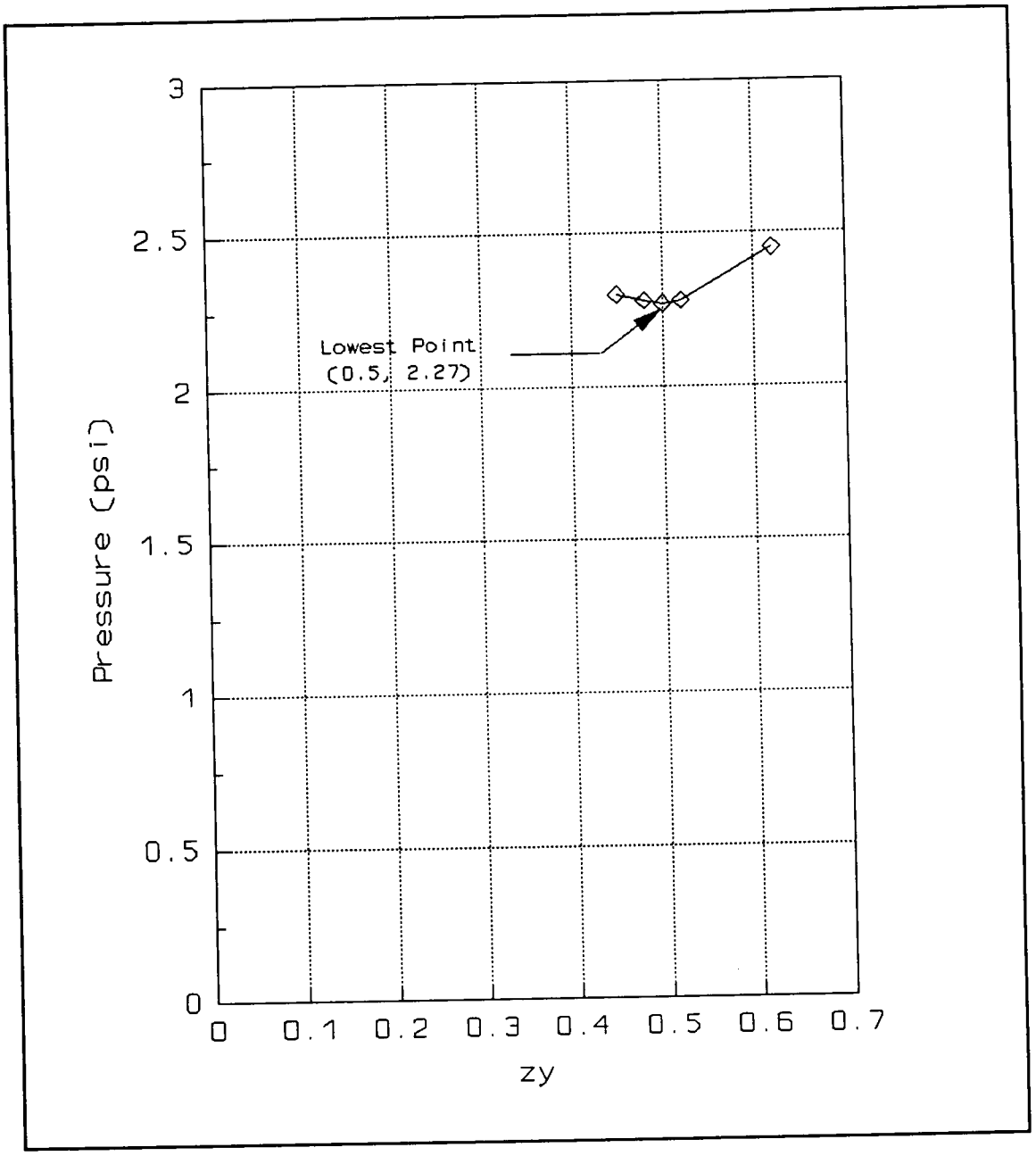


Figure 3.3.2 Pressure Versus zy, Mode A of Panel 28'x12' (Assuming zx1 = zx2 = 0.3)

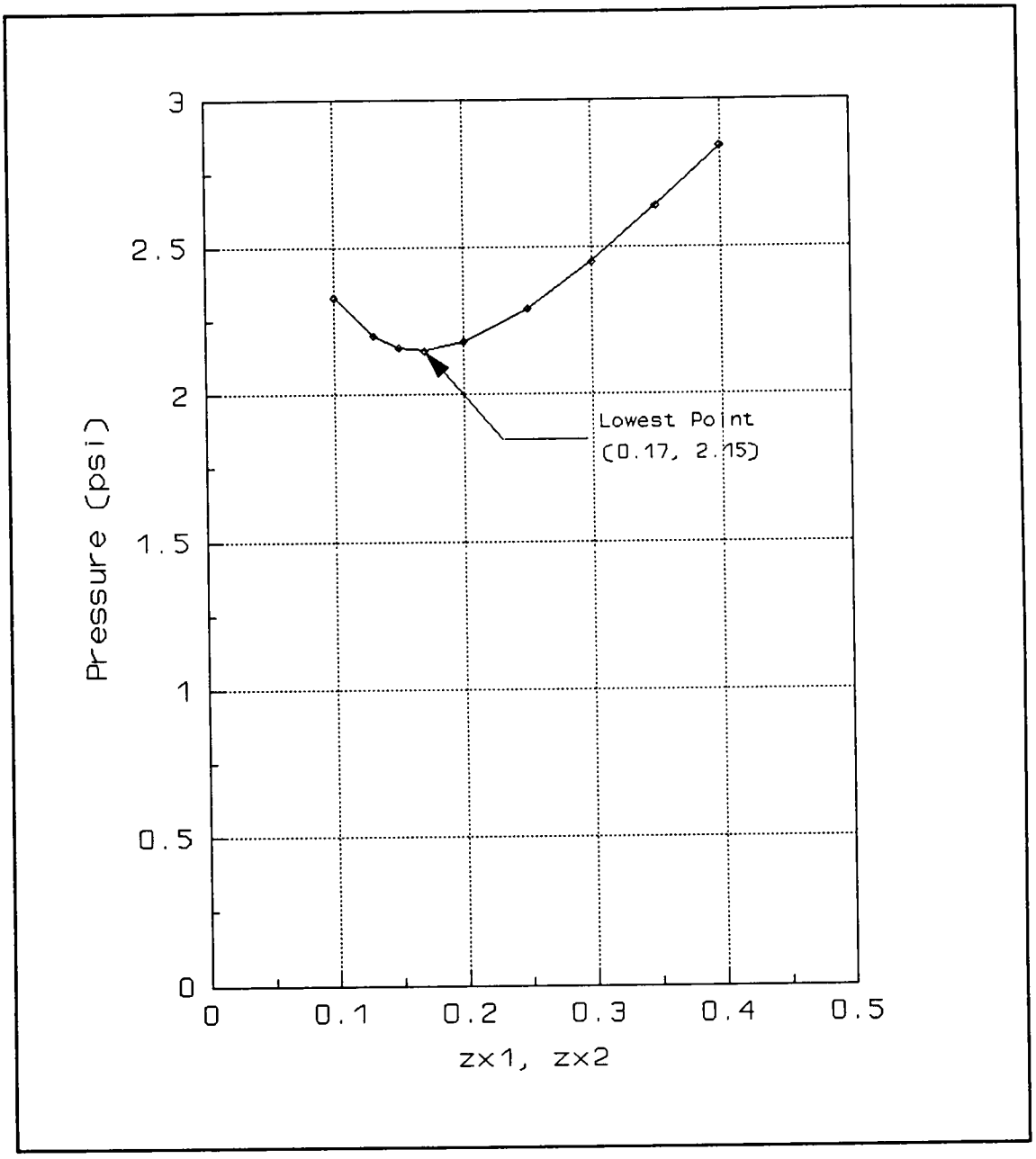


Figure 3.3.3 Pressure Versus zx1 and zx2, Mode A of Panel 28'x12' (Assuming zy = 0.62)

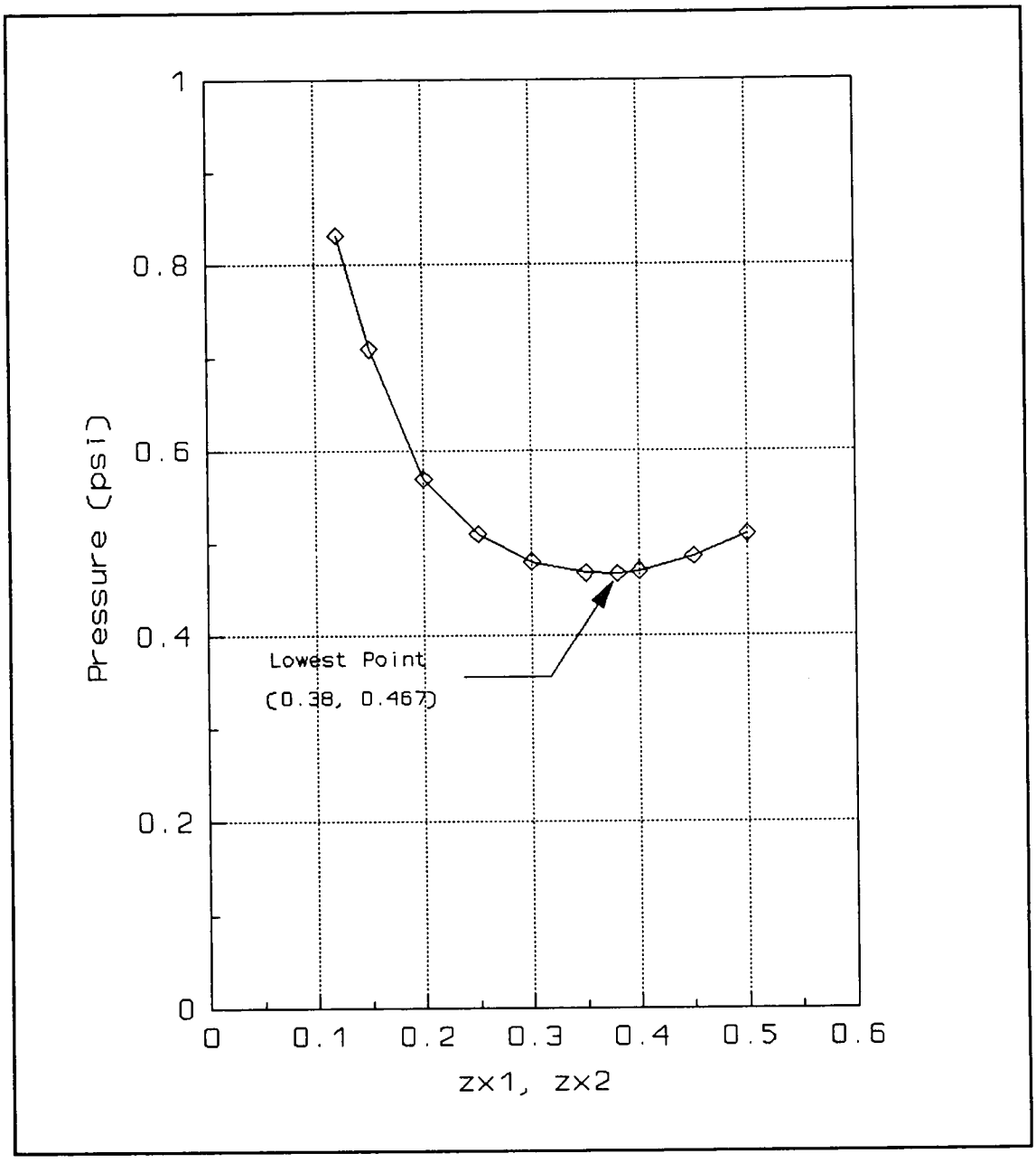


Figure 3.3.4 Pressure Versus zx1 and zx2, Mode C of Panel 28'x12' (Assuming zy = 0.5)

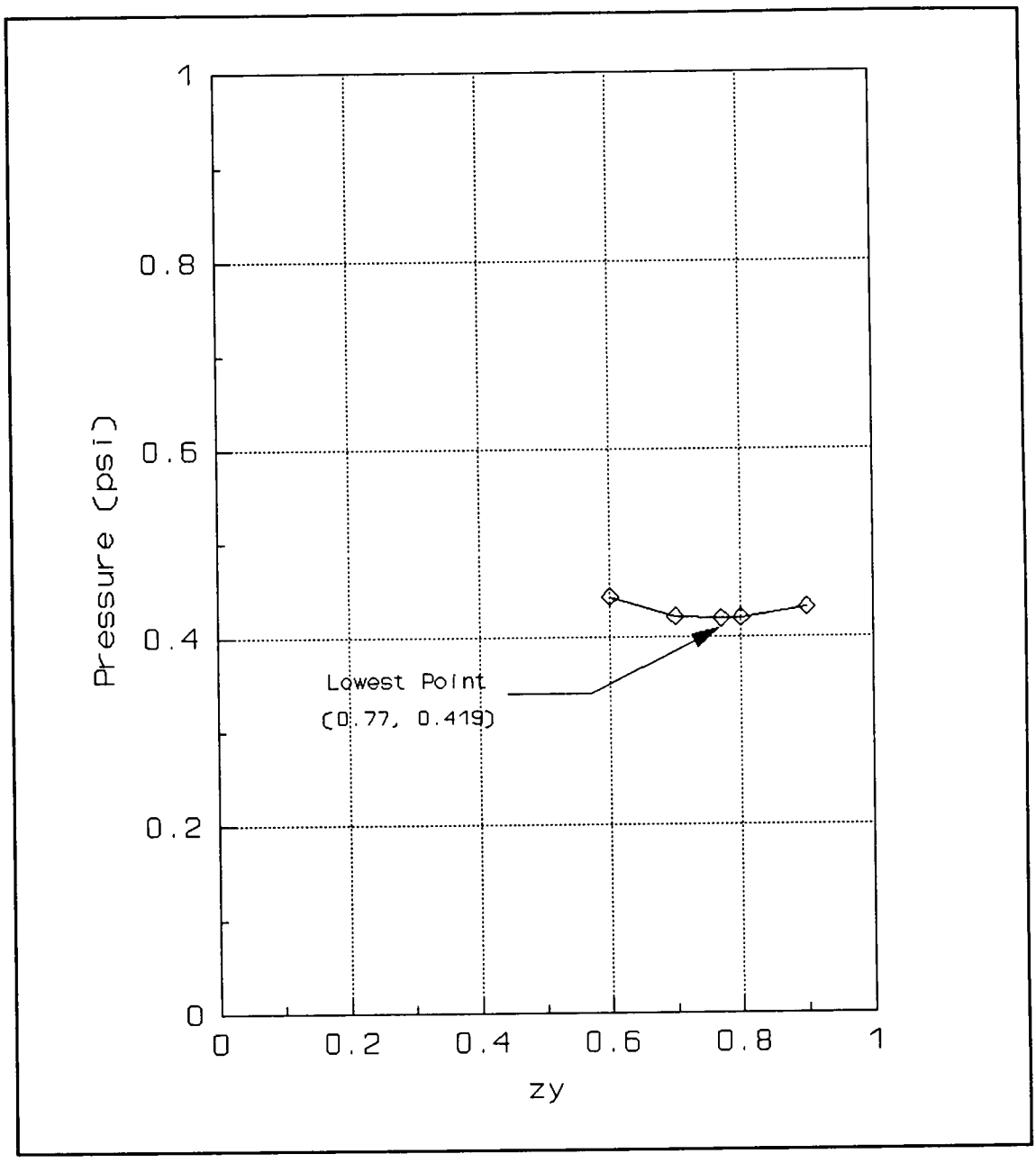


Figure 3.3.5 Pressure Versus zy, Mode C of Panel 28'x12' (Assuming zx1 = zx2 = 0.38)

TABLE 3.3.1

EFFECTS OF COEFFICIENT OF FRICTION ON ULTIMATE PRESSURE FOR PANEL 28'x12' IN BUILDING 9207

COEFFICIENT OF FRICTION	ULTIMATE PRESSURE (Psi)			
	MODE A	MODE B	MODE C	MODE D
0.0	2.023	----	0.420	1.013
0.25		----	0.646	
0.5		----	0.905	

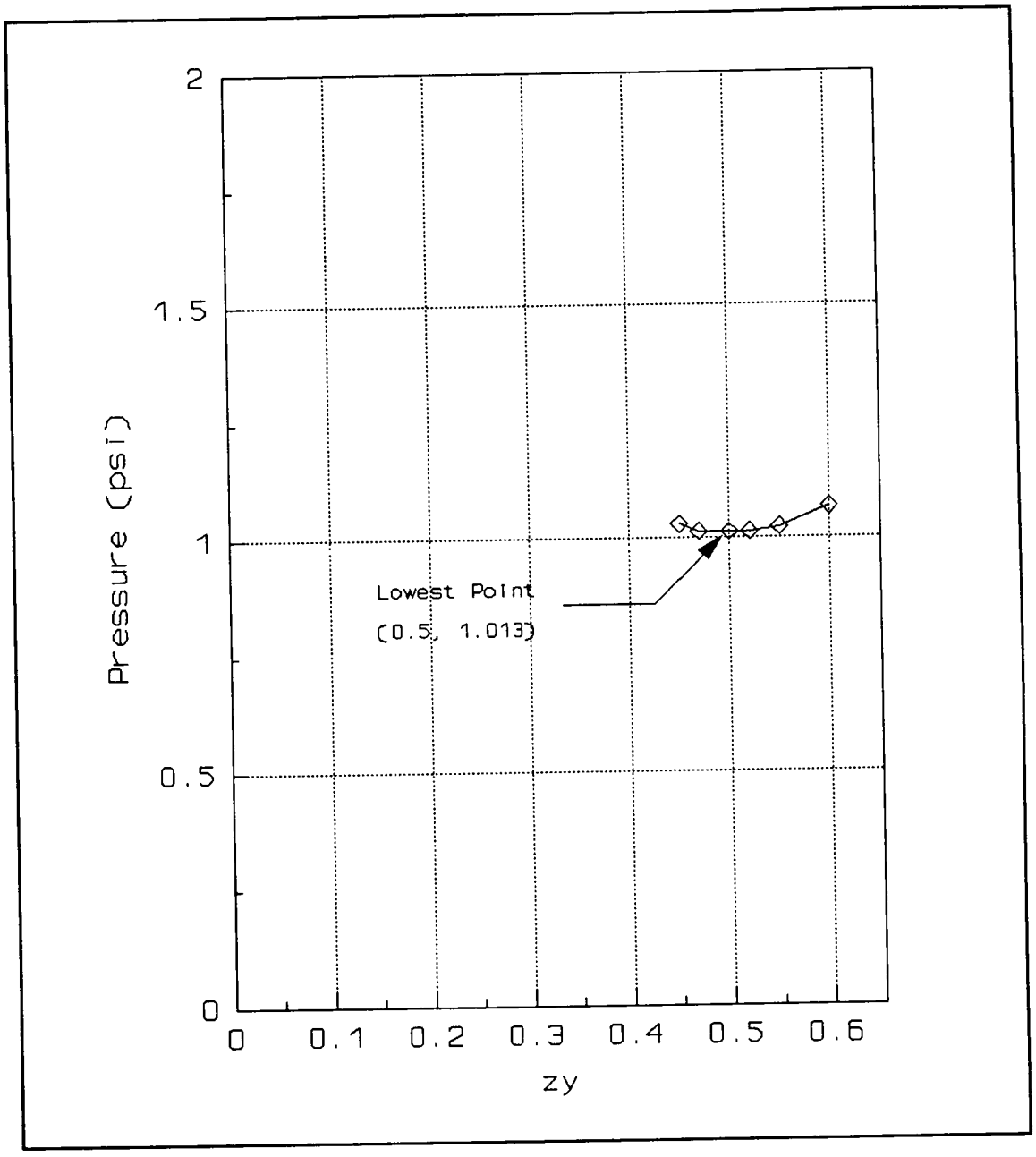


Figure 3.3.6 Pressure Versus zy, Mode D of Panel 28'x12'

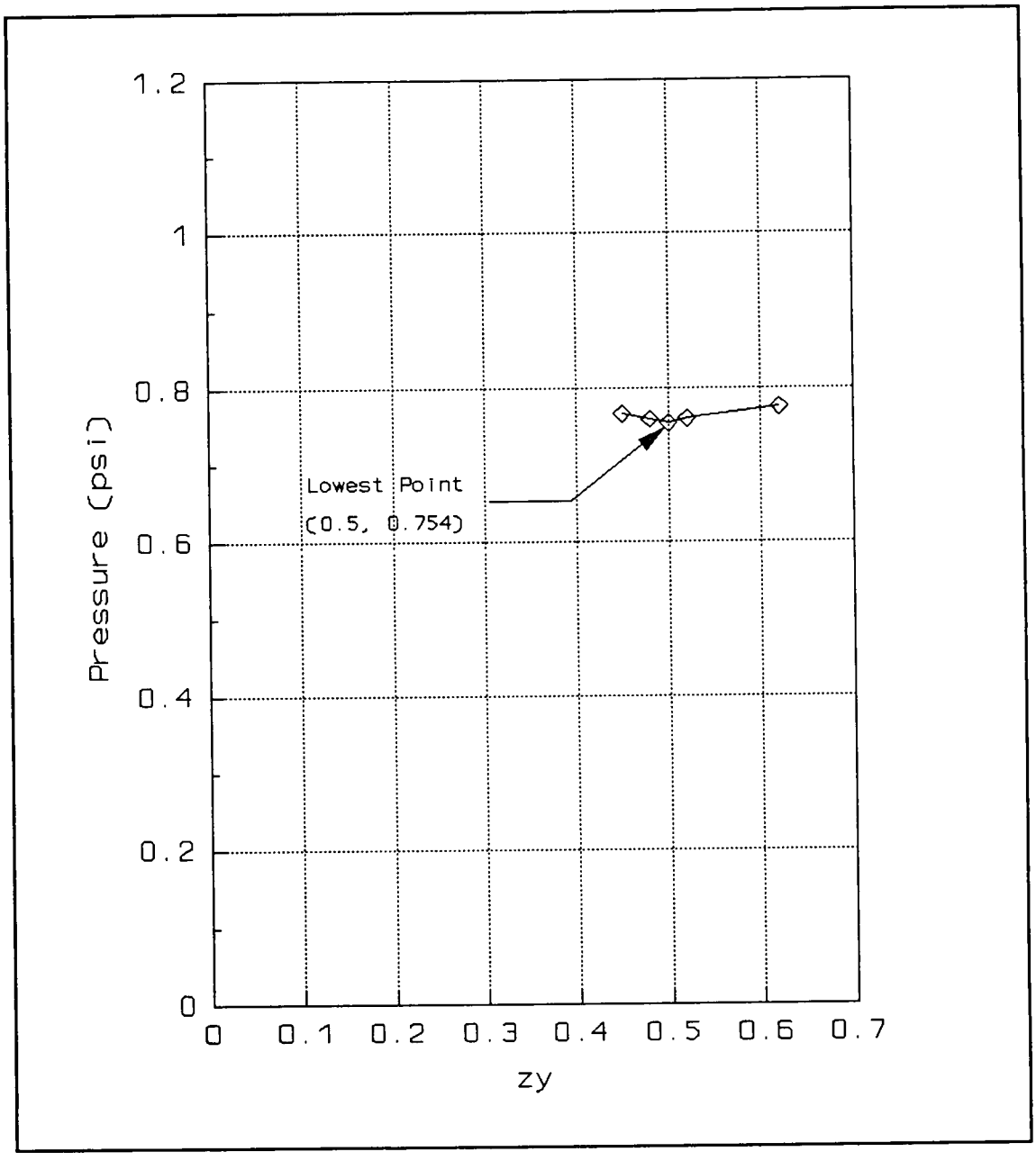


Figure 3.3.7 Pressure Versus zy, Mode A of Panel 24'x20.5' (Assuming zx1 = zx2 = 0.25)

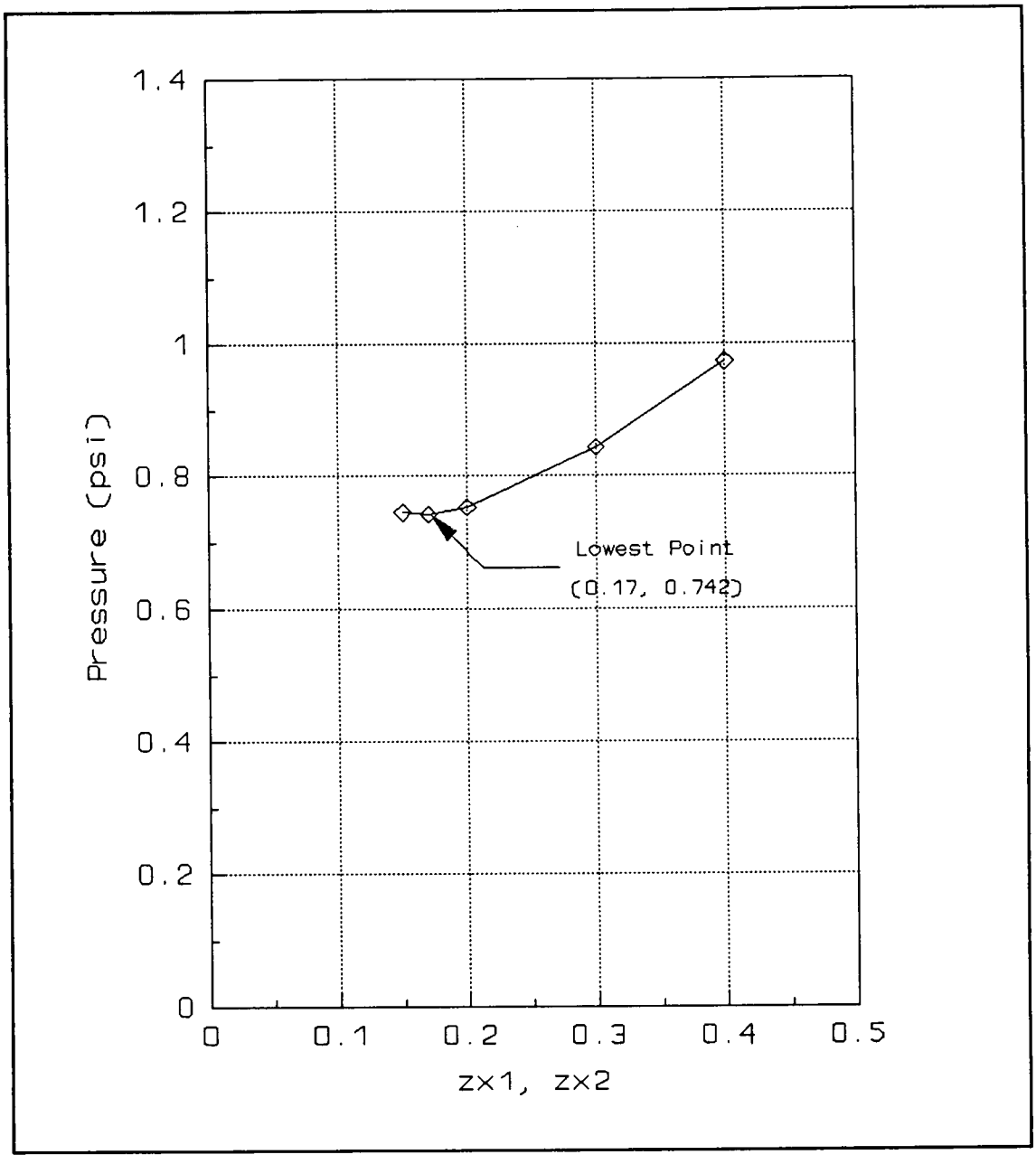


Figure 3.3.8 Pressure Versus zx1 and zx2, Mode A of Panel 24'x20.5' (Assuming zy = 0.5)

fracture line pattern and the dimensions of zx and zy were determined as in Figure 3.3.9, or zx=0.5, zy=0.9. The ultimate load capacity is also drastically reduced from Mode A, about 80%. The ultimate load capacity is also found to be a function of the coefficient of friction at the top interface of the wall panel such as shown in Table 3.3.2. The distance of zy for mode D was determined as shown in Figure 3.3.10. The ultimate load capacity was reduced to approximately one-third of the capacity of mode A.

The fracture line pattern for various modes of failures were examined and it is shown that slippage at the interface between the infills and the surrounding steel frame are important. If slippage occurs, the ultimate load capacity will be reduced significantly. Therefore, it is desirable to pay particular attention to the interface conditions, and to monitor the behavior at the interface between the infills and frame members during testing. Mode A is considered to be the most likely failure mode, therefore it is assumed to be the failure mode to predict the ultimate load capacity, maximum deflection and parametric study of the variables in the following.

3.3.3 Estimated Ultimate Strength

The predicted load-deflection curve for the infilled wall panel in building 9207 is shown in Figure 3.3.11, and for

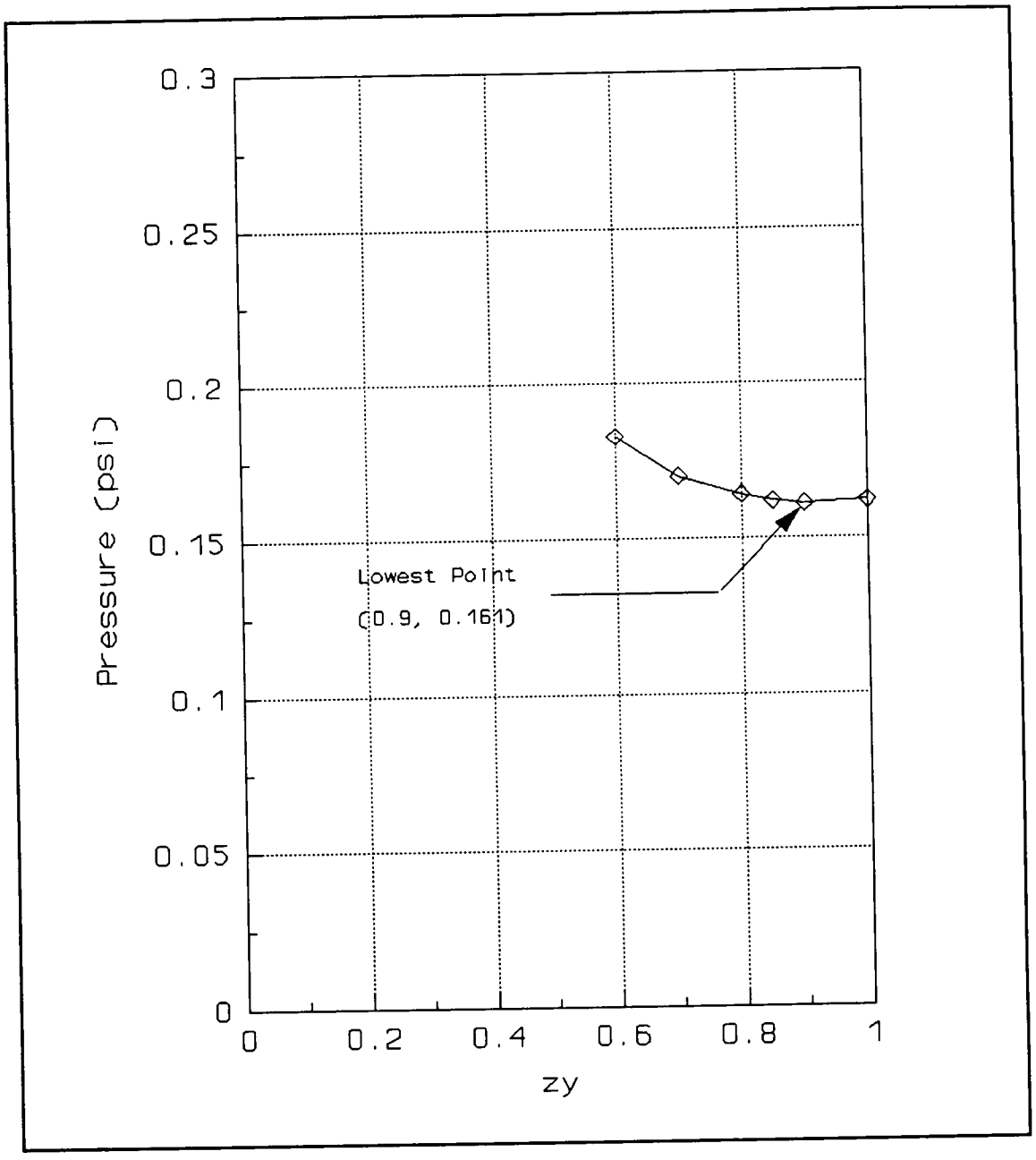


Figure 3.3.9 Pressure Versus zy, Mode B of Panel 24'x20.5' (Assuming zx = 0.5)

TABLE 3.3.2

EFFECTS OF COEFFICIENT OF FRICTION ON ULTIMATE PRESSURE FOR PANEL 24'x20.5' IN BUILDING 9212

COEFFICIENT OF FRICTION	ULTIMATE PRESSURE (PSI)			
	MODE A	MODE B	MODE C	MODE D
0.0	0.743	0.162	----	0.275
0.25		0.190	----	
0.5		0.221	----	

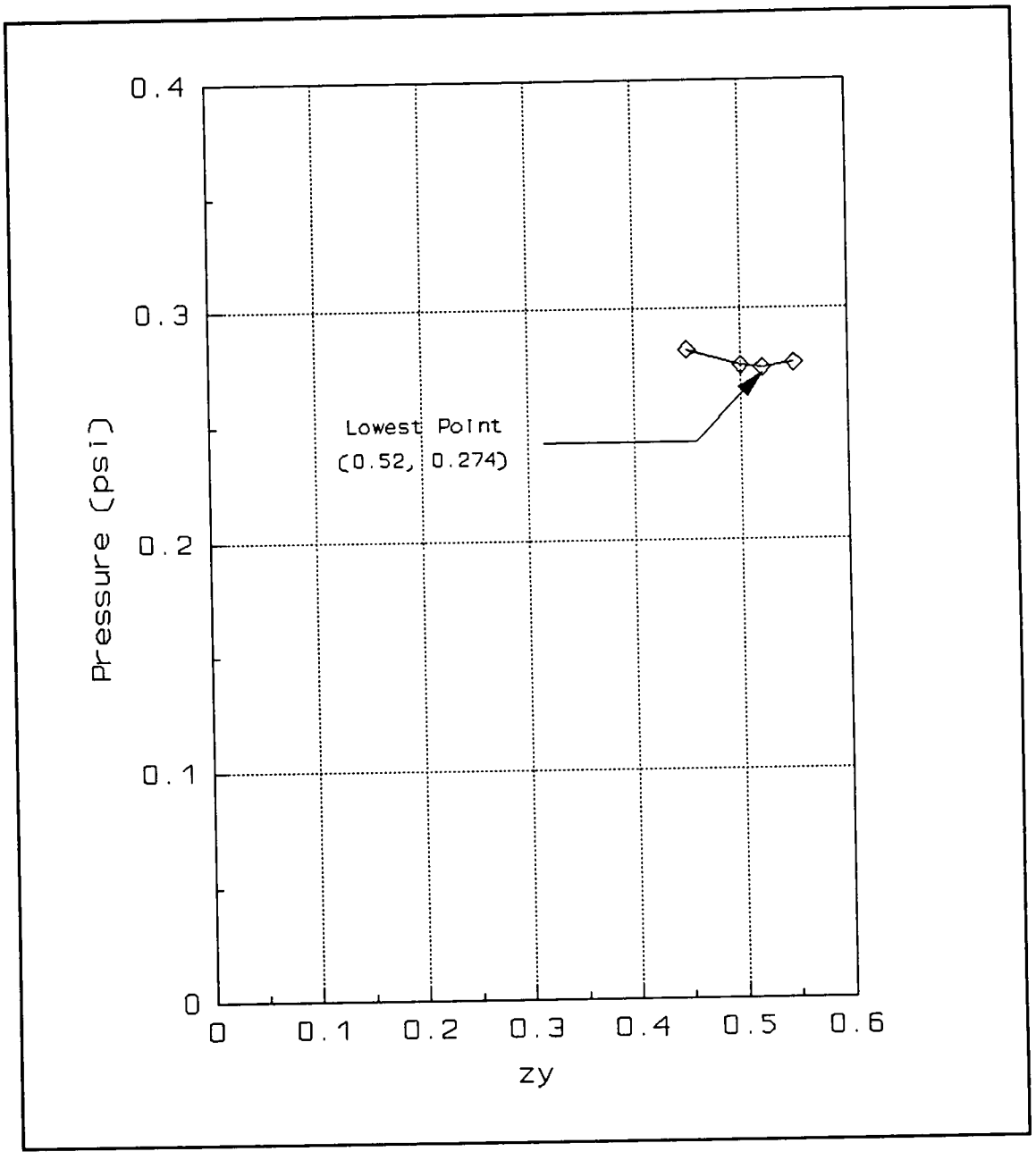


Figure 3.3.10 Pressure Versus zy, Mode D of Panel 24'x20.5'

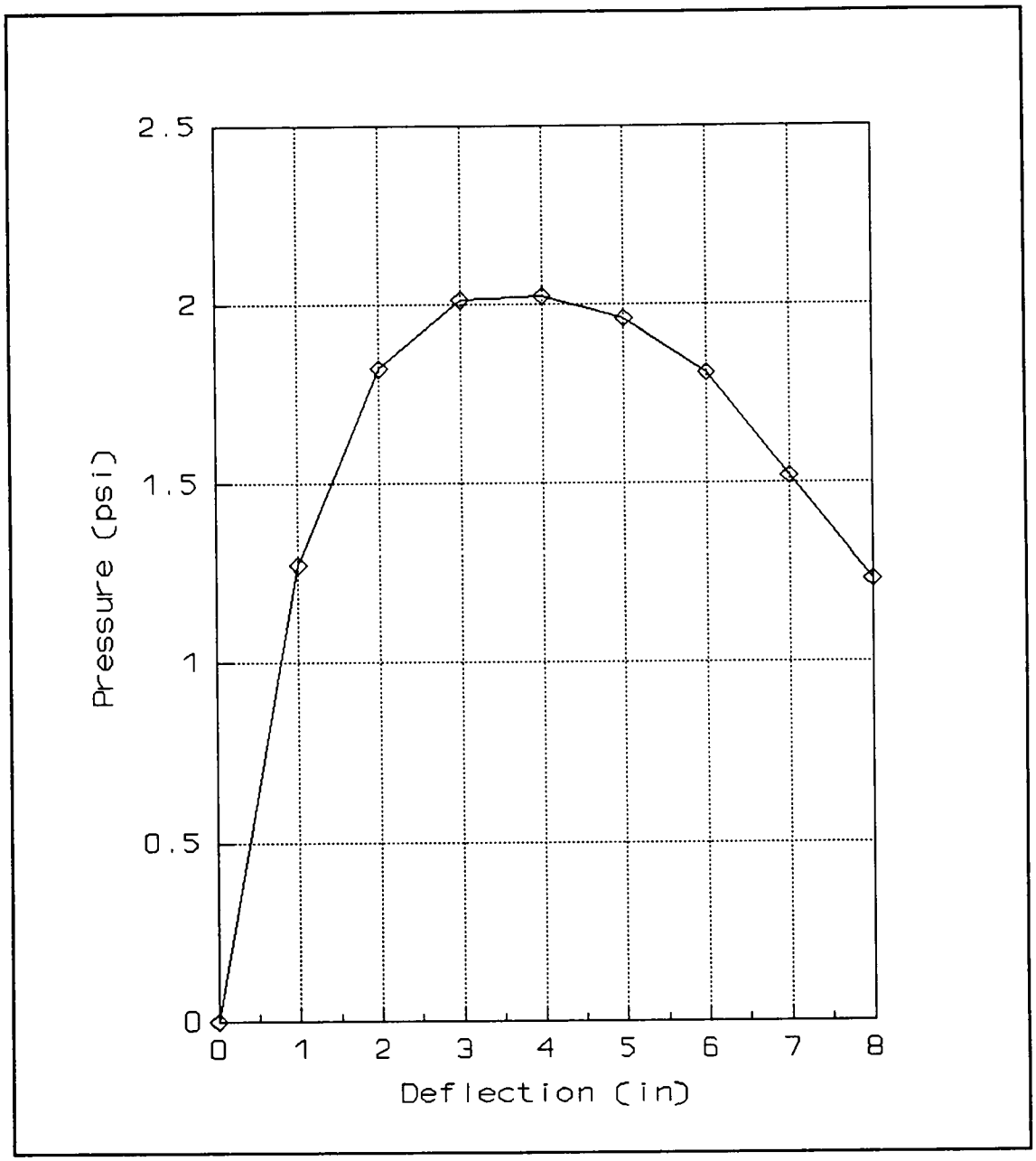


Figure 3.3.11 Pressure Versus Deflection for Wall Panel in Building 9207

building 9212 in Figure 3.3.12. In building 9207, the deflection at the maximum load centered around 3.0 inch to 5.0 inch with the ultimate pressure being about 2 psi, or approximately a total of 93 kips on the wall. The wall in 9212 displayed a broader range of deflection, ranging from 4.0 inch to 15.0 inch with a maximum pressure being approximately 0.74 psi, or approximately a total load of 51 kips.

Equation 3.2.2 (Dawe and Seah, 1989) was adopted and modified to accommodate the English Unit System as shown below:

$$q_{ult} = 800\,(f'_m)^{0.75}\,t^2\,(\alpha/L^{2.5} + \beta/H^{2.5}) \qquad [3.3.1]$$

where

$$\alpha = \frac{1}{H}(EI_cH^2+GJ_ctH)^{0.25} \quad \leq \quad 6.12$$

$$\beta = \frac{1}{L}(EI_bL^2+GJ_btL)^{0.25} \quad \leq \quad 6.12$$

q_{ult} = *ultimate load (Psi)*
t = *panel thickness (in)*
L = *panel length (in)*
H = *panel height (in)*
E = *Young's modulus of frame member (Ksi)*
G = *Shear modulus of frame member (Ksi)*
I_c, I_b = *Moments of inertia of columns and beams respectively* (in^4)
J_c, J_b = *Torsional constants of columns and beams respectively* (in^4)

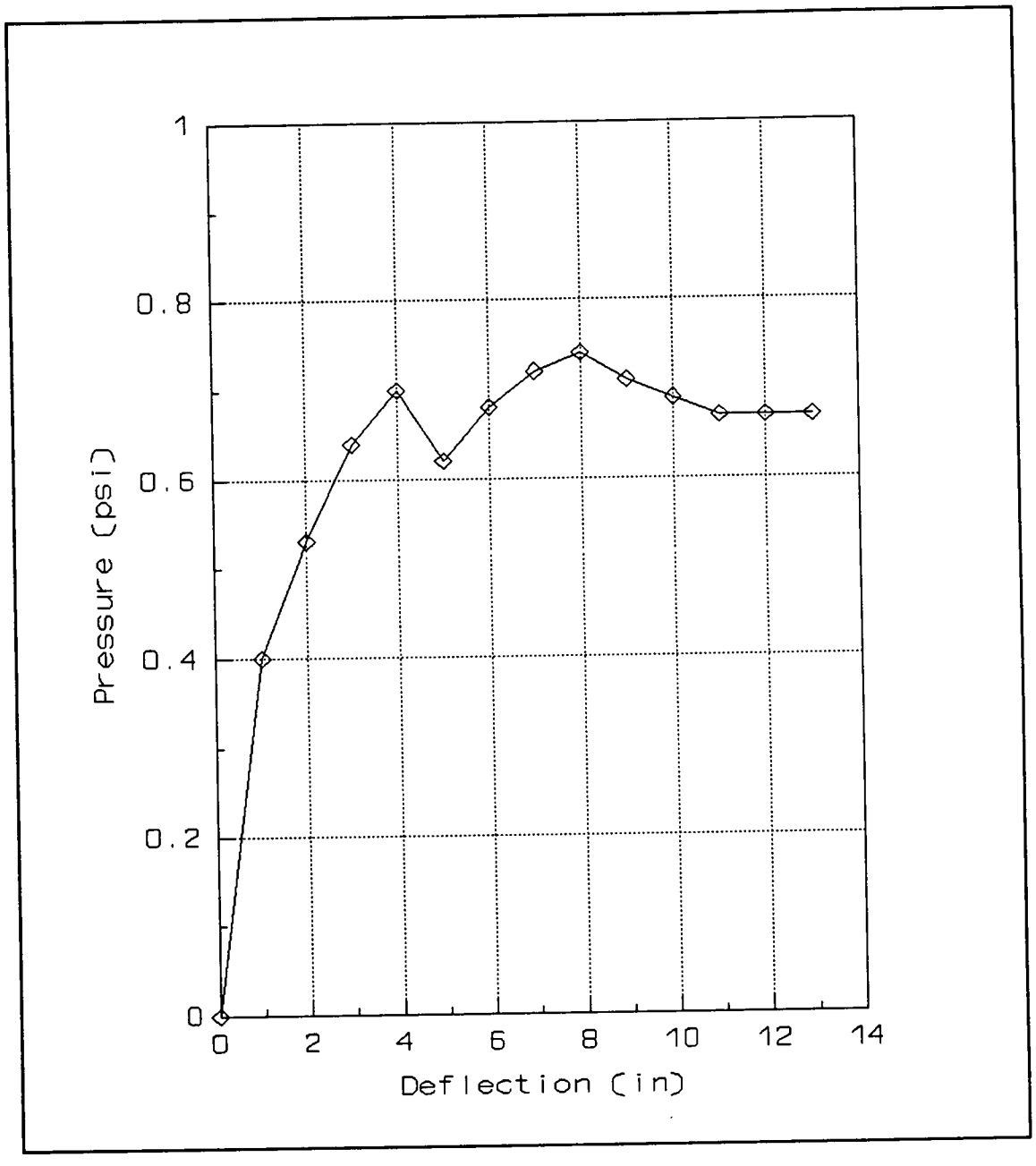


Figure 3.3.12 Pressure Versus Deflection for Wall Panel in Building 9212

The ultimate pressure predicted by Equation 3.3.1 was compared to the ultimate failure capacity predicted above. The ultimate strength for the 28 ft.x 12 ft. wall panel in Building 9207 was determined as 1.37 psi using Equation 3.3.1, about 47% less than the predicted ultimate load capacity. For the 24 ft.x 20.5 ft. wall panel in Building 9212, the ultimate load capacity was found to be around 0.6 psi, about 24% less than the predicted value of 0.74 psi. Thus the empirical equation gives a conservative estimate of the ultimate load, and it serves the purpose of preliminary estimation of the failure strength of an infilled masonry wall. It can also be used as a tool to check the design of masonry infilled walls simply supported on four sides.

3.3.4 In-plane Membrane Action

The in-plane forces developed due to the arching effects of the infills may induce adverse effects on the adjacent wall panels or panels on the floor above the test wall panel. The test wall panels in building 9207 and building 9212 were divided into 20 horizontal strips and 20 vertical strips and the axial thrust was calculated for each strip. The corresponding in-plane axial thrust per strip was determined when the ultimate strength and the maximum deflection were achieved. The forces for the 28 ft. x 12 ft. panel are plotted in Figure 3.3.13. The maximum horizontal in-plane

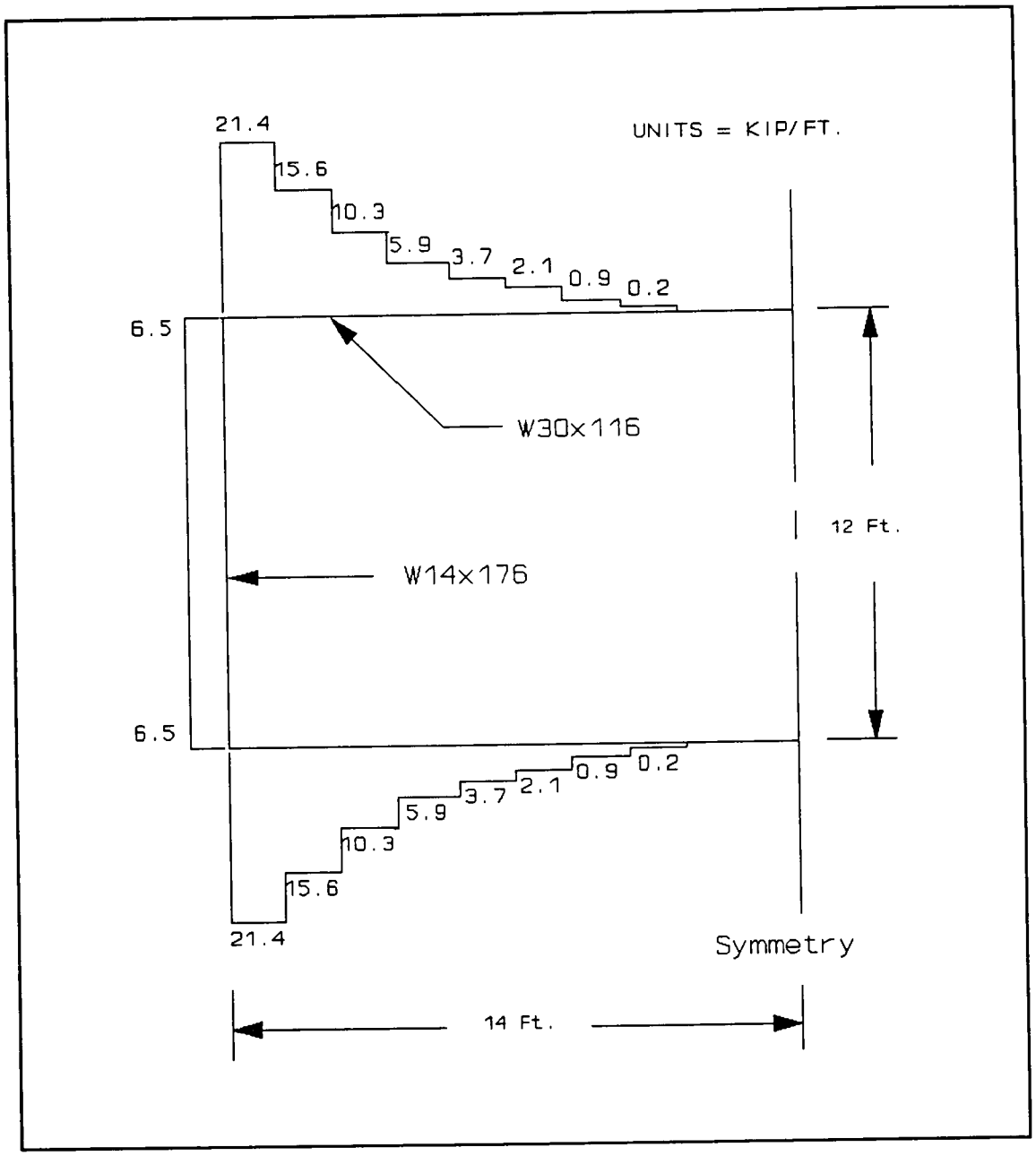


Figure 3.3.13 In-Plane Compressive Forces in Panel 28'x12'

force is 6.5 kips per foot, constant along the columns. In vertical direction, however, there was an in-plane force of 21.4 kips per foot at both ends of the panel, but this dropped off to zero near the mid-length of the panel.

In the parametric study, the effects of different steel frame sizes are examined. A brief examination of the effects of steel frame sizes on in-plane forces is conducted here. Increasing the top beam to a W36x300 results in no change in the axial thrust on the columns. The maximum in-plane force in vertical direction is approximately the same, 20 kips per foot at both ends of the panel. There is less of a decrease, and a 2.8 kips per foot force exists at the center of the panel. The axial thrusts are shown in Figure 3.3.14.

For the 24 ft. x 20.5 ft. wall panel, the distribution of the in-plane forces is plotted in Figure 3.3.15. The in-plane forces exerted on the columns and beams are critical around the corners of the panel primarily because the panel is relatively square. The maximum in-plane force is approximately 9 and 25 kips per foot in the horizontal and vertical directions respectively, and dropping off rapidly to zero within the next two strips towards the center of the panel. Increasing the top beam to a W36x300 causes a decrease in the maximum horizontal axial thrust of 20%. The maximum axial thrust for the vertical strips at both ends is also reduced by 20%, but the forces are distributed across the

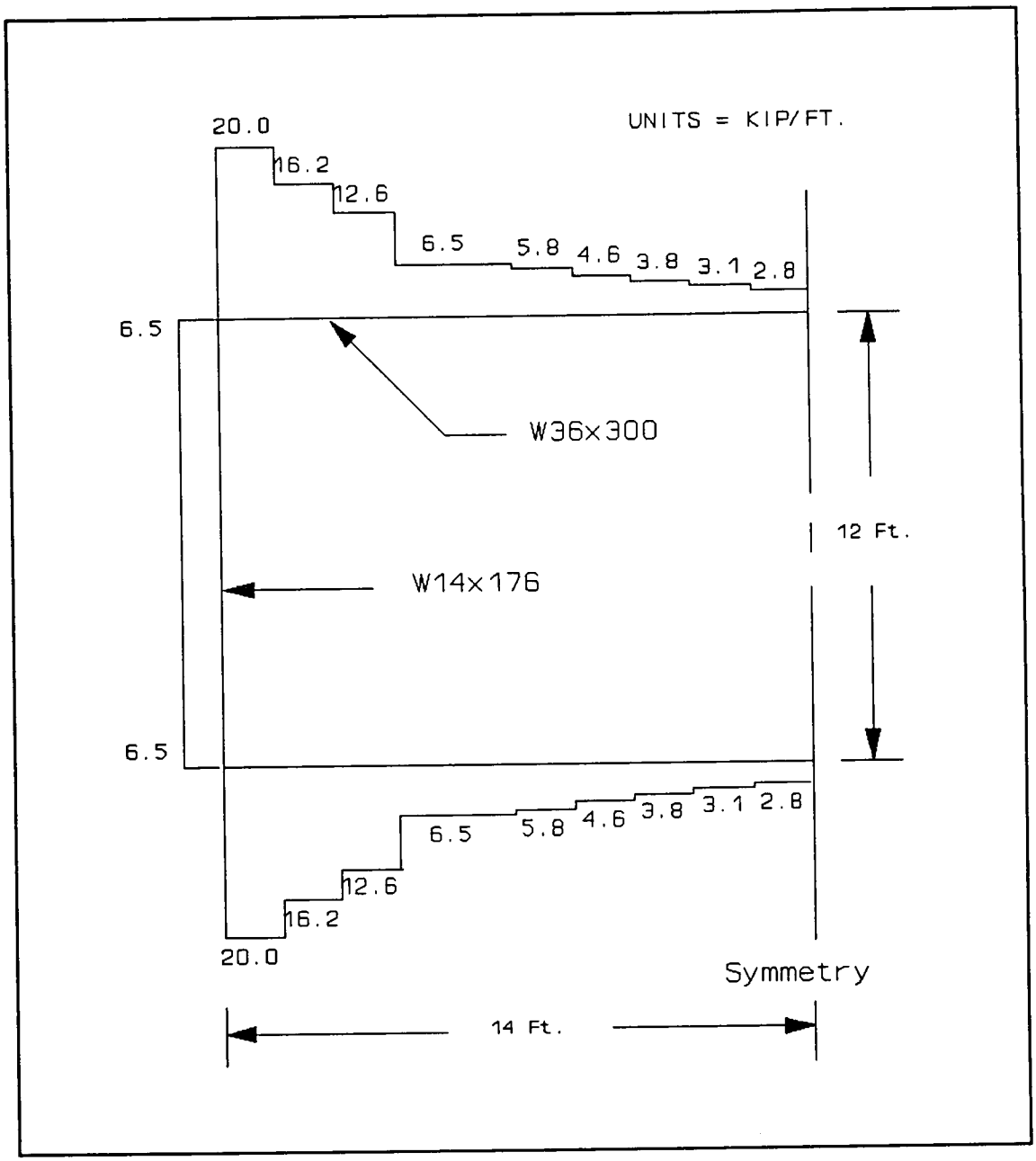


Figure 3.3.14 In-Plane Compressive Forces in Panel 28'x12', Top Beam = W36x300

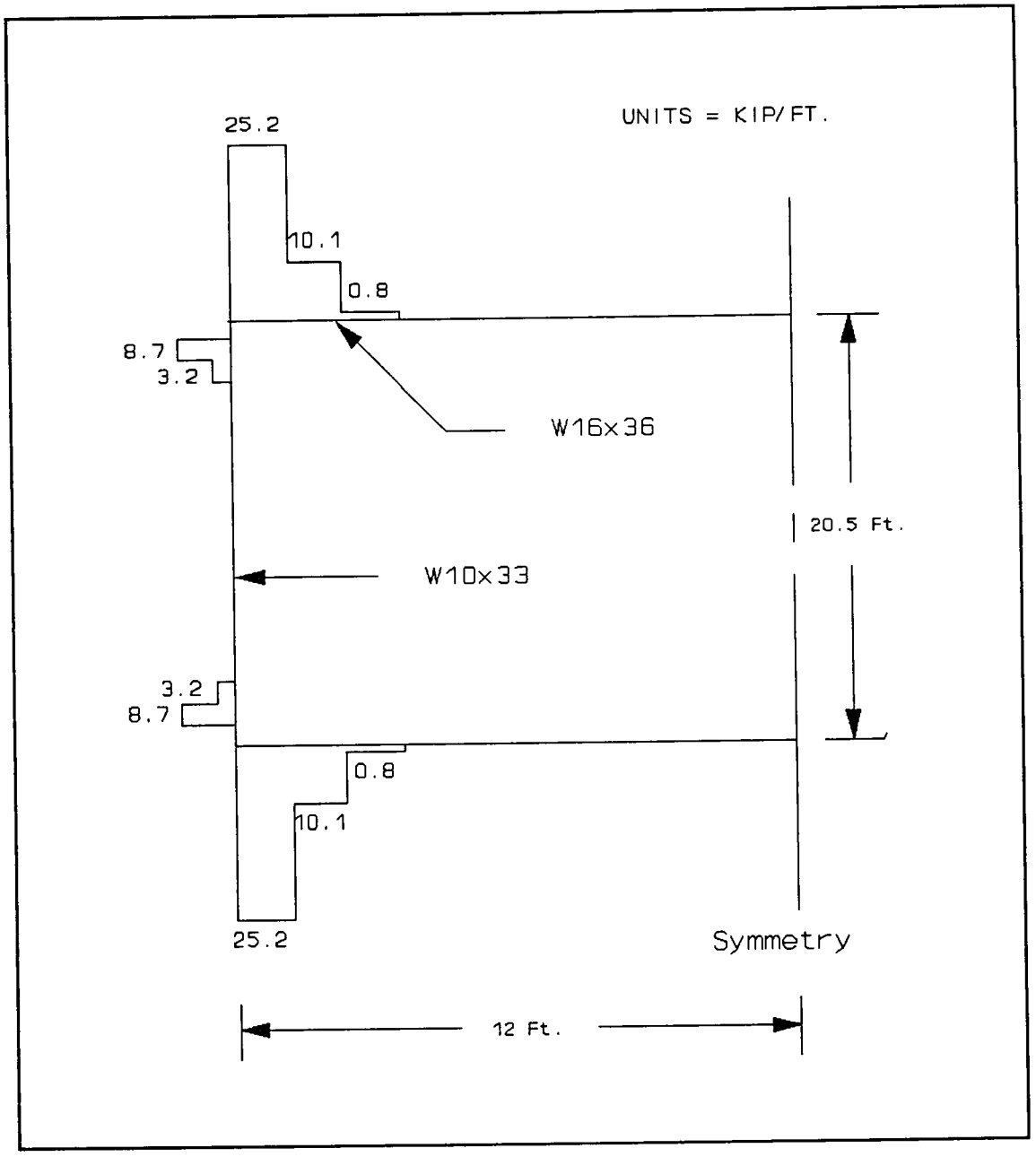


Figure 3.3.15 In-Plane Compressive Forces in Panel 24'x20.5'

entire beam, from 21 kips per foot at the corner to 4 kips per foot near the center, rather than concentrated at the corners. The plot in Figure 3.3.16 shows the distribution of the in-plane forces. Increasing the column sizes to W36x300's on both sides of the panel distributes the in-plane forces to most of the horizontal strips with a maximum force about 9 kips per foot at the top and bottom, and a minimum force about 1.5 kips per foot at the mid-height of the panel. The vertical strips experience a maximum of 16 kips per foot at both ends, which decreases rapidly to zero in next two strips towards the center of the panel. The distribution of in-plane forces is shown in Figure 3.3.17.

With the assumptions of the infills and enclosing frame members properties, the maximum in-plane uniform forces due to arching action exerted on the columns are estimated as 6.5 kips per foot and 9 kips per foot for the panels in building 9207 and 9212 respectively. The maximum axial thrust on the top and bottom beams are approximately 22 kips per foot and 25 kips per foot for panels in building 9207 and 9212 respectively.

3.3.5 Parametric Study

Several parameters suspected to be significant in determining the lateral resistance of the unreinforced hollow clay tile infilled wall panels were investigated. Among the

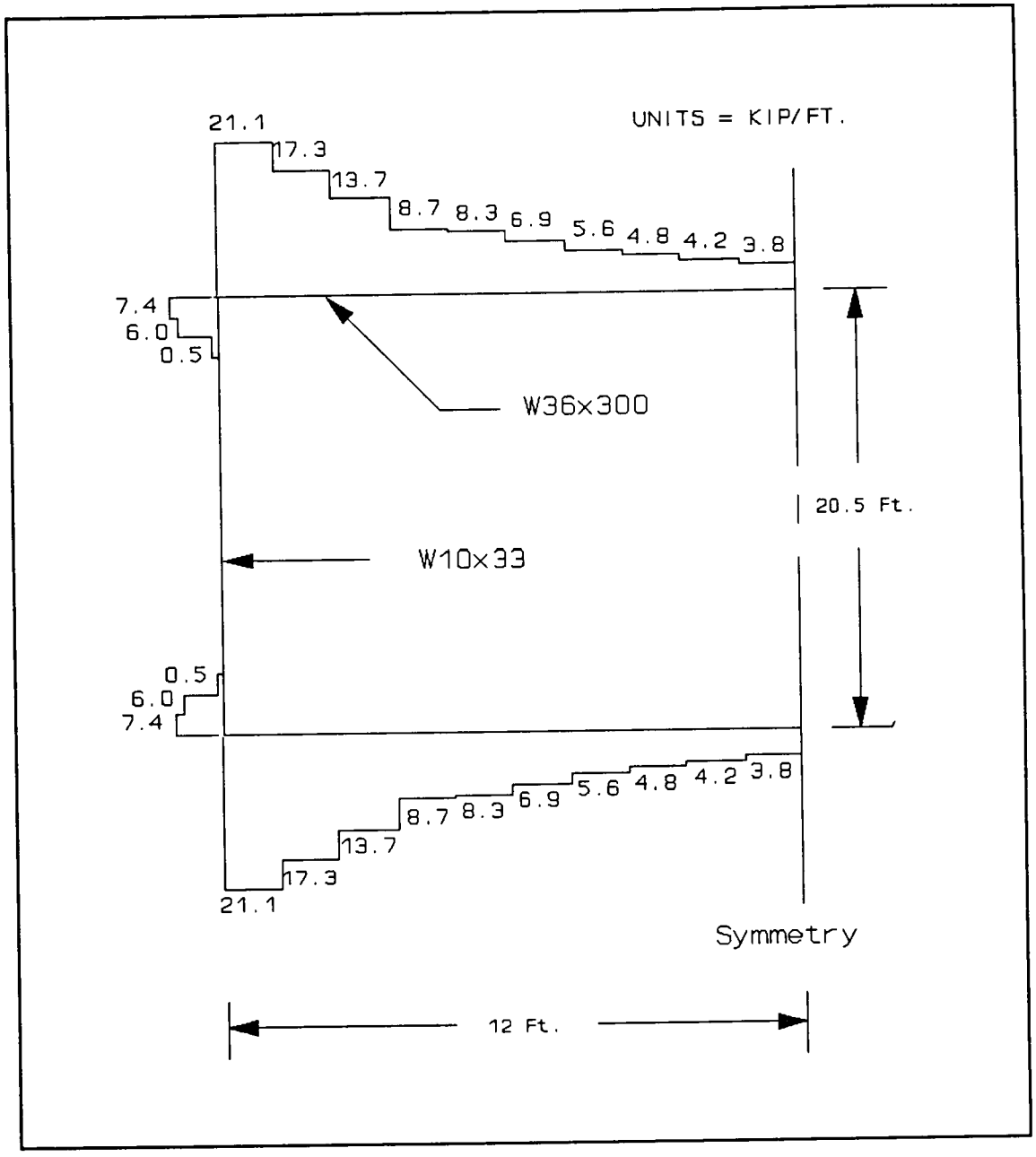


Figure 3.3.16 In-Plane Compressive Forces in Panel 24'x20.5', Top Beam = W36x300

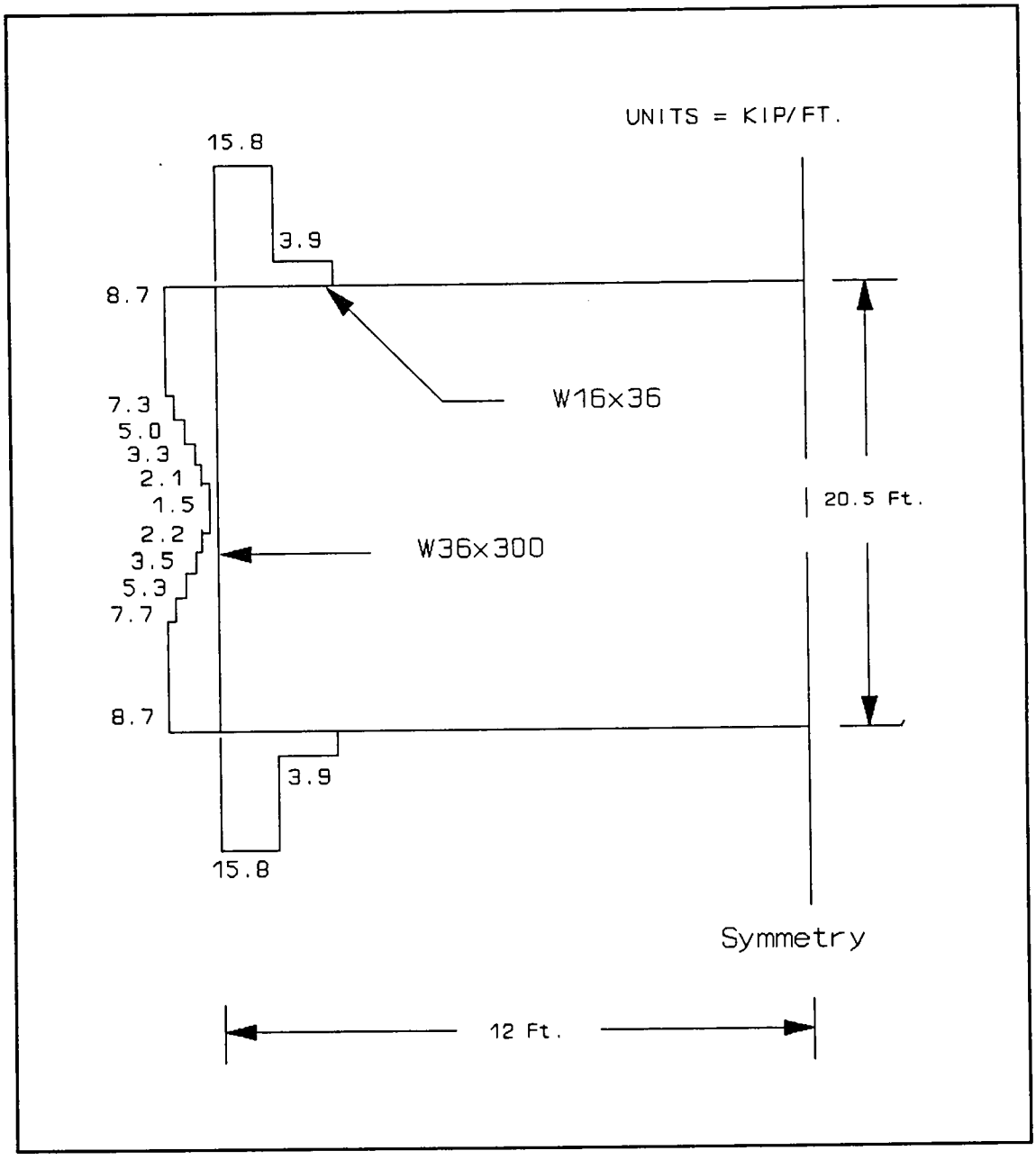


Figure 3.3.17 In-Plane Compressive Forces in Panel 24'x20.5', Column Sizes = W36x300's

parameters studied were compressive strength, modulus of elasticity, face shell thickness of the infills, and the member sizes of the steel frame.

(i) Compressive Strength

The compressive strength of the hollow clay tile masonry was found to be the main factor in determining the ultimate load capacity of the 28 ft. x 12 ft. wall panel in building 9207 as well as the 24 ft. x 20.5 ft. wall panel in building 9212. For compressive strengths between 500 and 3000 psi, an increase of compressive strength of 100 psi resulted in an approximate increase of 0.091 psi in ultimate load capacity of the wall panel in building 9207, as shown in Figure 3.3.18. Predicted load-deflection curves are shown in Figure 3.3.19 and Figure 3.3.20. There was an average increase of 0.034 psi in ultimate load capacity of the wall panel in building 9212 for an increase of 100 psi in the compressive strength. In other words, doubling the compressive strength from 1000 psi to 2000 psi would result in approximately a 50% increase in the ultimate capacity of the wall panel. The maximum deflection shifted from 3 inch to 5 inch with the increase of compressive strength for the wall panel in building 9207, whereas in building 9212 the maximum deflection occurred around the range of 4 inch to 6 inch.

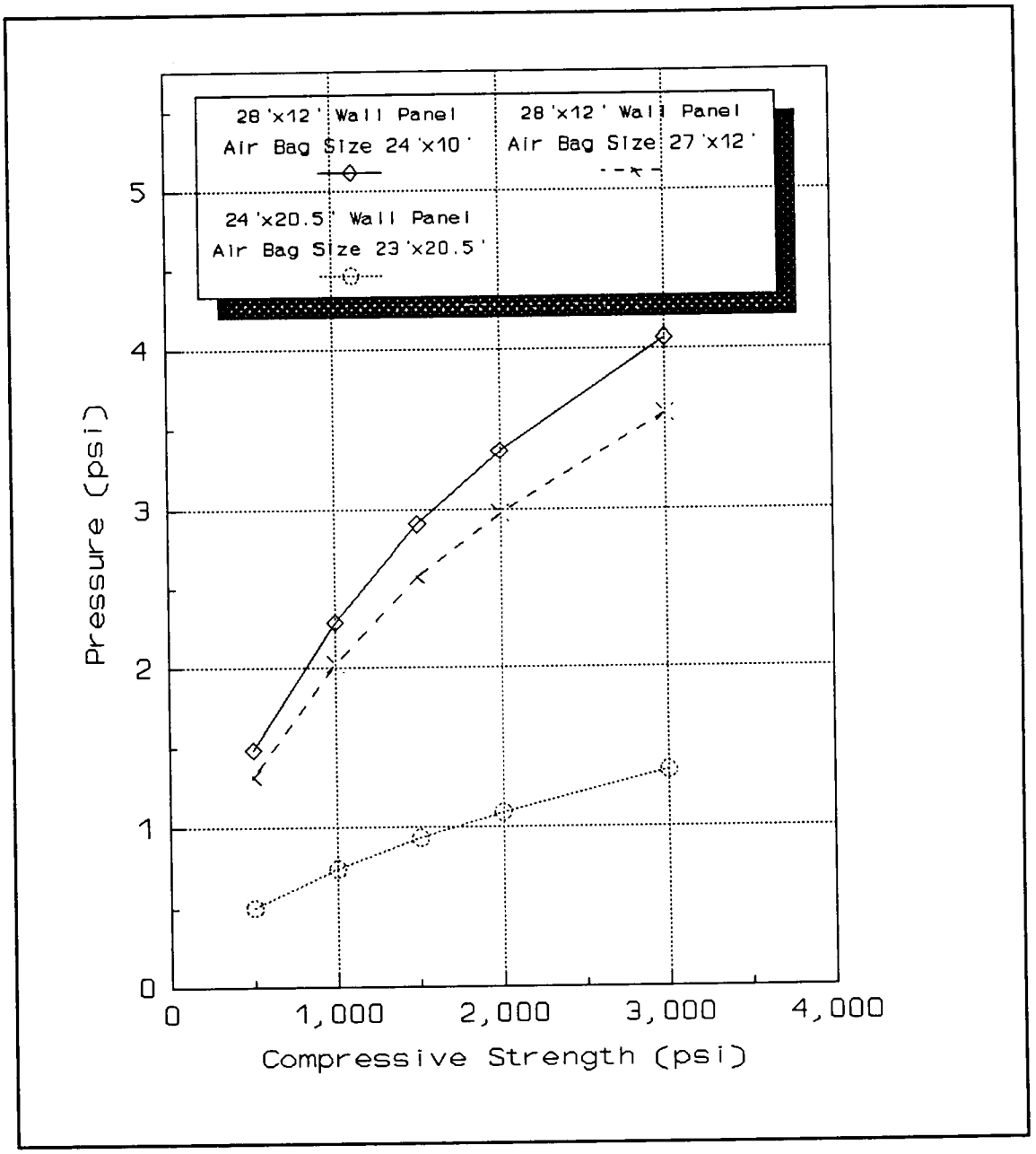


Figure 3.3.18 Pressure Versus Compressive Strength

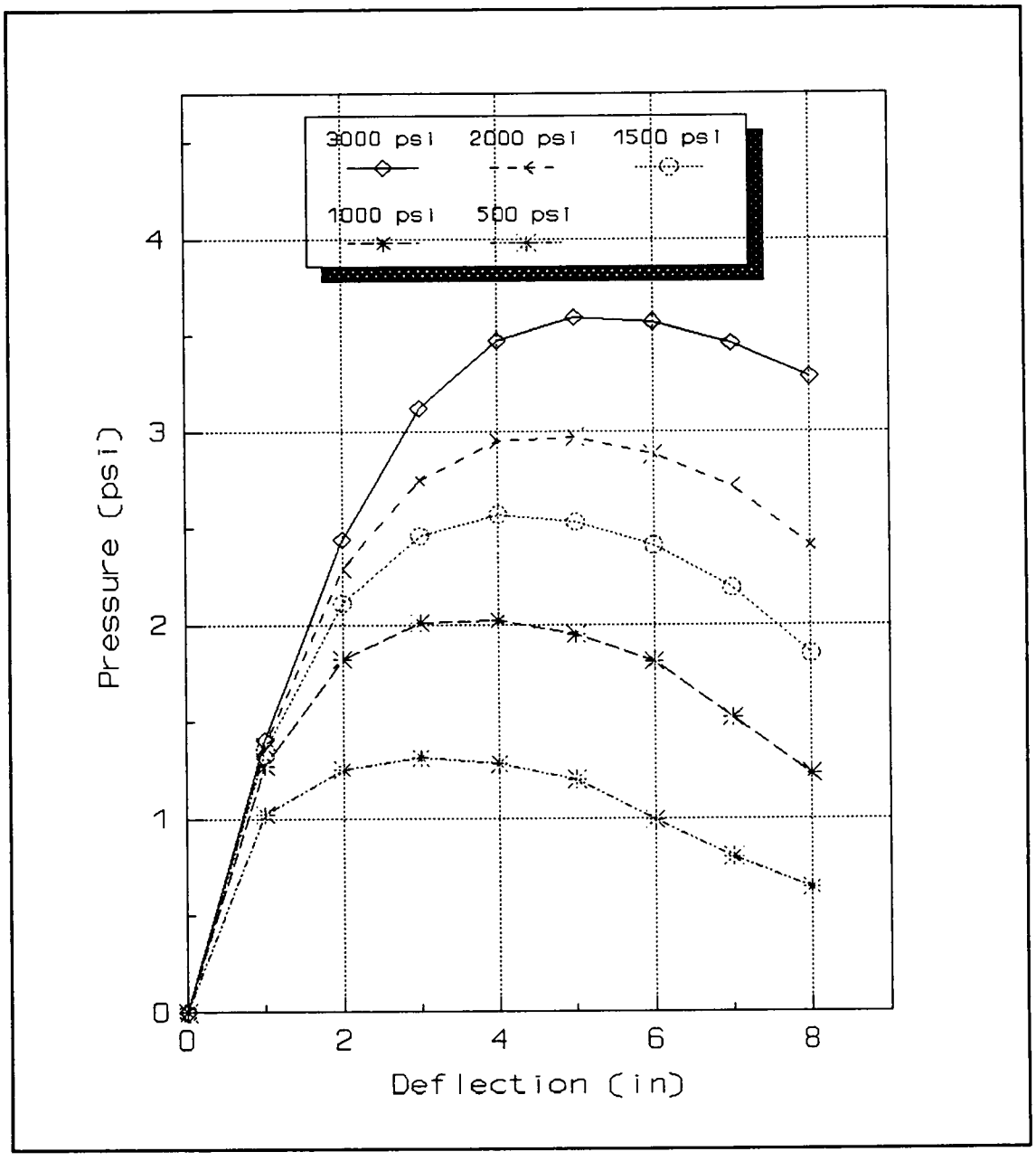


Figure 3.3.19 Pressure Versus Deflection with Various Compressive Strength for Panel 28'x12'

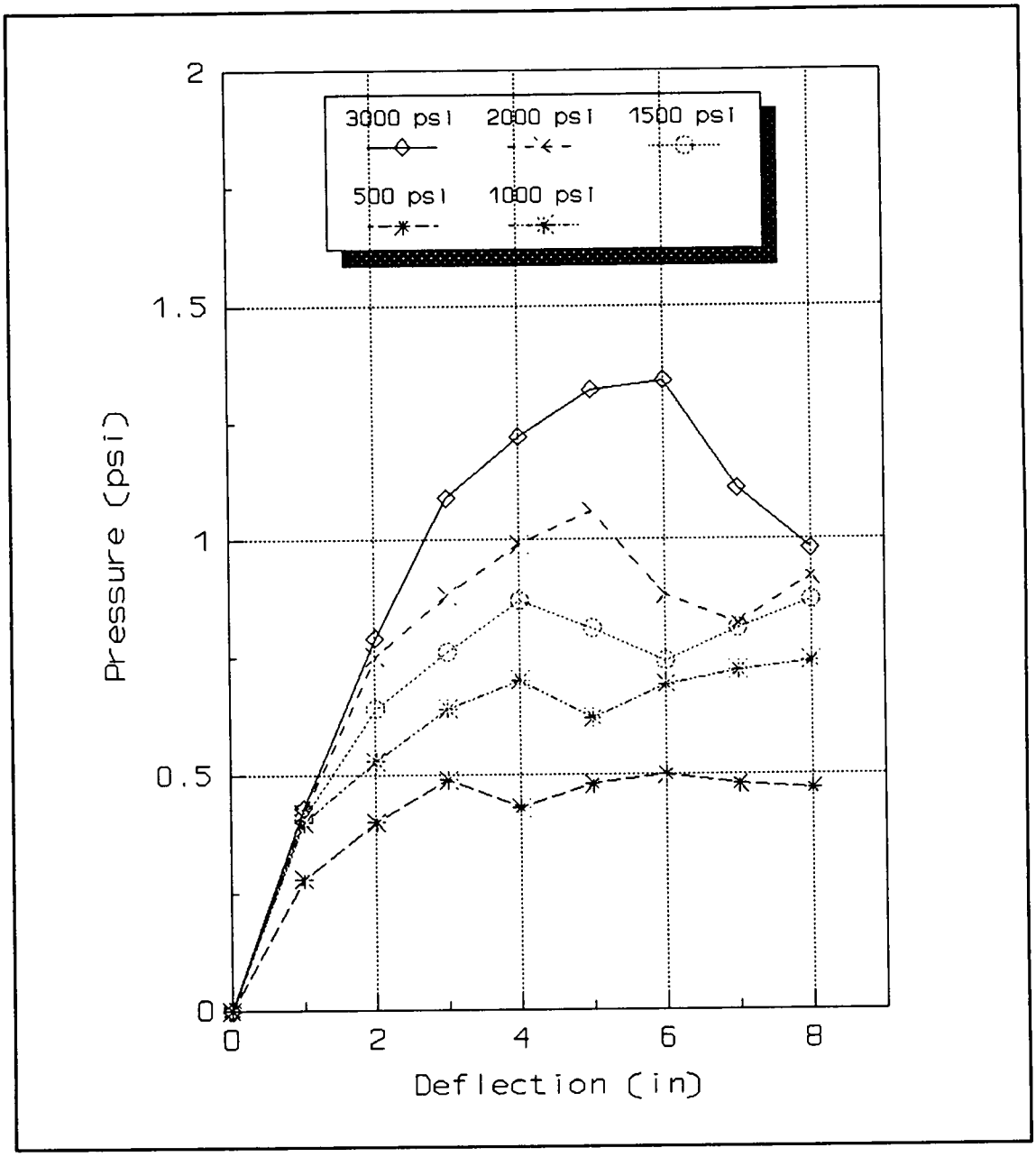


Figure 3.3.20 Pressure Versus Deflection with Various Compressive Strength for Panel 24'x20.5'

(ii) Modulus of Elasticity

The modulus of elasticity of the hollow clay tile masonry was another parameter contributing to the ultimate load capacity of infilled wall panels. An increase of 1000 ksi in the modulus of elasticity will cause an increase of 0.19 psi and 0.049 psi in the ultimate capacity in building 9207 and building 9212 respectively, as shown in Figure 3.3.21. In other words, doubling the modulus of elasticity from 1500 to 3000 ksi would result in a 10 to 15% increase in the ultimate capacity. Load-deflection curves are shown in Figure 3.3.22 and Figure 3.3.23. The maximum deflection shifted slightly to 3 inches from 4 inches in the panel in building 9207, while the maximum deflection ranged from 3 to 9 inches for the wall panel in building 9212.

(iii) Face Shell Thickness

The original analytical method was developed for masonry that had only two webs, one in the front and one in the back. Although the method could be modified to account for the additional webs on the hollow clay tile, there would be difficulties encountered. This is particularly true for the 12 inch wall which is built up of alternating 4 inch and 8 inch tiles. As an approximation to the behavior with additional webs, the effect of varying the face shell thickness was examined. This was the purpose of using a one

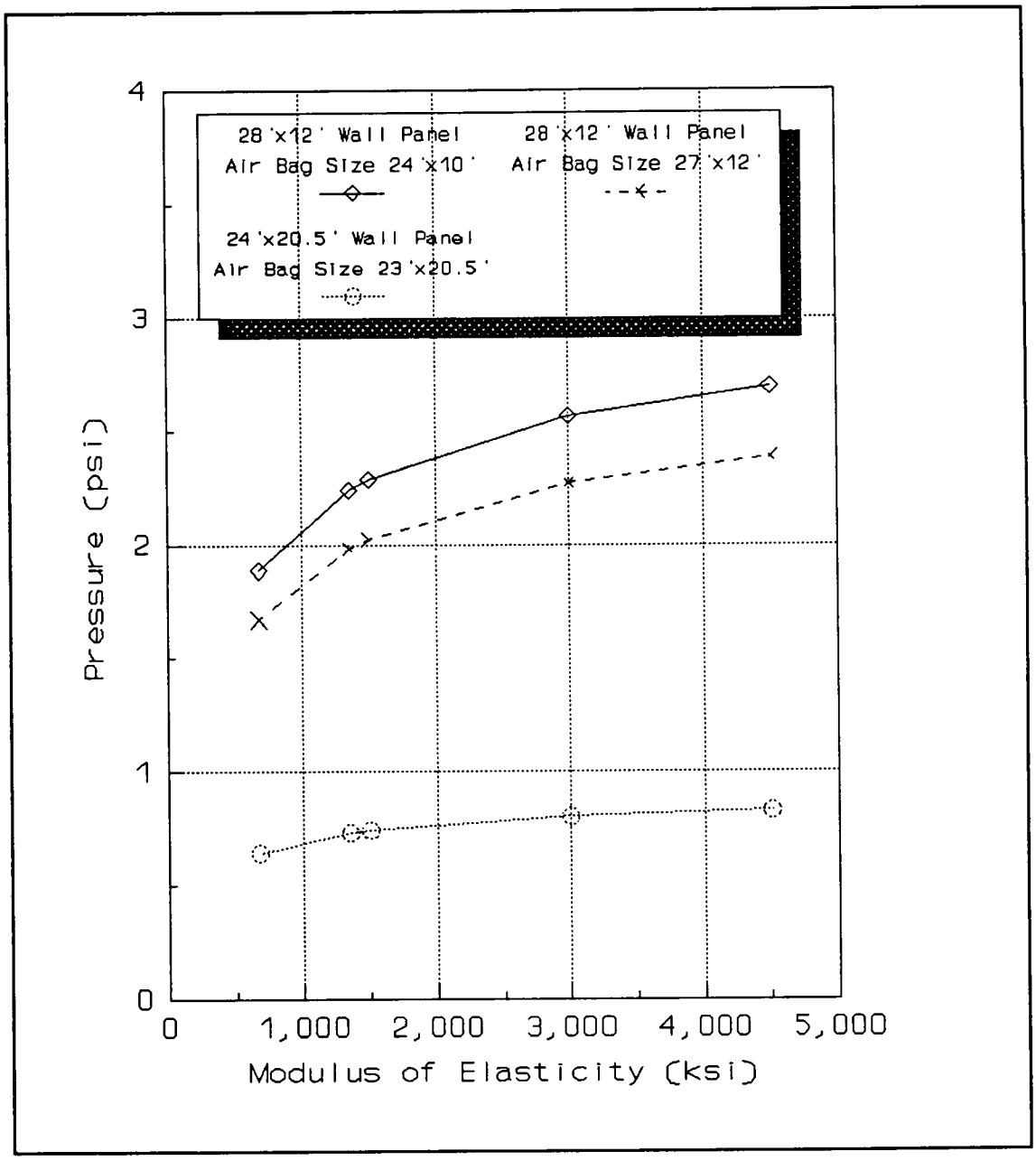


Figure 3.3.21 Pressure Versus Modulus of Elasticity

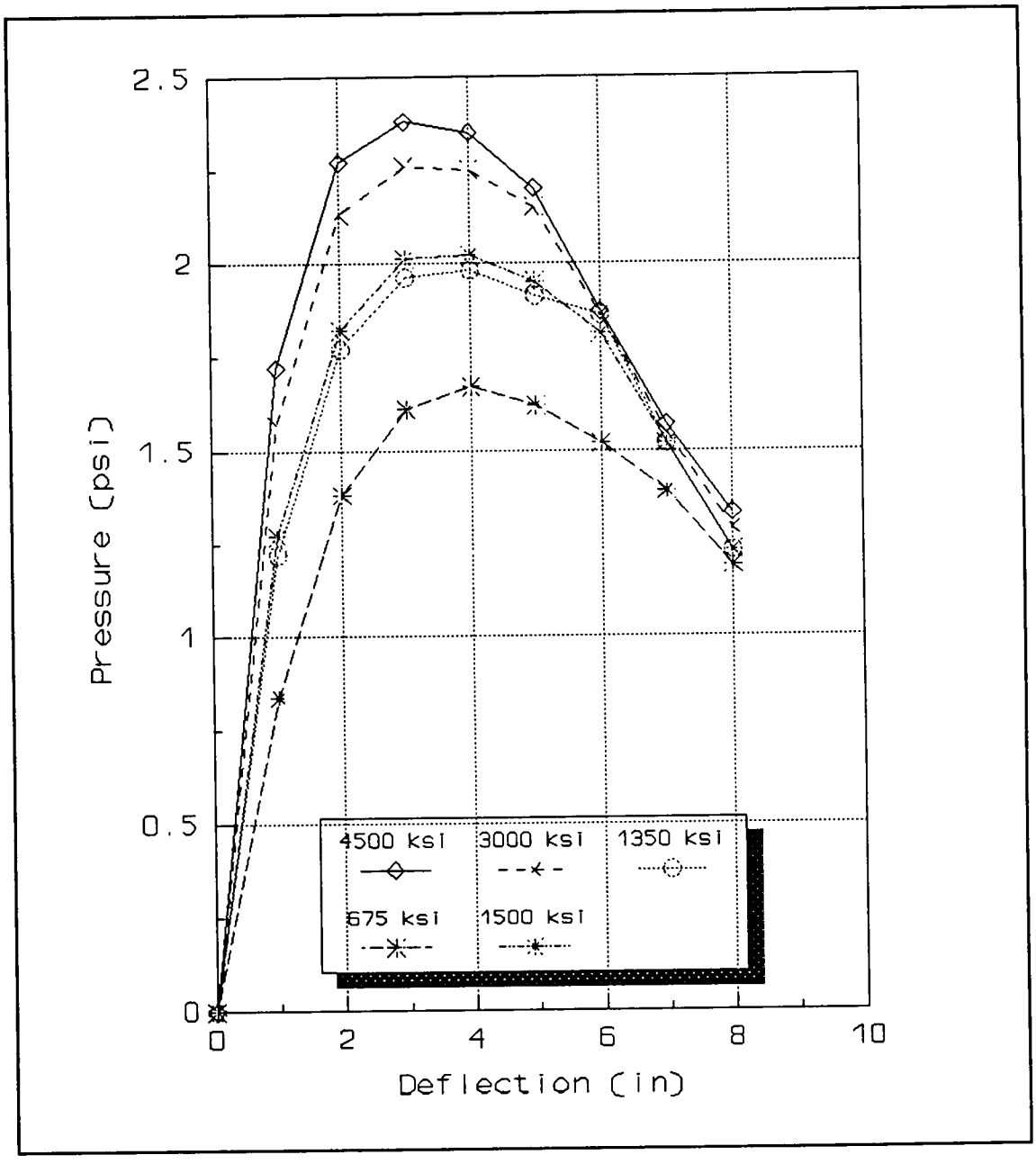


Figure 3.3.22 Pressure Versus Deflection with Various Modulus of Elasticity for Panel 28'x12'

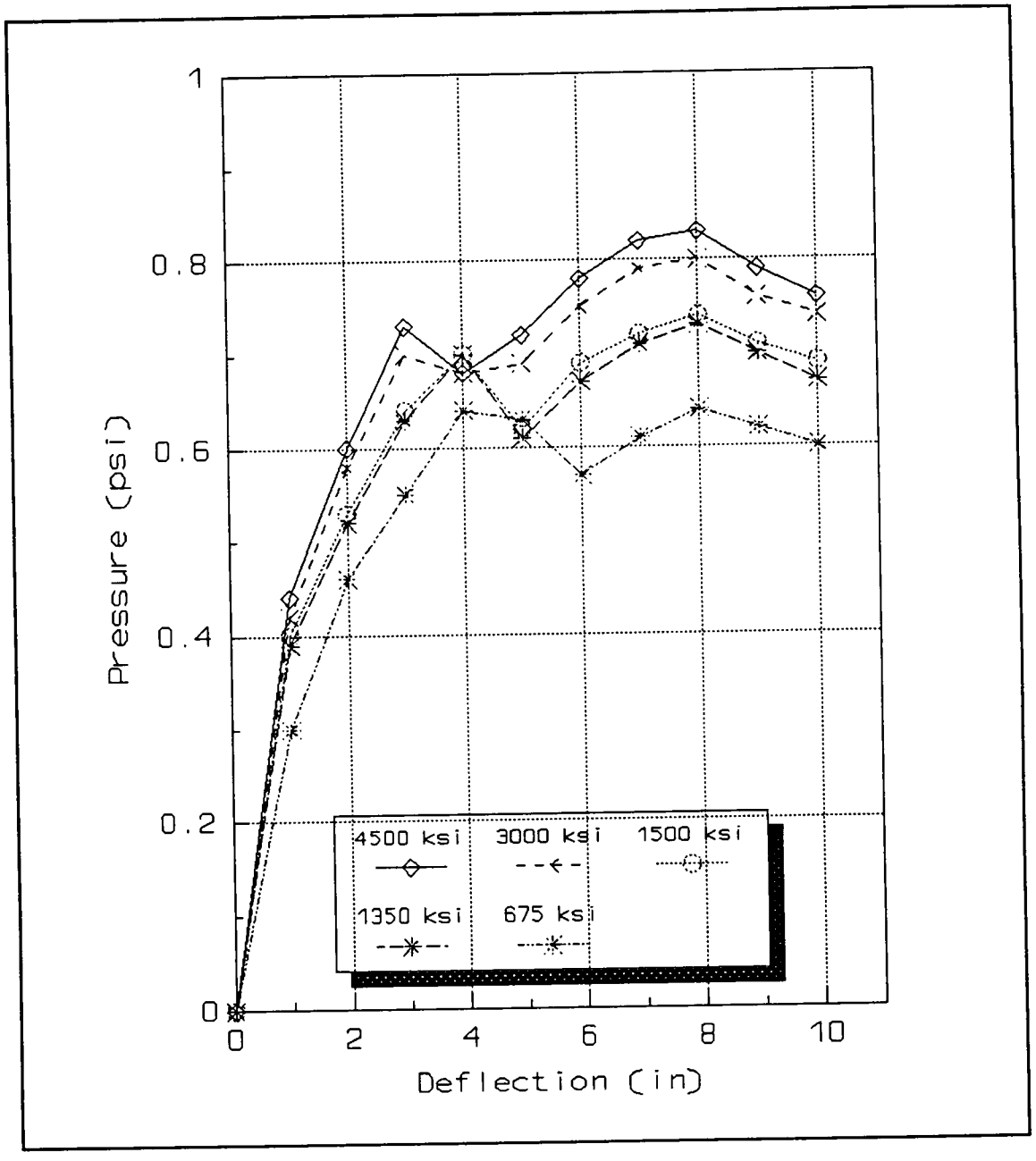


Figure 3.3.23 Pressure Versus Deflection with Various Modulus of Elasticity for Panel 24'x20.5'

inch face shell thickness for the 12 inch wall, the one inch thickness being an assumed "equivalent" face shell thickness.

As the face shell thickness increased, the ultimate load increased to a point. Once a certain value of the face shell thickness was reached, the ultimate load started to drop. Face shell thickness in the range between 1.0 inch and 2.0 inches. resulted in the highest ultimate loads. Increasing the face shell thickness to 1.0 inch in building 9207 (an 8 inch wall) increased the ultimate load to 2.5 psi, or 25%. Either a decrease of the face shell thickness to 0.5 inch, or increasing it to 4.0 inches resulted in a slight decrease in the ultimate load, as shown in Figure 3.3.24. The wall panel in building 9212 had an ultimate load capacity of 0.8 psi at a face shell thickness of 2.0 inches, or 7% increase from 0.74 psi at the thickness of 1.0 inch. The ultimate pressure capacity decreased slightly when the face shell thickness was reduced to 0.5 inch or increased to 6.0 inches, as shown in Figure 3.3.25.

(iv) Steel Frame Sizes

The above analyses have assumed that the panel is a single isolated panel. Thus, the columns and beams are free to translate in the in-plane direction, and to twist about their axes. In reality, the panel may be a part of a wall that is restraining either the beams or the columns from

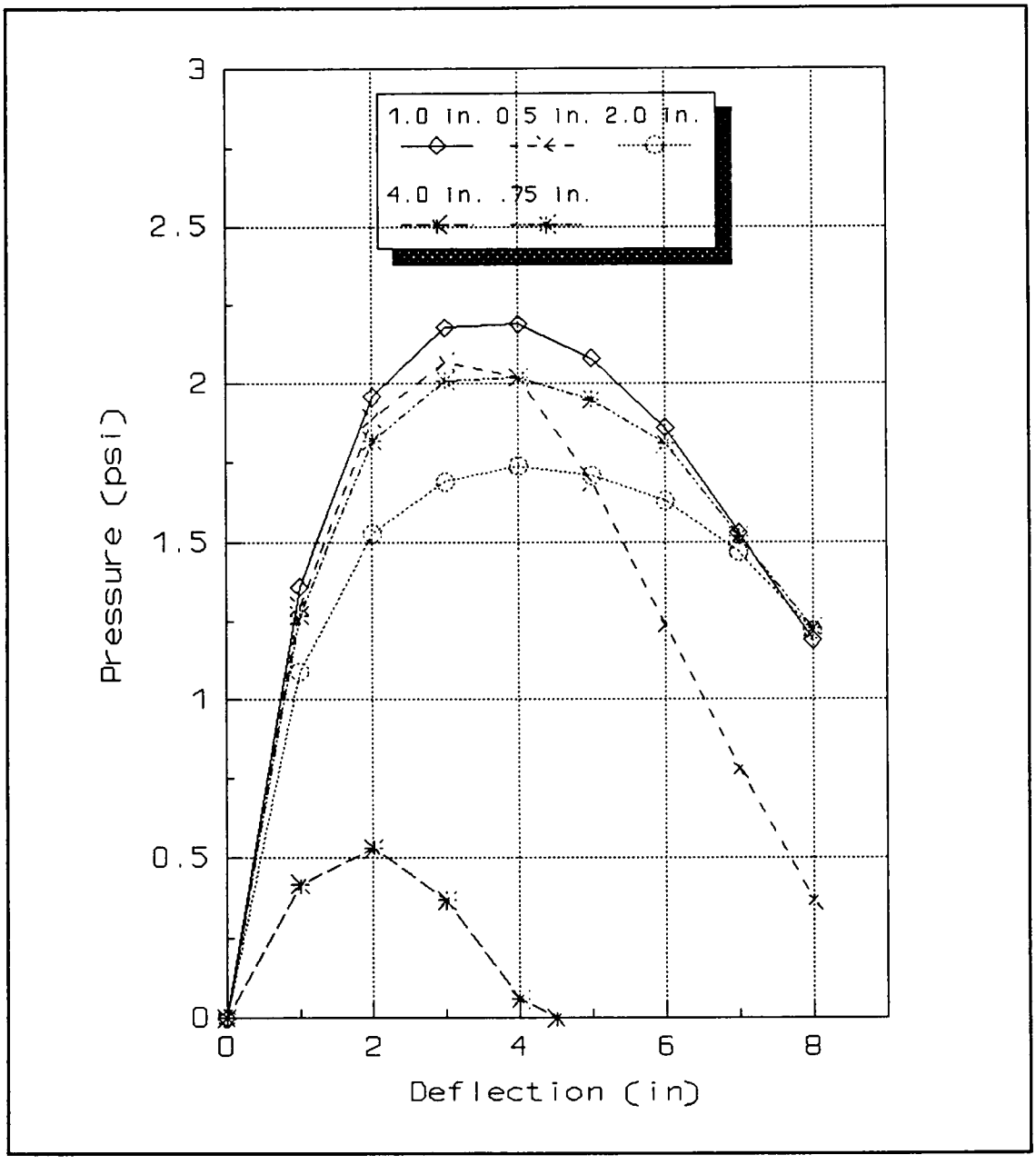


Figure 3.3.24 Pressure Versus Deflection with Various Face Shell Thickness for Panel 28'x12'

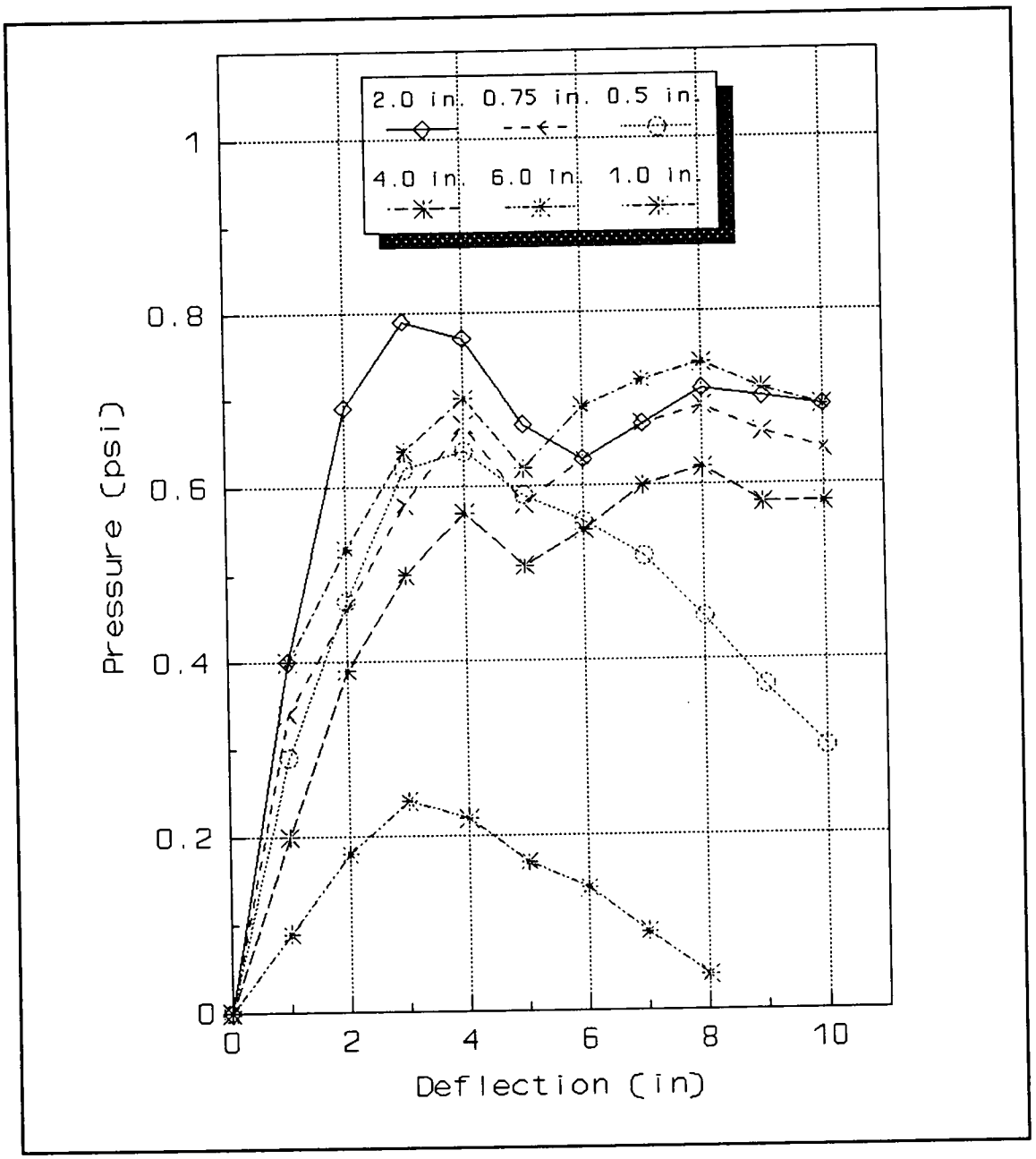


Figure 3.3.25 Pressure Versus Deflection with Various Face Shell Thickness for Panel 24'x20.5'

translation and/or twisting. To examine this effect, the columns and beam sizes were varied as a means of simulating different restraint conditions provided by adjacent walls and members.

Tables 3.3.3 and 3.3.4 show the results for varying sizes of top and bottom beams for building 9207. Increasing the upper beam in building 9207 to a W36x300, which has a moment of inertia of about four times that of a W30x116, resulted in an increase in the ultimate pressure of 25%. The bottom beam size had little effect on the results unless a very small and flexible bottom beam was used. The ultimate loading capacity of the infilled wall panel in building 9207 was not affected by a change of column sizes, either equal or unequal column sizes on both sides as shown in Figure 3.3.26. This is probably due to the panel being relatively long with respect to its height. The arching action primarily occurs as spanning from top to bottom rather than side to side.

In building 9212, an increase of the top beam to a W36x300 doubled the ultimate pressure as shown in Table 3.3.5. However, this is about a forty-five fold increase in moment of inertia. Using a W16x100, or tripling the moment of inertia, resulted in a 40% increase in ultimate pressure. Changing the bottom beam size did not affect the ultimate load capacity significantly, as shown in Table 3.3.6. Figure 3.3.27 indicated that increasing both columns to W36x300s increased

TABLE 3.3.3

EFFECTS OF TOP BEAM SIZES ON ULTIMATE PRESSURE FOR PANEL 28'x12' IN BUILDING 9207

TOP BEAM SIZES	MOMENT OF INERTIA ($Inch^4$)	TORSIONAL CONSTANT ($Inch^4$)	WARPING CONSTANT ($Inch^6$)	AIR BAG SIZES (Ft.xFt.)	ULTIMATE PRESSURE (Psi)
W10x100	623	10.9	5150	27 x 12	---
				24 x 10	1.787
W16x100	1490	7.73	11900	27 x 12	1.793
				24 x 10	2.026
W30x116	4930	6.43	34900	27 x 12	2.023
				24 x 10	2.286
W36x135	7800	6.99	68100	27 x 12	2.154
				24 x 10	2.434
W36x300	20300	64.2	398000	27 x 12	2.528
				24 x 10	2.857

TABLE 3.3.4

EFFECTS OF BOTTOM BEAM SIZES ON ULTIMATE PRESSURE FOR PANEL 28'x12' IN BUILDING 9207

BOTTOM BEAM SIZES	MOMENT OF INERTIA ($Inch^4$)	TORSIONAL CONSTANT ($Inch^4$)	WARPING CONSTANT ($Inch^6$)	AIR BAG SIZES (Ft.xFt.)	ULTIMATE PRESSURE (Psi)
W16x36	448	0.54	1460	27 x 12	---
				24 x 10	1.431
W16x100	1490	7.73	11900	27 x 12	1.592
				24 x 10	1.799
W36x135	7800	6.99	68100	27 x 12	1.924
				24 x 10	1.959
W36x260	17300	41.5	330000	27 x 12	2.023
				24 x 10	2.286
W36x300	20300	64.2	398000	27 x 12	2.033
				24 x 10	2.025

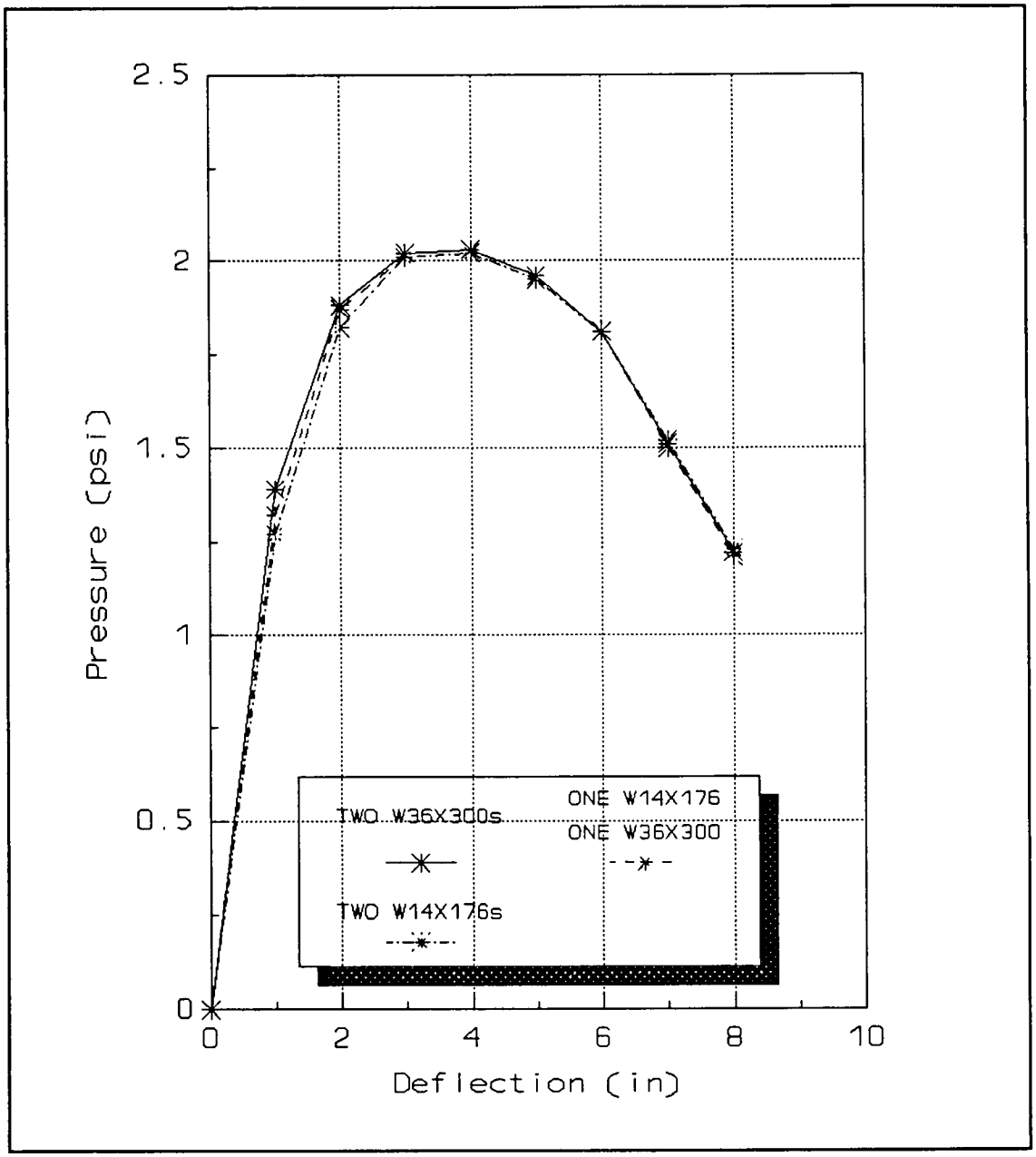


Figure 3.3.26 Pressure Versus Deflection with Various Column Sizes for Panel 28'x12'

TABLE 3.3.5

EFFECTS OF TOP BEAM SIZES ON ULTIMATE PRESSURE FOR PANEL 24'x20.5' IN BUILDING 9212

TOP BEAM SIZES	MOMENT OF INERTIA ($Inch^4$)	TORSIONAL CONSTANT ($Inch^4$)	WARPING CONSTANT ($Inch^6$)	AIR BAG SIZES (Ft.xFt.)	ULTIMATE PRESSURE (Psi)
W16x36	448	0.54	1460	23 x 20.5	0.743
W10x100	623	10.9	5150	23 x 20.5	1.027
W16x100	1490	7.73	11900	23 x 20.5	1.041
W36x135	7800	6.99	68100	23 x 20.5	1.204
W36x300	20300	64.2	398000	23 x 20.5	1.416

TABLE 3.3.6

EFFECTS OF BOTTOM BEAM SIZES ON ULTIMATE PRESSURE FOR PANEL 24'x20.5' IN BUILDING 9212

BOTTOM BEAM SIZES	MOMENT OF INERTIA ($Inch^4$)	TORSIONAL CONSTANT ($Inch^4$)	WARPING CONSTANT ($Inch^6$)	AIR BAG SIZES (Ft.xFt.)	ULTIMATE PRESSURE (Psi)
W16x36	448	0.54	1460	23 x 20.5	0.646
W10x100	623	10.9	5150	23 x 20.5	0.744
W16x100	1490	7.73	11900	23 x 20.5	0.728
W36x135	7800	6.99	68100	23 x 20.5	0.739
W36x260	17300	41.5	330000	23 x 20.5	0.743
W36x300	20300	64.2	398000	23 x 20.5	0.743

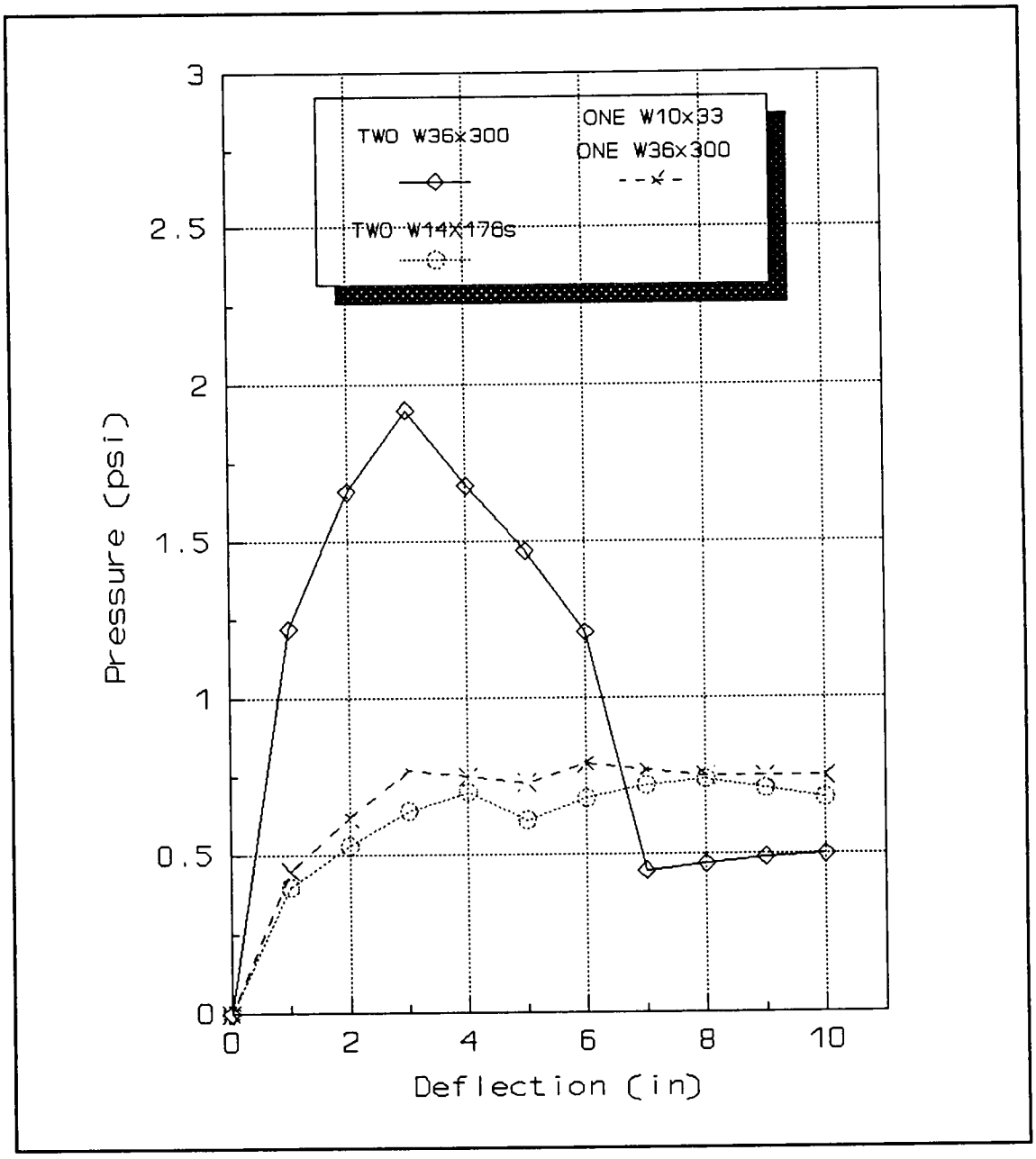


Figure 3.3.27 Pressure Versus Deflection with Various Column Sizes for Panel 24'x20.5'

the ultimate capacity by about 150%. In addition, the ultimate capacity occurred at a smaller deflection, 3 inches, and the load capacity dropped off significantly beyond this. Thus, although the capacity increases, the behavior was more brittle in nature. Increasing the column size on only one side just had a marginal effect on the results.

(v) Air Bag Size

Current plans are to test the wall in building 9207 with an air bag that is slightly smaller than the wall panel itself. The air bag will have a size of 24 ft. x 10 ft., or only about 71% of the wall will be loaded. The effect of this reduced size of the air bag loading was investigated. Under the identical compressive strength, modulus of elasticity and face shell thickness, the ultimate pressure when the wall is loaded with a 24 ft. x 10 ft. air bag instead of a 27 ft. x 12 ft. air bag increased approximately 12% as shown in Figure 3.3.28. The total load that the wall will carry will only be about 80% of the total load for a full size air bag, due to the reduced area. Thus, under the postulated conditions for the wall that were used to predict the ultimate load, it is expected that only 80 kips is necessary to fail the wall in 9207.

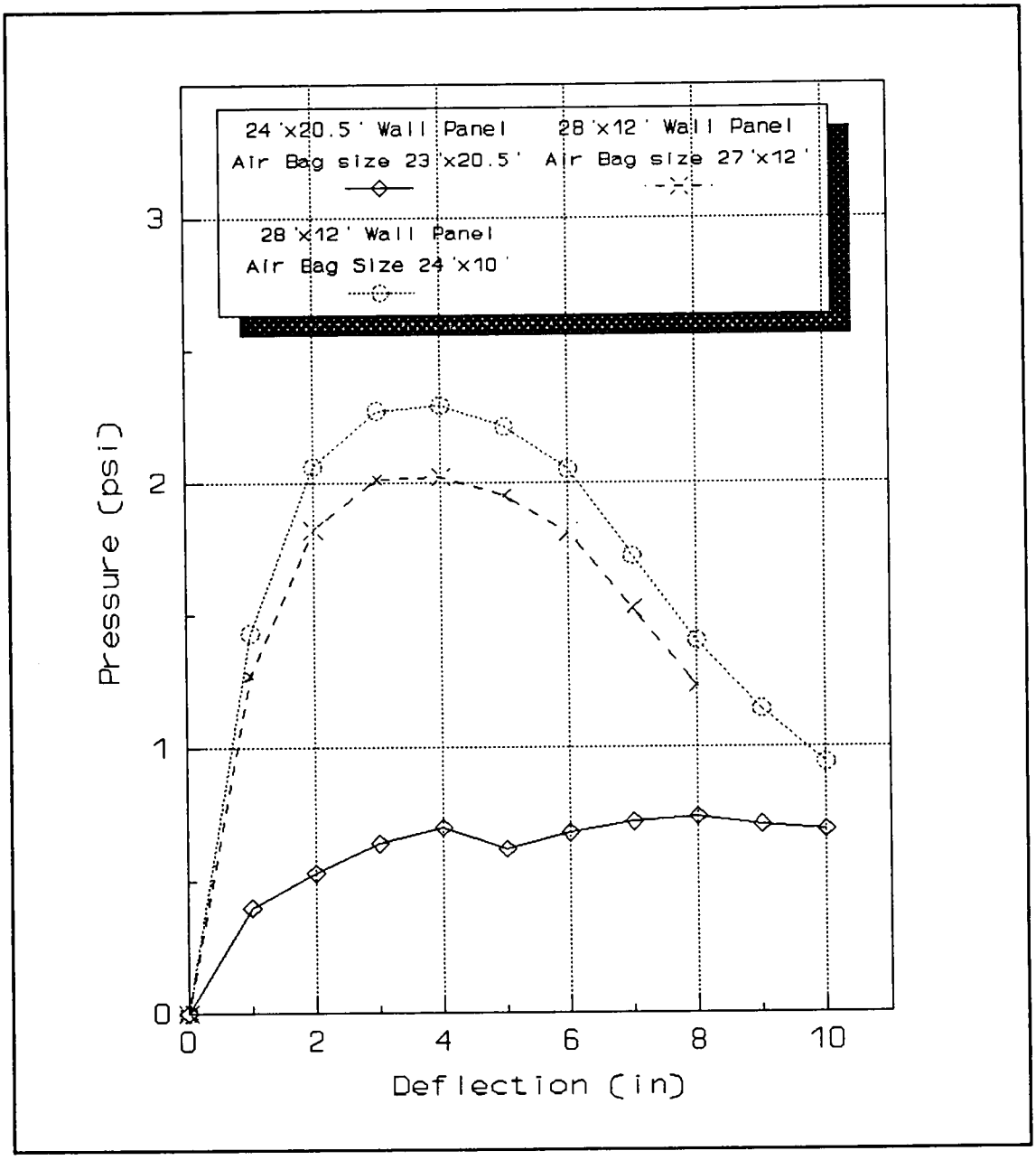


Figure 3.3.28 Pressure Versus Deflection with Different Air Bag Sizes

3.4 SUMMARY OF RESULTS

Predicted capacities of the experimental wall panel in building 9207 and building 9212 were determined using assumed material properties. Results were 93 kips for the wall in 9207 and 51 kips for the wall in 9212. These results are significantly affected by the compressive strength of the wall, and can be modified and updated as compressive strengths become available from the prism testing program. Using an air bag size different from the wall panel size causes a change in the results, but it can be accounted for in the analysis. The other parameter having a significant effect on the results is the restraint provided by the confining steel frame. Adjacent wall panels, which will serve to provide additional restraint to the columns and beams, can cause a profound effect on the capacity. These conditions need to be closely examined at the test sites. Instrumentation has been specified in the test plan to measure column and beam in-plane movements and rotations. The other parameters examined, modulus of elasticity and face shell thickness, did not have a large effect, and probably do not need any further examination before the tests.

CHAPTER 4

CONCLUSIONS AND RECOMMENDATIONS

4.1 CONCLUSIONS

Analytical methods for predicting the strengths of two existing wall panels with respect to their limit states were investigated. The failure theory proposed by Thurlimann and Guggisberg (1988), in combination with the ABAQUS (1988) finite element technique for linear elastic analysis, results in reasonably good predictions of the first cracking loads. The analytical technique adapted from Seah (1988), proven to have good correlation with experimental results, was utilized to predict the ultimate strength of the panels. The technique included arching action in a yield line analysis to predict the maximum load capacities.

For the panel in Building 9207, the first cracking pressure is 0.52 Psi or a total load of 24 Kips on the wall. The ultimate pressure is about 2.0 Psi or a total load of 93 Kips on the wall. The first cracking load is about 26% of the ultimate load. For the panel in Building 9212, the first crack and ultimate pressure are about 0.34 Psi and 0.74 Psi

respectively, or total loads of 23 Kips and 51 Kips. The first cracking load is about 45% of the ultimate load. The trend of these results are consistent with the experimental results obtained by Seah (1988) and Drysdale and Essawy (1988), despite the difficulties of modeling the boundary conditions. The difference between 26% and 45% for the panels in Building 9207 and 9212 respectively is probably caused by the stiffness of the enclosing frame, especially the top beam. The panel in Building 9207 has a W30x116 top beam compared to a W16x36 in panel in Building 9212. Based on the parametric study on the steel frame sizes in Section 3.3.5, it was evident that the stiffness provided by the larger beam size in Building 9207 restrains the infilled panel and increases the ultimate load capacity of the panel to a larger extent.

The results from the parametric studies showed that modulus of rupture and modulus of elasticity have significant effects on the first cracking load. The ultimate load capacity is significantly influenced by the compressive strength of the wall. As a result, the wall panel strength is dependent primarily on the flexural strength of the wall before cracking. The post-cracking strength depends on the membrane action or arching effects due to the in-plane thrust developed when the panel cracked out of the plane and is restrained by the enclosed steel frame.

Although air bag size has an effect on the strengths of

the wall panels, it can be easily accounted for in the analysis. Other parameters, such as Poisson's ratio and face shell thickness, have marginal effects on the first crack and ultimate loads.

The boundary conditions are critical in predicting the wall panel capacity. One of the characteristics of infill arching action is that the perimeter strips tend to develop significant in-plane thrusts that cause membrane action while less thrust is developed in the middle strips. Comparing Case 2 in pre-cracking prediction and failure Mode B or Mode C in post-cracking prediction in Building 9207 and 9212 shows that the first cracking load is very close to that of the ultimate strength. The restraint and stiffness provided by the enclosing steel frame will influence the ultimate strength. The confinement of the wall panel by a large size of top beam increases the ultimate load substantially. The affect on the ultimate strength by restraint in the columns are dependent on the aspect ratio. The longer length of the panel with respect to its height decreases the effect of the columns on the ultimate strength.

4.2 RECOMMENDATIONS

Some of the difficulties encountered in this study are related to:

(i) Uncertainties in modeling the support conditions

The boundary conditions of the panels in Building 9207 and 9212 are not well defined. Therefore, assumptions are made in modeling the actual panel. It is recommended that careful observation and monitoring be conducted of the actual infill to frame boundaries while testing is in progress.

(ii) Approximation and simplification of the material properties

The hollow clay tile masonry is a highly variable material and there is a scarcity of experimental and analytical data on the material properties. This results in the approximation of the elastic constants, modulus of rupture, and compressive strength used in this study. These are the primary factors affecting the strength of the panels. Simplification was also assumed in the 12-inch walls, which were made of 8-inch and 4-inch units. The effects of the masonry units' horizontal cores, continuity, homogeneity and workmanship are obtainable through a prism testing program.

Although assumptions are made to analyze the hollow clay tile wall panels using a linear elastic model, the actual behavior of the infilled clay tile panel may be non-linear.

(iii) Completeness of the analytical model

Arching action for the infilled wall panel is assumed to occur when the panel cracks out of the plane of the wall. The results of the analyses and other experimental work indicate that the wall panel capacity is significantly greater than the first cracking strength. The analyses in this thesis are for monotonic loading, whereas earthquake generated forces consist of load reversal. The validity of the arching effect and the ability of in-plane membrane action to develop under dynamic loading is presently unknown. To better understand the actual behavior of the infilled wall panel in the event of an earthquake, it is recommended that further research, analysis, and testing include dynamic loadings in the out-of-plane as well as in-plane directions.

REFERENCES

REFERENCES

ABAQUS. (1989). Version 4.8, Hibbitt, Karlsson, and Sorensen, Inc.

Abboud, B.E., and Hamid, A.A. (1990). "Behavior of Model Concrete Masonry Slender Walls Under Out-of-Plane Lateral Loads." Fifth North American Masonry Conference, University of Illinois at Urbana-Champaign.

Anderson, C. (1985). "Test on Wall Subjected to Uniform Lateral Loading and Edge Loading." Proceedings of the Seventh International Brick and Block Masonry Conference, Melbourne, Australia, 889-900.

Axley, J.W. (1979). "Infill Panels: Their Influence on Seismic Response of Buildings." Dissertation of Doctor of Philosophy, University of California, Berkeley, California.

Baker, L.R. (1979). "A Failure Criterion for Brickwork in Biaxial Bending." Proceeding of the Fifth International Brick Masonry Conference, Washington.

Bennett, R.M., and Burdette, E.G. (1989). "Final Report on Structural Behavior of Clay Tile Walls Proposed Evaluation Program." The University of Tennessee, Knoxville, Tennessee.

Cavanagh, C., Webb, W.F., and Hodgkinson, H.R. (1982). "In-situ Lateral Load Tests on an Old Brickwork Building." Heavy Clay Division, British Ceramic Research Association, Technical Note 345.

Dawe, J.L., and Seah, C.K. (1988). "Lateral Load Resistance of Masonry Panels in Flexible Steel Frames." Proceedings of Eighth International Brick and Block Masonry Conference, Ireland, 606-616.

Dawe, J.L., and Seah, C.K. (1989). "Out-of-plane Resistance of Concrete Masonry Infilled Panels." Canadian Journal of Civil Engineering, 16, 854-864.

DOE Order 6430.1A (1987). "General Design Criteria." United States Department of Energy, Washington, D.C.

Drysdale, R.G., and Essawy, A.S. (1988). "Out-of-plane Bending of Concrete Block Walls." Journal of Structural Engineering, ASCE, 114(1), 121-132.

Drysdale, R.G., and Hamid, A.A. (1984). "Tension Failure Criteria for Plain Concrete Masonry." Journal of Structural Division, ASCE, 110(2), 228-244.

Essawy, A.S., and Drysdale, R.G. (1986). "Macroscopic Failure Criterion for Masonry Assemblages." Proceedings of the Fourth Canadian Masonry Symposium, Fredericton, N.B., Canada, 263-277.

Essawy, A.S., and Drysdale, R.G. (1987). "Evaluation of Available Design Methods for Masonry Walls Subject to Out-of-plane Loading." Proceedings Fourth North American Masonry Conference, University of California, Los Angeles, California, 32-1 - 32-13.

Fricke, K.E. (1990). Personal Communication.

Fricke, K.E., and Jones, W.D. (1989). "Seismic Analysis and Testing of Clay Tile Walls at the Oak Ridge Y-12 Plant." Martin Marietta Energy Systems, Inc., Oak Ridge, Tennessee.

Fried, A., Anderson, C., and Smith, D. (1988). "Predicting the Transverse Lateral Strength of Masonry Walls." Proceedings of the Eight International Brick and Block Masonry Conference, Dublin, Ireland, 1171-1183.

Gazzola, E., Drysdale, R.G., and Essawy, A.S. (1985). "Bending of Concrete Masonry Wallettes at Different Angles to the Bed Joints." Proceedings of the Third North American Masonry Conference, University of Texas, Arlington, Texas, 27-1 - 27-14.

Hamid, A.A., and Drysdale, R.G. (1981). "Proposed Failure Criteria for Concrete Block Masonry Under Biaxial Stresses." Journal of Structural Division, ASCE, 107(8), 1675-1687.

Haseltine, B.A., West, H.W.H., and Tutt, J.M. (1977). "Part 2 : Design of walls to resist lateral loads." The Structural Engineer, 55(10), 422-430.

Hendry, A.W. (1973). "The Lateral Strength of Unreinforced Brickwork." The Structural Engineer, 51(2), 43-50.

Huff, T.E. (1990). Personal Communication.

Johnson, F.B., and Matthys, J.H. (1973). "Structural Strength of Hollow Clay Tile Assemblages." Journal of Structural Division, ASCE, 99(2), 259-275.

Kemp, K.O. (1965). "The Yield Criterion for Orthotropically Reinforced Concrete Slabs." Int. Journal of Mech. Science, Progamon Press Ltd., 7, 737-746.

Martin Marietta Energy Systems Committee for the Structural Testing of Hollow Clay Tile Wall Panels. (1990). "Test Procedure for out-of-plane Full Scale Static Testing of a Hollow Clay Tile Wall Panel." HCTP-6, Rev. 0.

Park, R. (1964). "Ultimate Strength of Rectangular Concrete Slabs Under Short-term Uniform Loading with Edges Restrained Against Lateral Movements." Proceedings of the Institute of Civil Engineers, 28(6), 125-150.

Plummer, H.C. (1962). "Brick and Tile Engineering." Brick Institute of America, McLean, Virginia.

Seah, C.K. (1988). "Out-of-plane Behavior of Masonry Infilled Panels." Master of Science Thesis, University of New Brunswick.

Sinha, B.P. (1978). "A Simplified Ultimate Load Analysis of Lateral Loaded Model Orthotropic Brickwork Panels of Low Tensile Strength." The Structural Engineer, 56B(4), 81-84.

Sinha, B.P., Loftus, M.D., and Temple, R. (1979). "Lateral Strength of Model Brickwork Panels." Proceedings of the Institute of Civil Engineers, 67(2), 191-197.

Thurlimann, B., and Guggisberg, R. (1988). "Failure Criterion for Laterally Loaded Masonry Walls : Experimental Investigations." Proceedings of the Eighth International Brick and Block Masonry Conference, Dublin, Ireland, 1, 699-706.

Weaver, W., and Johnston, P.R. (1984). "Finite Elements for Structural Analysis." Prentice-Hall, inc., New Jersey.

VITA

Lek Song Chua [蔡 立 松] was born in Pulau Ketam, Malaysia on Jan 4, 1961. He graduated from La Salle High School and Tunku Abdul Rahman College in Malaysia on December 1979 and 1982 respectively. To pursue higher education, he attended the University of Miami in Florida for two semesters and transferred to the University of Tennessee at Knoxville where he majors in Civil Engineering. The author received his Bachelor of Science degree in Civil Engineering with high honors in August 1988.

The author started his graduate studies in the graduate school of the University of Tennessee at Knoxville the following year. He accepted a Graduate Assistantship from the Civil Engineering Department and a research position with Martin Mariatta Energy System while completing his studies. He received his Master of Science degree with a major in Structural Engineering in May 1991.

The author is a former Secretary/Treasurer of Chi Epsilon National Honor Society for Civil Engineers, Members of Tau Beta Pi National Honor Society for Engineers, Gamma Beta Phi National Honor Society, and American Society of Civil Engineers.